APPLICATION OF X-RAY CT FOR INVESTIGATING FLUID FLOW AND CONFORMANCE CONTROL DURING CO_2 INJECTION IN HIGHLY HETEROGENEOUS MEDIA

A Thesis

by

DEEPAK CHAKRAVARTHY

Submitted to the Office of Graduate Studies of
Texas A&M University
in partial fulfillment of the requirements for the degree of

MASTER OF SCIENCE

May 2005

Major Subject: Petroleum Engineering

APPLICATION OF X-RAY CT FOR INVESTIGATING FLUID FLOW AND CONFORMANCE CONTROL DURING CO_2 INJECTION IN HIGHLY HETEROGENEOUS MEDIA

A Thesis

by

DEEPAK CHAKRAVARTHY

Submitted to Texas A&M University
in partial fulfillment of the requirements
for the degree of

MASTER OF SCIENCE

Approved as to style and content by:

David S. Schechter (Chair of Committee)	Daulat D. Mamora (Member)
Eyad Masad (Member)	Stephen A. Holditch (Head of Department)

May 2005

Major Subject: Petroleum Engineering

ABSTRACT

Application of X-Ray CT for Investigating Fluid Flow and Conformance Control During CO_2 Injection in Highly Heterogeneous Media. (May 2005)

Deepak Chakravarthy, B.E., PSG Institute of Technology, India

Chair of Advisory Committee: Dr. David S. Schechter

Fractured reservoirs have always been considered poor candidates for enhanced oil recovery. This can be attributed to the complexities involved in understanding and predicting performance in these reservoirs. In a fractured system, the high permeability fracture forms the preferred pathway for the injected fluids, and a large amount of oil that is stored in the matrix is bypassed. Hence, a good understanding of multiphase fluid flow in fractures is required to reduce oil bypass and increase recovery from these reservoirs. This research investigates the effect of heterogeneity and injection rates on oil bypass and also the various techniques used for the improvement of sweep efficiency in heterogeneous systems. Several coreflood experiments were performed using homogeneous and heterogeneous cores and a 4^{th} generation X-Ray CT scanner was used to visualize heterogeneity and fluid flow in the core. Porosity and saturation measurements were made during the course of the experiment.

The experimental results indicate that injection rates play a very important role in affecting the recovery process, more so in the presence of fractures. At high injection rates, faster breakthrough of CO_2 and higher oil bypass were observed than at low injection rates. But very low injection rates are not attractive from an economic point of view. Hence water viscosified with a polymer was injected directly into the fracture to divert CO_2 flow into the matrix and delay breakthrough, similar to the WAG process. Although the breakthrough time reduced considerably, water “leak off” into the matrix was very high. To counter this problem, a cross-linked gel was used in the fracture for conformance control. The gel was found to overcome “leak off” problems and effectively divert CO_2 flow into the matrix. This experimental research will serve to increase the understanding of fluid flow and conformance control methods in fractured reservoirs.

DEDICATION

To Mom, Kib, Divya, Tuffy and Jerry and all my friends who have always stood by me.

ACKNOWLEDGMENTS

I would like to express my deepest gratitude and appreciation to my advisor and committee chair, Dr. David S. Schechter, for believing in me and helping me out when everything looked bleak. His constant encouragement and creative ideas have always motivated me to work beyond my ability.

I would like to thank Dr. Daulat Mamora for his constant guidance and help in the laboratory during the course of this work. I'd also like to thank Dr. Eyad Masad for having agreed to serve on my graduate committee and reviewing my work.

I wish to thank Dr. Erwinsyah Putra for his continuous support and guidance. He has been my mentor, guide and friend throughout my graduate study and for that, I'll always be grateful to him.

I would also like to thank Dr. Blasingame for giving me the opportunity to be a part of this department. I would also like to thank Dr. Scott for having helped me during my initial days at the department.

I would like to thank Vivek Muralidharan for everything he has done for me. Without his help, I'm not sure where I'd be today. Many thanks to Deepak, Sandeep and Ashish for their support and guidance. Thanks are also due to Manoj, Kartik, Harshal, Patel and Prasanna for making my stay at A&M a memorable one. I'd like to thank Mirko and Dayo for their friendship and for making my office a more cheerful place. I'd also like to thank my roommate Chandru for his support and encouragement.

It has been a pleasure to work with the members of the NFR group and all the other graduate students in the department. I can never forget those sleepless nights at the lab, the countless Hot and Spicy's I've had at four in the morning or the six hour naps that I've taken on my desk. Thank you very much.

TABLE OF CONTENTS

CHAPTER Page

LIST OF FIGURES

FIGURE Page

FIGURE Page

FIGURE Page

FIGURE Page

LIST OF TABLES

TABLE Page

CHAPTER I

INTRODUCTION

1.1 Introduction

Fractured reservoirs form a large and increasing percentage of the world's hydrocarbon reserves, with millions of barrels of oil left uncovered in them. However, in spite of their wide occurrence and huge reserves, the oil recovery from most of these reservoirs is extremely low. This can be attributed to their poor response to both secondary and tertiary recovery operations. A thorough understanding of multiphase flow in fractures is required to improve oil recovery from fractured reservoirs. Therefore studies on naturally fractured reservoirs have gained vast importance in the recent years.

Numerous secondary and tertiary recovery methods have been used over the years in an attempt to improve oil recovery from hydrocarbon reservoirs. Of the various tertiary recovery methods used, CO_2 flooding has seen growing importance, especially in the medium to light oil reservoirs. There are several factors that make CO_2 flooding an excellent enhanced oil recovery (EOR) process, the primary ones being its easy solubility in crude oil and its ability to "swell" the net volume of oil and thereby reduce oil viscosity by a vaporizing-gas-drive mechanism[1]. The success of a CO_2 flood is decided on the basis of the number of thousands of cubic feet (Mcf) of CO_2 injected per barrel of oil recovered, termed "Utilization Factor". The quantity of hydrocarbons that can be recovered from a reservoir and hence the utilization factor are influenced by several characteristics of the reservoir including reservoir rock properties, reservoir pressure and temperature, physical and compositional properties of the fluid and structural relief, to name a few. However, the predominant factor in deciding the success of a CO_2 flood is the reservoir heterogeneity. Highly heterogeneous reservoirs with variable lateral and vertical relative permeability characteristics can cause potential problems during CO_2 injection.

This thesis follows the style of *Journal of Petroleum Technology*.

Roebuck[2] reports that the injected CO_2 would tend to finger ahead into areas with high mobility ratios. As displacement progresses, the mobility ratio continues to increase in the portions of the reservoir previously contacted by the displacing gas. Hence, there is a decreasing tendency of the gas to enter regions of low permeability or regions of low gas saturation. This results in the gas forming preferential paths and "bypassing" large volumes of oil. The degree of bypassing is enhanced to a large extent by the presence of natural or hydraulic fractures. In a fractured reservoir, the displacement process is dependent on the fracture-matrix geometry, size and interaction apart from other physical phenomena. Uleberg and Hoier[3] suggest that the injection gas tends to flow in the highly permeable fractures, instead of the normally expected displacement path. These fractures are often responsible for early and excessive breakthrough of CO_2, thus greatly affecting the economics of the project[4, 5]. It therefore becomes essential to understand the complexities involved in the yet unexplored fracture-matrix interactions.

In order to better understand multiphase flow, visualization of fluid flow inside the medium is essential. Several techniques have been adopted to visualize fluid flow, from as early as 1960. But in the recent years, X-Ray computerized tomography (CT) has seen increasing application for non-intrusive determination of variables in rock properties and fluid flow visualization. Invented for medical purposes, the CT scanner is now being used for a wide variety of applications. Many researchers have used CT for rock property determination (Bergosh *et al.*[6], (1985); Hornapur *et al.*[7], (1985); Hornapur *et al.*[8], (1986); Narayanan and Deans[9], (1987); Jasti *et al.*[10], (1988); Hidajat *et al.*[11], (2002)). These include study of heterogeneous rocks, fractures, vuggy carbonates and determination of rock properties like porosity and bulk density. Application of X-Ray CT in various coreflood experiments has also been discussed by many researchers. MacAllister *et al.*[12] (1990) conducted three-phase oil/water and gas/water experiments using CT scanner to investigate the dependence of relative permeability on wettability. Withjack[13] (1987) demonstrated the use of X-Ray CT for flow visualization and determination of fluid saturations. Vinegar and Wellington[14] (1987) used CT to visualize three phase fluid flow during miscible and immiscible displacements using CO_2. They used iodated dopant to distinguish between the different phases. They also proposed methods to determine two phase and three phase fluid saturations. Hicks *et al.*[15] (1994) conducted a study of

miscible displacements in heterogeneous carbonate cores using X-Ray CT. Apart from these works, there are a few others that deal with investigation of oil bypassing using X-Ray CT. Wellington and Vinegar[16] (1985) tested the use of surfactants for CO_2 mobility control. They concluded that surfactant can prove to be an effective mobility control agent for CO_2. Yamamoto *et al*[17] (1994) conducted coreflood experiments to analyze the performance CO_2 WAG injection in layered reservoirs. Oshita *et al*[18] (2000) discussed the possible reasons for early water breakthrough in oil-wet cores. Alajmi and Grader[19] (2000) conducted two-phase oil/water experiments in fractured cores to study oil bypassing caused during waterflooding in fractured porous media. This review of literature suggests that a thorough investigation of gas injection in the presence of extreme heterogeneities like fractures has not been carried out and many uncertainties still exist in this area.

This research uses a fourth generation X-Ray CT scanner for the investigation of various factors that cause oil bypass in fractured reservoirs. Experiments were performed at various flow rates and the effects of injection rates and heterogeneity have been investigated. Also, experiments were conducted to investigate the effectiveness of various mobility control and conformance control techniques like Water Alternating Gas (WAG) and the usage of polymer gel in a fractured system. This experimental research will improve the understanding of fluid flow occurring in fractured reservoir systems, which in turn would help in improving oil recovery from these reservoirs.

1.2 Objectives

The goal of this work is to investigate CO_2 flooding in fractured systems. Determining the effect of various factors like the presence of general heterogeneities like changes in porosity and permeability and the presence of extreme heterogeneities like fractures are the primary objectives. Water Alternating Gas (WAG) has proven to be mostly effective in fairly homogeneous reservoirs. This research investigates the performance of WAG in highly heterogeneous systems. The other objective is to perform CO_2 flooding experiments in the presence of a conformance control agent like polymer gel and observe the effect on oil recovery and breakthrough.

1.3 Rationale and significance

In the United States, oil that is potentially producible by advanced methods amounts to 200 of the remaining 351 billion barrels. Of the available enhanced oil recovery methods, gas injection has the greatest potential for additional oil recovery from light oil reservoirs, for which incremental oil recoveries may exceed 10% of the stock tank oil initially in place (STOIIP)[20]. CO_2 flooding has evolved to be the most promising gas injection technique for widespread use in enhanced oil recovery due to a number of factors, including the fact that CO_2 is one of the most plentiful compounds available in the planet[21].

Rapid advancement in technology has led to the commencement of a large number of improved oil recovery (IOR) projects, especially in areas where CO_2 production wells are being drilled to increase its supply. However, there are a large number of reservoirs that are not being considered for CO_2 flooding and other IOR techniques due to the presence of extreme heterogeneities or natural fractures. The fluid flow experiments performed will help in achieving a better understanding of the complexities involved in flow through fractures. A good understanding of these complexities is required before commencing IOR projects in these reservoirs and this is important for both technical and economic success of the project. Also, the preliminary experiments performed to determine fracture aperture will help in better characterizing fractured reservoirs.

1.4 Methodology

Several experiments were performed to study the effect of injection rates and heterogeneity on oil recovery and breakthrough time. Continuous CO_2 injection experiments were first performed on homogeneous (unfractured) cores at different injection rates and the oil recovery in each case was observed. The X-Ray scanner was used to obtain cross-sectional scans of the cores and these scans were combined to obtain ortho reconstructions. Using these scans, saturations were determined at different points along the length of the core to identify the effect of heterogeneity on oil saturation in the core. Average values of saturations were also determined for each experiment. The cores were than artificially fractured in the laboratory using a core splitter and experiments were performed on fractured cores. The main objective of these experiments was to

compare the recovery and breakthrough times with the homogeneous core experiments. In order to reduce breakthrough times and increase recovery, WAG experiments were carried out. Experiments were also performed using water whose viscosity was artificially increased using a polymer, so as to improve conformance in the fractured system. Finally, experiments were performed in the presence of a polymer gel, which again was used to improve conformance.

CHAPTER II

EXPERIMENTAL SETUP

The experimental setup can be divided into five main components – the injection system, the coreflood cell, HD 200 X-Ray CT scanner, the production system and the data acquisition system. A brief description of each of the components is given below.

2.1 Injection system

The injection system consists of two sets of one-liter accumulators one each for the oil and water. These accumulators can withstand a maximum pressure of 3000 psi. There is also a two-liter Temco^{TM} accumulator with a maximum pressure rating of 2500 psi. Each of these accumulators is connected to an ISCO 5000 D syringe pump using stainless steel tubing. The syringe pump, with a nominal cylinder capacity of 508 ml, consists of a programmable pump controller with an RS-232 serial interface for computer control or monitoring of operating parameters. The pump can operate at flow rates starting from 0.01 cc/min. The maximum pressure rating for the pump is 3000 psi @ 200 ml/min. Using the programmable controller, the pump can be set to deliver at a constant pressure or at a constant flow rate. Water is injected from the pump under set conditions below the piston in the accumulator. This increases the pressure of the fluid above the piston to the desired level. A Swagelok SS-41XS2 ball valve is used to switch the flow from the pump to either the CO_2 accumulator or the secondary ball valve which divides the flow between the oil and the water accumulator.

2.2 Coreflood cell

The core holder measuring 21 in. long is made up of aluminum and was designed specially for use with the CT scanner. It is capable of holding cores up to 1 ft. in length and 1 in. in diameter. The maximum pressure rating of the coreflood cell is approximately 7000 psi. The cell consists of detachable end pieces with plungers on both ends. One end has a fixed plunger while at the other end, the plunger can be moved by rotating a screw at the end piece, to make sure that the core is in contact with the plungers.

A viton Hassler sleeve surrounds the core and is secured to the plungers. When cores less than 1 ft. in length are used, aluminum spacers with spider grooves are used in the remaining space. The coreflood cell has an inlet for hydraulic oil, which is used to apply overburden pressure. A hydraulic hand pump is used to pressurize the cell by injecting hydraulic oil into the Hassler sleeve – inner wall annulus and pressures up to 7000 psi can be obtained in this manner. Another inlet in the core holder can be used to fix a thermocouple for temperature measurement or another device like a pressure tap. The layout of the core holder is shown in Fig. 2.1 and Fig. 2.2

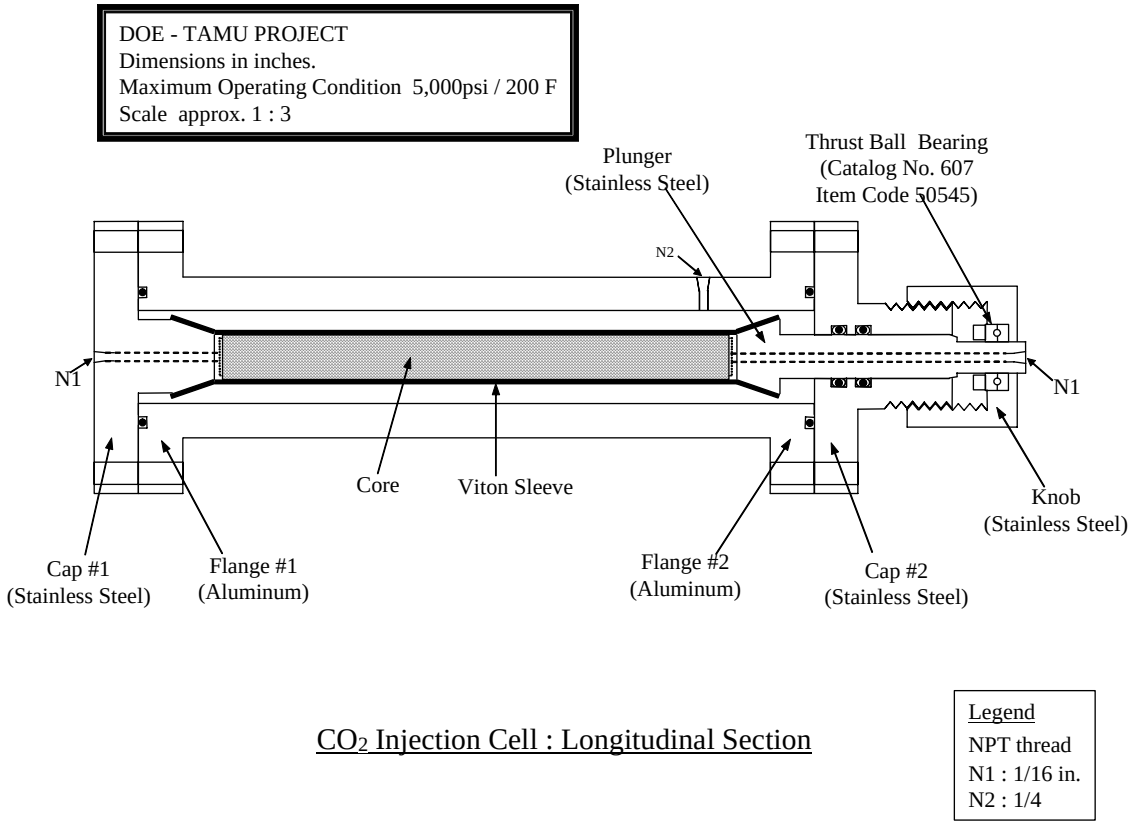

Fig. 2.1 – Design of aluminum core holder used for X-ray CT scanning.

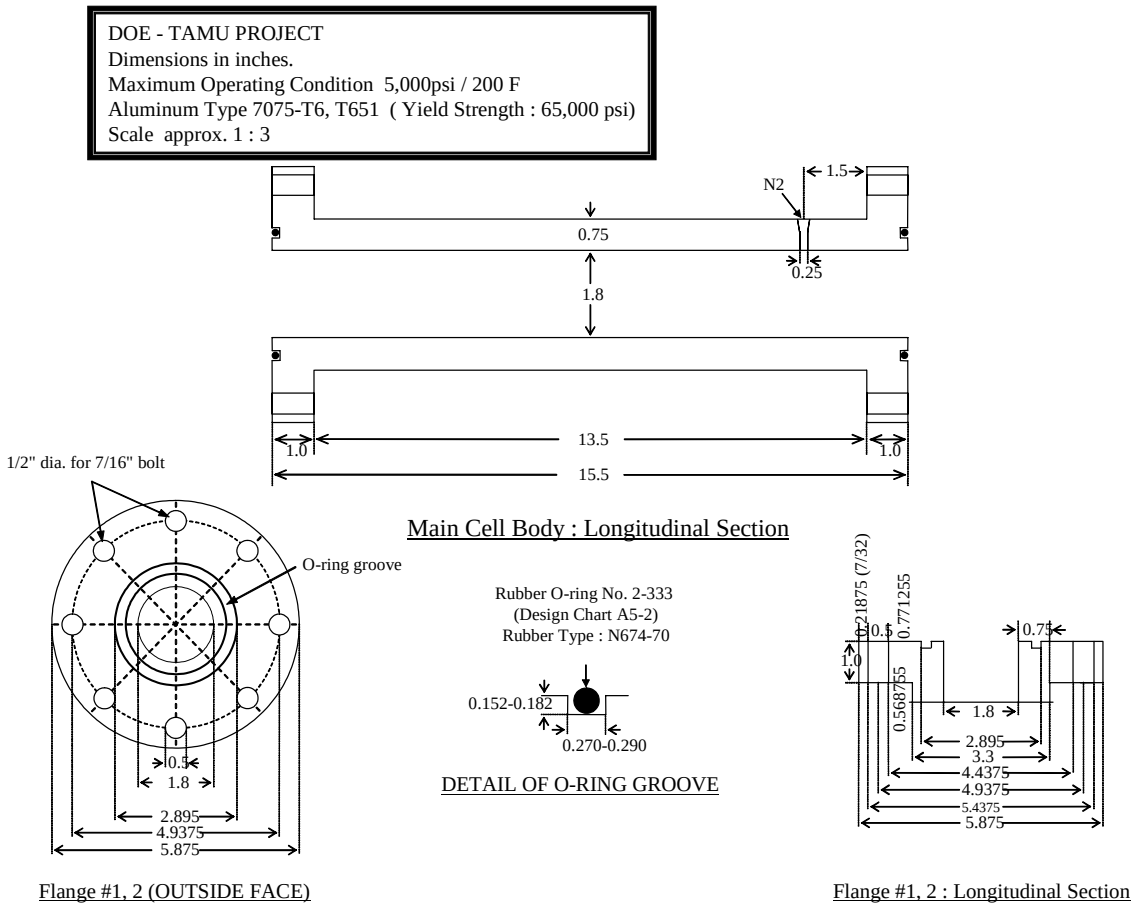

Fig. 2.2 – Cross-sectional view of the core holder.

2.3 X-Ray CT scanner

The X-Ray CT scanner is a fourth generation Universal systems HD 200 system with a resolution of 0.3 mm x 0.3 mm. This scanner can be used to scan a maximum diameter of 48 cm with a maximum scan time of 4 sec per scan. Cross-sectional scans of the core sample are made at regular intervals during the experiment. An image appears on the video screen as a filled in circle, and the image information is in a 512 by 512 matrix. Each pixel represents a CT number that is related to the average absorption coefficient of

a spatial volume within the scanned field. The volume of each pixel varies according to scanned field size and beam thickness selections. The CT numbers are compared to that of water, which is assigned a value of zero. The data obtained from the CT scanner is transferred to the image processing system installed in a Sun workstation. The cross-sectional images can then be used for porosity and saturation determination or reconstructed for flow visualization.

2.4 Production system

The outlet end of the core holder is connected to a Swagelok SS-ORS2 precision needle valve which serves as the back pressure regulator and is used to increase pressure in the system. Connected further down is a Swagelok SS-SS2-VH high precision metering valve with a vernier handle. This valve was required to allow minute adjustments to the fluid flow rate so as to avoid a large pressure drop. The produced fluid is collected in a graduated cylinder and any gas produced is allowed to flow to a gas chromatograph and then measured using a wet test meter.

2.5 Data Acquisition System (DAQ)

Two Omega pressure transducers one each at the inlet and the outlet are used to measure pressure at the two ends. The pressure data is then transferred to an Omega OMB-DAQ-55 data acquisition system. The OMB-DAQ-55 Personal DAQ is a full-featured data acquisition system that utilizes the Universal Serial Bus (USB), which is built into almost every new PC. Designed for high accuracy and resolution, the 22-bit OMB-DAQ-55 data acquisition system directly measures multiple channels of voltage, thermocouple, pulse, frequency, and digital I/O. A single cable to the PC provides high-speed communication and power to the OMB-DAQ-55. No additional batteries or power supplies are required, except when using bus-powered hubs. This DAQ is connected to a Pentium III computer system and the pressures can be observed and acquired real time using the software that is available with the DAQ.

A schematic of the experimental setup is shown in Fig. 2.3.

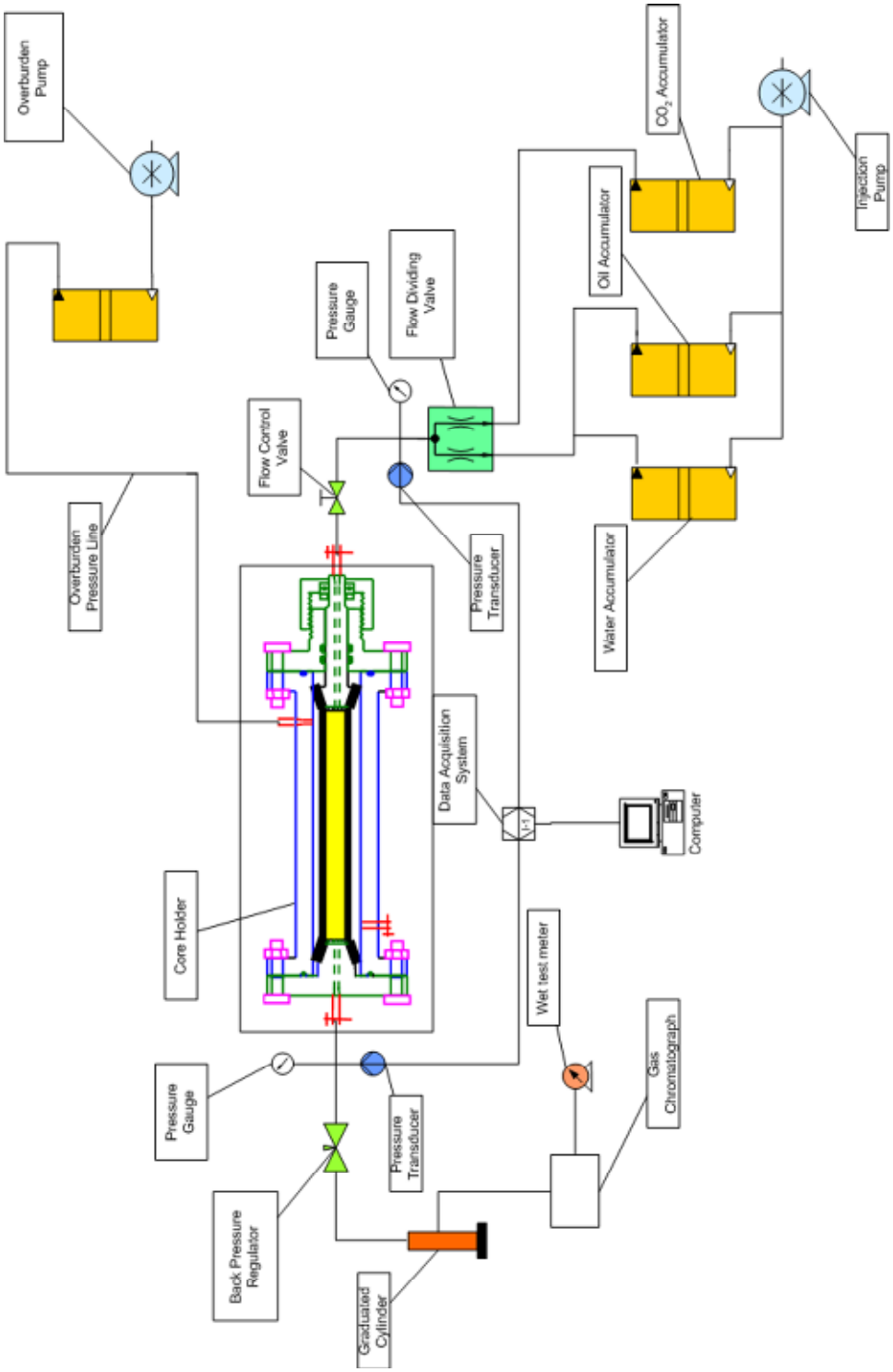

Fig. 2.3. Schematic of the experimental setup.

CHAPTER III

INTRODUCTION TO X-RAY TOMOGRAPHY

3.1 Introduction

X-ray computer tomography (X-ray CT) is a method in the area of non-destructive testing (NDT). It was developed during the seventies for medical purposes and was subsequently introduced for industrial applications in the latter part of the eighties. It is an imaging technique, similar to X-ray radiography, the only difference being the way X-ray radiation penetrates an object. Figs. 3.1 and 3.2 show the basic difference between X-ray radiography and X-ray CT. A CT image generates a slice through the object in a true geometrical manner whereas X-ray radiography image projects a three-dimensional picture into two-dimension. Thus the CT image shows maps of the amount of radiation that is taken away (attenuated) in the form of linear attenuation coefficient, μ, from a beam of X-ray at each point (voxel -3D value) of the object. The value of μ depends on the density and the atomic composition of the matter in which X-ray propagates. In contrast, the X-ray radiographic image pixel values are proportional to the radiation attenuated along the line from the X-ray source to the detector element (film in Fig. 3.1 but a digital detector in Fig. 3.2). Radiography is faster as compared to CT scanning, but it is inferior when it comes to revealing interior details of the imaged object.

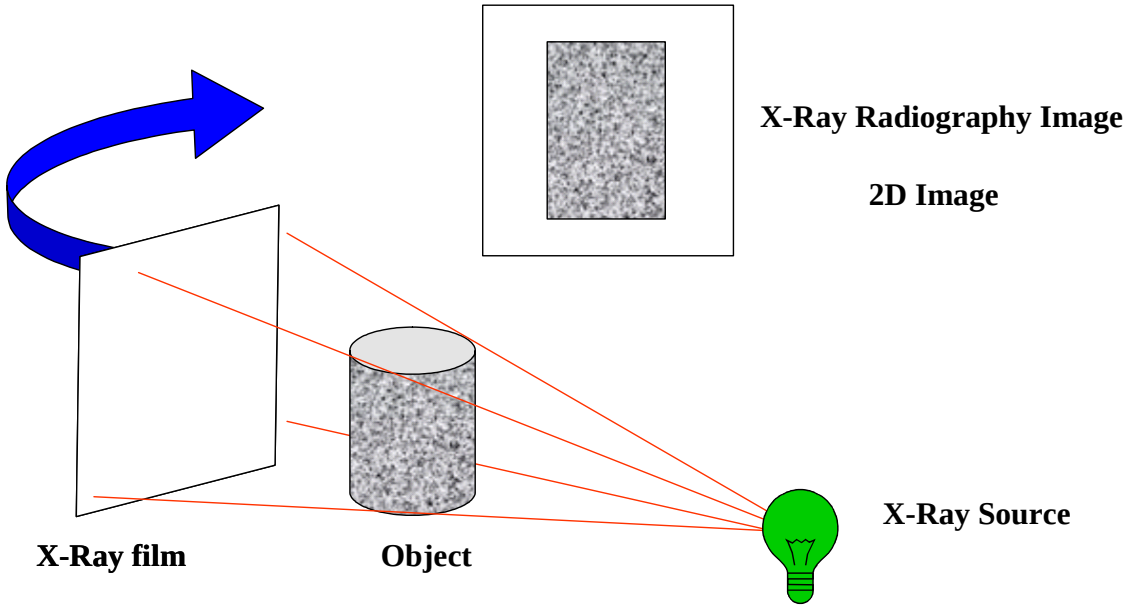

Fig. 3.1 Conceptual representation of X-ray radiography.

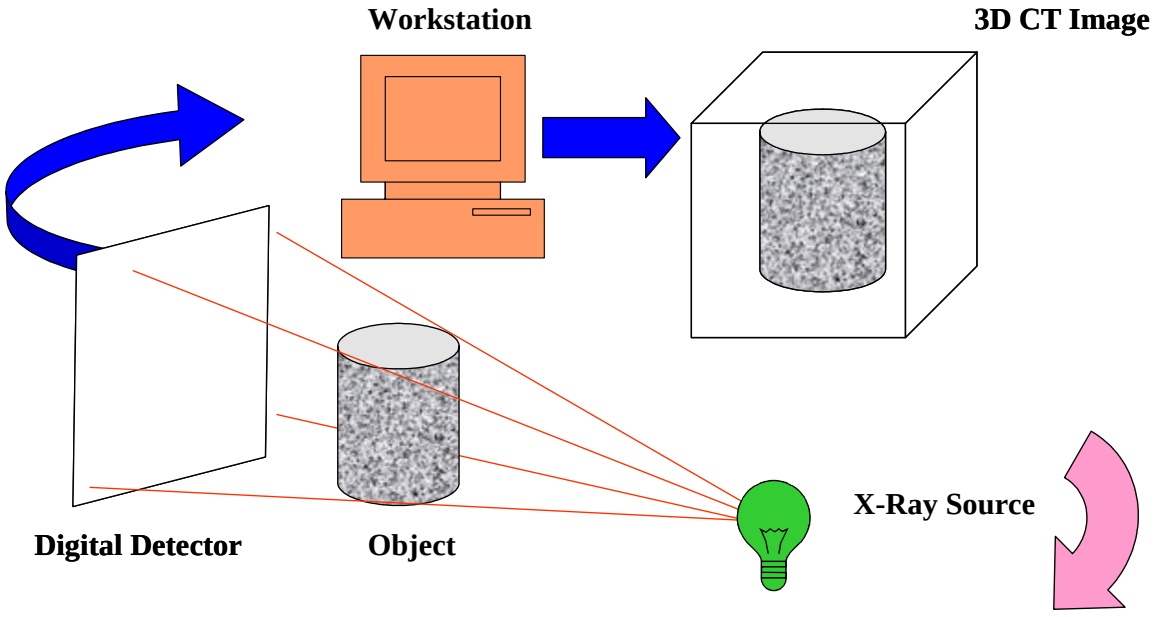

Fig. 3.2 Conceptual representation of X-ray tomography.

In our experiments we obtain CT images of cores and rock objects, which give the projection of internal structures. It sometimes becomes necessary that over-laying grains obscure certain important details, which need study. By using slice-imaging techniques (tomography), we can selectively have a layer by layer structural detail of the given core sample. With computerized tomography, we can see sequence images of thin consecutive slices of the cores or rock object in three dimensions. Unlike conventional, classical tomography, computerized tomography does not suffer from interference from structures in the object outside the slice being imaged. This is done by irradiating only thin slices of the object with a fan-shaped beam. Also, the CT images (tomograms) of the object's structure can give more selective information within the object than conventional planar projection radiographs. Compared to planar radiography, CT images have superior contrast resolution, i.e., they are capable of distinguishing very small differences in attenuation (contrasts), but have inferior spatial resolution. The maximum spatial resolution of X-ray scan is 0.5 mm, which implies that the smallest details in the image that can be resolved, must be separated at least 0.5 mm. This drawback in X-ray CT has lead to the refinement in X-ray microtomography. In X-ray microtomography, a spatial resolution of 2 micron (2 thousandths of a millimeter) and below can be achieved.

X-ray CT scanners used nowadays are either third- generation or fourth-generation. Fig. 3.3(a) shows a third-generation CT scanner. The X-ray tube and the receptor array are located on opposite sides of the object and both rotate around the object during data acquisition. Fig. 3.3(b) is a fourth-generation CT scanner. Here, only the X-ray tube rotates around the object; the receptor array, which is situated in the outside of the scanning frame, remains stationary. The receptors are made from solid-state material and can be as many as 4000. CT scanners are also available in which the X-ray tube circles the object while the table moves continuously, so that the X-ray tube moves in a spiral orbit around the object. These are called spiral CT scanners. Department of Petroleum Engineering, Texas A&M University, now has a fourth generation spiral CT scanner.

3.2 Principles of operation

In order to generate a CT image two steps are necessary. Firstly we should have physical measurements of the attenuation of X-rays along the core in different directions, and secondly we have to make mathematical calculations of the linear attenuation coefficients, μ, all over the slice.

A fan-shaped beam, wide enough to pass on both sides of the core or rock object, is used. The image receptor is an array of several hundred small separate receptors. Readings from the receptors are fed into a computer, which after numerous calculations produces a tomogram of the object, i.e., a map of linear attenuation coefficients, μ. The data acquisition time is a few seconds and a 512 pixel x 512 pixel image matrix. Typically medical CT scanners today use a fan-beam, ones which are having about 700 receptors (3rd generation) or 4000 receptors (4th generation), complete data acquisition in approximately 1-2 seconds and a few seconds to reconstruct the 512x512 image matrix with 12 or 16 bits depth.

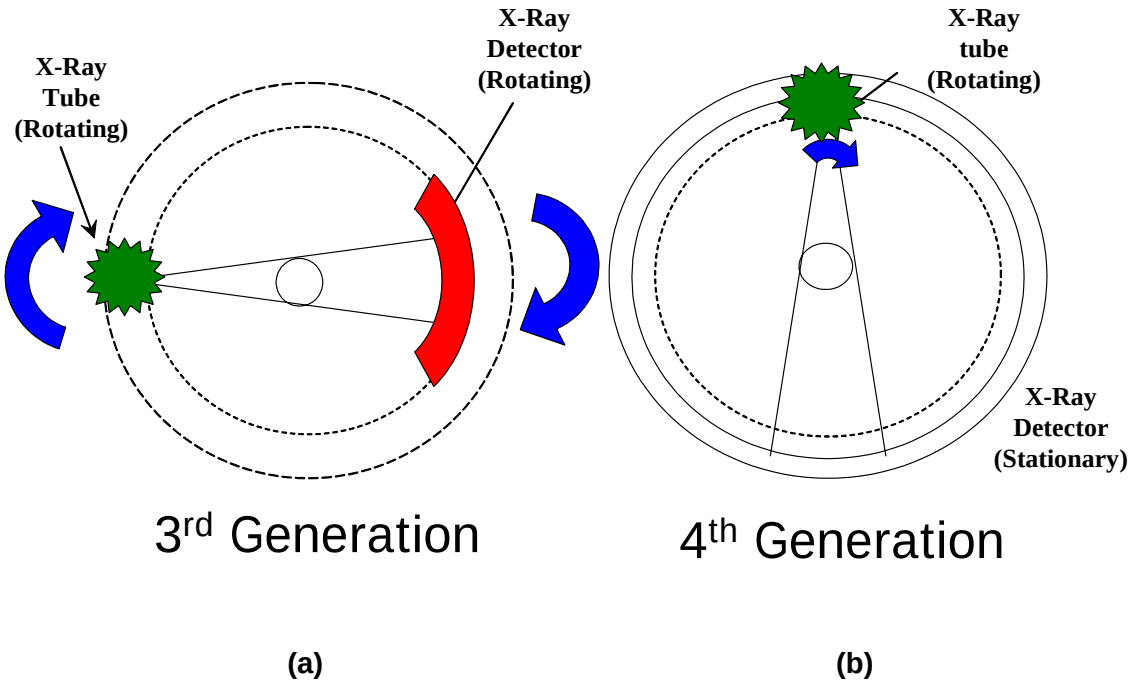

Fig. 3.3 Conceptual representation of 3rd generation and 4th generation X-ray CT scanner.

X-ray CT is one of the forms of digital radiology. When X-rays interact with matter, there are three primary interaction modes: photoelectric, Compton and coherent. When the photoelectric effect occurs, a photon from the incident beam disappears, and an electron is ejected from the inner shell of an atom. As shown in Fig. 3.4(a) an incident photon loses all its energy on entering an atom, being absorbed in the process. The atom responds, by ejecting an inner shell electron, which becomes a photoelectron (Fig. 3.4(b)). The atom reaches an excited state and an electron from a higher energy level fills the vacancy and emits a characteristic X-ray photon Fig. 3.4(c).

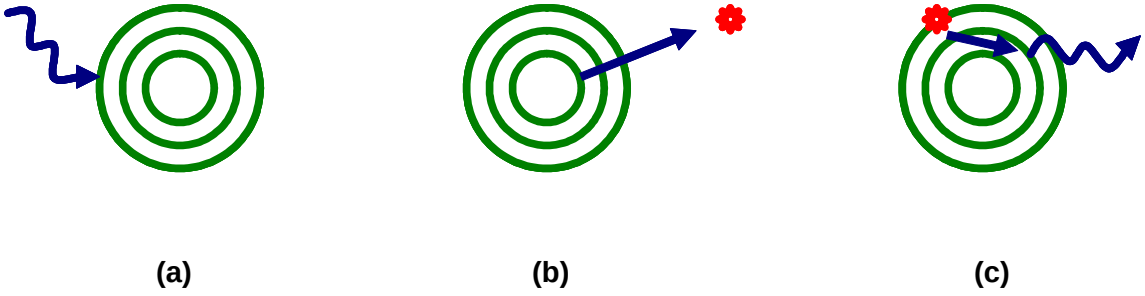

Fig. 3.4 Photoelectric effect.

In Compton scattering, Fig. 3.5, a photon from the incident beam collides with an electron, loses some of its energy and is deflected from its original direction.

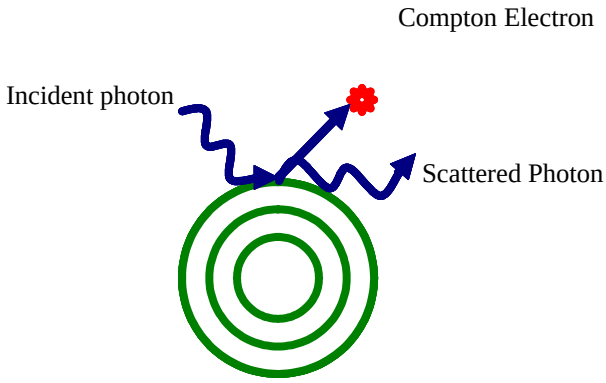

Fig. 3.5 Compton effect.

In coherent (or Rayleigh) scattering, Fig. 3.6, an incident photon is scattered by bound atomic electrons without losing energy and the atom is neither ionized nor excited. Thus, when a narrow beam of monoenergetic photons passes through a medium of thickness *x*, the beam will be attenuated and scattered because of the three above cited effects. The receptors measure the X-rays passing through a slice of the object in different positions. This forms one projection of the object. Its reading gives us a measure of the attenuation in the object along the path of a particular ray.

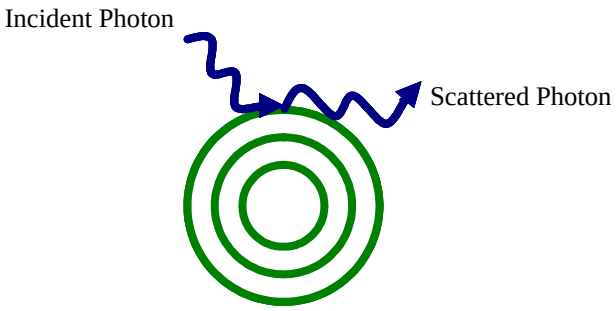

Fig. 3.6 Rayleigh scattering.

For a homogeneous object, the receptor reading, as stated by *Huang* [1987], is given by:

$$I = I_0 e^{-\mu x} \quad \text{.....(1)}$$

where,

I_0 is the receptor reading without the object,

μ the linear attenuation coefficient for the object,

x is the object thickness along the path of that ray, and

e the base of the natural logarithm (e = 2.718).

For an inhomogeneous object such as a core or a rock, the product μx is a sum over all the different grains/crystal types, i, $\Sigma\mu_i x_i$. After the readings from one of the receptors have been stored in the computer, the tube is rotated to another angle and a new projection profile measured. This procedure, called reconstruction, is applied to data from sets of projection profiles through all volume elements (voxels) and for all rotation angles (projections), in a slice of the object. An average linear attenuation coefficient, μ, for each voxel is calculated. Each value of μ is assigned a grey scale value on the display-monitor and is presented in a square picture element (pixel) of the image.

3.3 Reconstruction algorithms

The computer reconstructs an image, a matrix of μ-values for all voxels in a slice perpendicular to the rotation axis. The procedure to reconstruct the image is made with the help of reconstruction algorithm. The objective of this algorithm is to find the μ-values in each voxel based on all the measured data in the projection profiles. A filtering procedure helps in removing the smearing-out of the detail.

3.4 Display of CT numbers, N_{CT}

In the digital display computer monitor, the measured μ - values is distributed over a grey scale with the lowest values of μ black and the highest white. A CT number, N_{CT} , is defined as:

$$N_{CT} = \mu \frac{\mu - \mu_w}{\mu_w} \qquad \text{.....(2)}$$

where,

μ is the average linear attenuation coefficient for the material in a given voxel

μ_w that for water, and

N_{CT} is given in the dimensionless unit, *Hounsfield number*

The CT number scale has two fixed values independent of photon energy. For vacuum, air or body gas,

$$N_{CT} = -1000$$

and for water,

$$N_{CT} = 0.$$

The common method used for calculating porosity from CT images is:

$$\phi = \frac{N_{CT100\%Sat} - N_{CTDry}}{N_{CTWater} - N_{CTAir}} \quad \text{.....(3)}$$

For water displacing air in the core, then saturation is given by:

$$S_w = \frac{N_{CTMat} - N_{CTDry}}{N_{CT100\%Sat} - N_{CTDry}} \quad \text{.....(4)}$$

For oil-water phase, the saturation is calculated with the help of the following relation:

$$S_w = \frac{N_{CTMat} - N_{CT100\%Sat}}{\phi\left(N_{CTOil} - N_{CTWater}\right)} \quad \text{.....(5)}$$

where, $N_{CT100\%Sat}$ is the CT number of 100% saturated voxel,

N_{CTDry} is the CT number of dry voxel,

$N_{CTWater}$ is the CT number of Water = 0.0,

N_{CTAir} is the number of Air = -1000.0,

N_{CTMat} is the CT number of the matrix,

N_{CTOil} is the CT number of Oil.

3.5 Image display

In order to give contrast to the object, we give a narrow interval of the CT numbers, called the window, to the entire grey scale on the display-monitor. The entire range of CT numbers is displayed on this grey scale, called the 'window width' and the average attenuation value is the 'window level'. Changes in window width, as shown in Fig. 3.7 alter the contrast and changes in window level help in selecting the structures in the image, displayed on the grey scale. As the window width is made narrower, the structure is assisted with higher contrast. Structures that are on the lower and higher sides of the window width (low and high CT numbers) are either completely black or white. As the window width is made even narrower, the contrast of the structures displayed increases. Combinations of these techniques enable small differences in attenuations at various points in the object and its composition to be visualized.

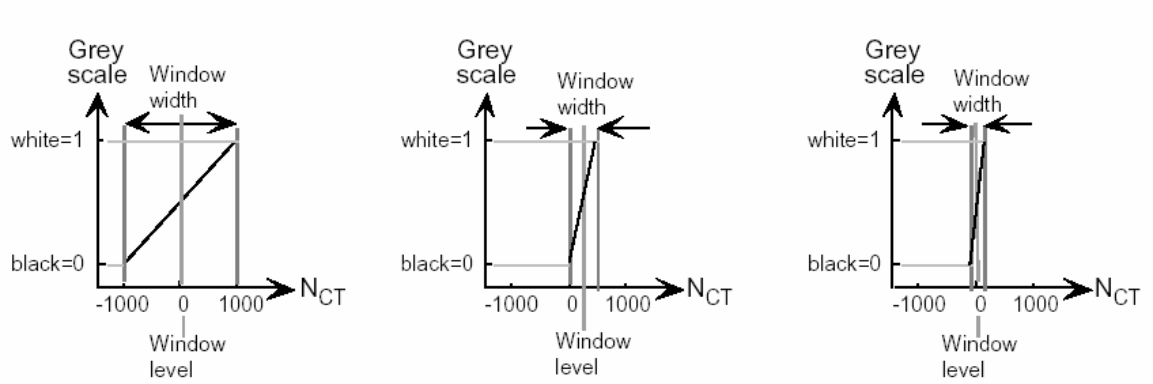

Fig. 3.7 Effect of window width and window level after *Huang*

3.6 Artifacts

Computerized tomography is based on physical measurements followed by mathematical computations. These computations are based on idealized assumptions that do not entirely correspond to physical reality. This creates artifacts or errors in the measurement and reconstruction of the μ - values. Artifacts in the image are patterns that do not correspond to the object's structure. Beam hardening artifacts, as for example, are

found when a spectrum of photon energies is used and is the most common form of artifact.

3.7 Porosity determination

Porosity distribution in the core is determined using CT-analysis method using simple correlations presented by *Qadeer*[22] [1988]. Each CT image is in the matrix form, in which each element, a voxel, represents a volume of 0.5 x 0.5 x 2.0 mm^3. As previously defined in eqn. 2, CT numbers are taken along the entire cross-section of the core. For a dry unfractured core, for average CT numbers, we have the following relation:

$$N_{CTdry} = (1-\phi)N_{CTmatrix} + \phi N_{CTAir} \quad \text{.....(6)}$$

The dry core is then flooded with brine. The resulting CT image can be represented by the following relationship:

$$N_{CT100\%Brine} = (1-\phi)N_{CTmatrix} + \phi N_{CTBrine} \quad \text{.....(7)}$$

Subtracting eqn. (6) from eqn. (5), we have:

$$N_{CT100\%Brine} - N_{CTdry} = \phi(N_{CTBrine} - N_{CTAir}) \quad \text{.....(8)}$$

Rearranging, we derive the relation to determine the porosity of the core as:

$$\phi = \frac{N_{CT100\%Brine} - N_{CTDry}}{N_{CTBrine} - N_{CTAir}} \quad \text{.....(9)}$$

3.8 Saturation determination

We apply the same concept in determining the saturation of the core. If there is a mixture of two fluids in the core which is scanned, then:

$$N_{CTmixture} = (1-\phi)N_{CTmatrix} + \phi S_{FluidA} N_{CTFluidA} + \phi(1-S_{FluidA})N_{CTFluidB} \quad \text{……} \quad (10)$$

Rearranging,

$$N_{CTmixture} = (1-\phi)N_{CTmatrix} + \phi S_{FluidA}(N_{CTFluidA} - N_{CTFluidB}) + \phi N_{CTFluidB} \quad \ldots\ldots \quad (11)$$

Subtracting eqn. 18 from eqn. 23, we have:

$$N_{CTdry} - N_{CTmixture} = \phi N_{CTAir} - \phi S_{FluidA}(N_{CTFluidA} - N_{CTFluidB}) - \phi N_{CTFluidB} \quad \ldots\ldots \quad (12)$$

Rearranging,

$$S_{FliudA} = \frac{N_{CTdry} - N_{CTmixture} + \phi(N_{CTFluidB} - N_{CTAir})}{\phi(N_{CTFluidA} - N_{CTFluidB})} \quad \ldots\ldots\ldots\ldots\ldots\ldots\ldots\ldots\ldots\ldots\ldots\ldots (13)$$

From eqn. 21, for fluid B we have:

$$\phi = \frac{N_{CTMat} - N_{CTDry}}{N_{CTFluidB} - N_{CTAir}} \quad \ldots\ldots\ldots\ldots\ldots\ldots\ldots\ldots\ldots\ldots\ldots\ldots\ldots\ldots\ldots\ldots\ldots\ldots\ldots\ldots\ldots\ldots (14)$$

Substituting this in eqn. 13, we have eqn. 5 as given previously.

CHAPTER IV

EXPERIMENTAL CONDITIONS AND PROCEDURE

4.1 Background

The experimental conditions and parameters were decided largely based on whether the displacements would be miscible or immiscible. In order to better understand the rationale behind our experimental conditions, a basic knowledge of the mechanisms by which CO_2 displaces a fluid is required. CO_2 can displace oil from reservoirs by various mechanisms. These mechanisms include solution gas drive, immiscible CO_2 drive, hydrocarbon vaporization, direct miscible drive and multiple contact miscible drive[23]. The recovery of oil by CO_2 flooding is increased due to the following reasons:

1. Reduction in viscosity of oil.
2. Swelling of oil.
3. Increase in the oil density.
4. Vaporization and extraction of portions of crude oil.

CO_2 has a critical temperature of 89º F and a critical pressure of 1070 psia (Fig. 4.1). The extraction of hydrocarbons from oil takes place only above a particular pressure called the Minimum Miscibility Pressure (MMP). The extraction can be one due to single contact miscibility which occurs at relatively high pressures and is usually not seen in most reservoirs or due to multiple contact miscibility where CO_2 extracts the lighter components from the oil by multiple contacts between the oil rich CO_2 phase and the crude oil. The MMP is dependent on a number of factors among which are, the temperature of the oil in the system and the oil composition. As the temperature increases, the density of CO_2 decreases and hence the pressure required for hydrocarbon extraction increases. Also, this pressure increases with the amount of heavier ends present in the oil. There are several correlations available for the determination of MMP. These correlations take into consideration the temperature and the amount of asphaltenes present in the oil.

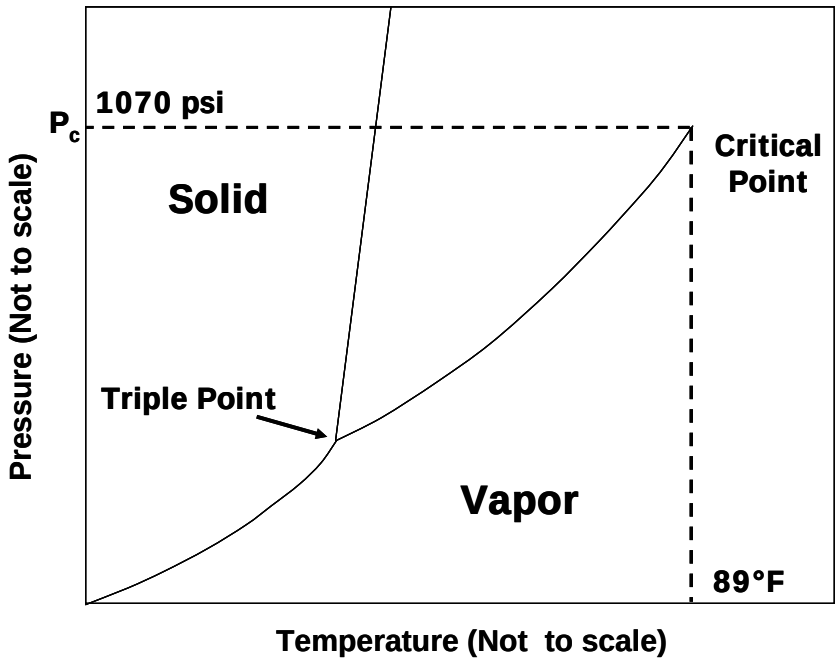

Fig .4.1 – Phase diagram of CO_2.

The objective of our experiments is to first investigate immiscible displacement of oil by CO_2 and extend this to fractures, before proceeding to miscible displacements. Holm and Josendal[23] report that for miscible displacement to take place, the density of CO_2 should be at least 0.25 to 0.35 gm/cc. There are various reservoir pressure-temperature combinations that yield these densities. In order to have immiscible displacement, the density of CO_2 must be less than this range. Fig. 4.2 shows the density of CO_2 for different pressures and temperatures. One important point to be noted is the abrupt shift in densities that occur at pressures below the critical temperature. But the density turns out to be a continuous function of pressure at temperatures above the critical temperature. For our immiscible displacements we decided to maintain the density of CO_2 around 0.l5 gm/cc. This density can be achieved at a temperature of 70º F and a pressure of 800 psia. At this temperature and pressure, the major mechanisms of oil recovery are swelling of oil, reduction in viscosity and an internal solution gas drive[24].

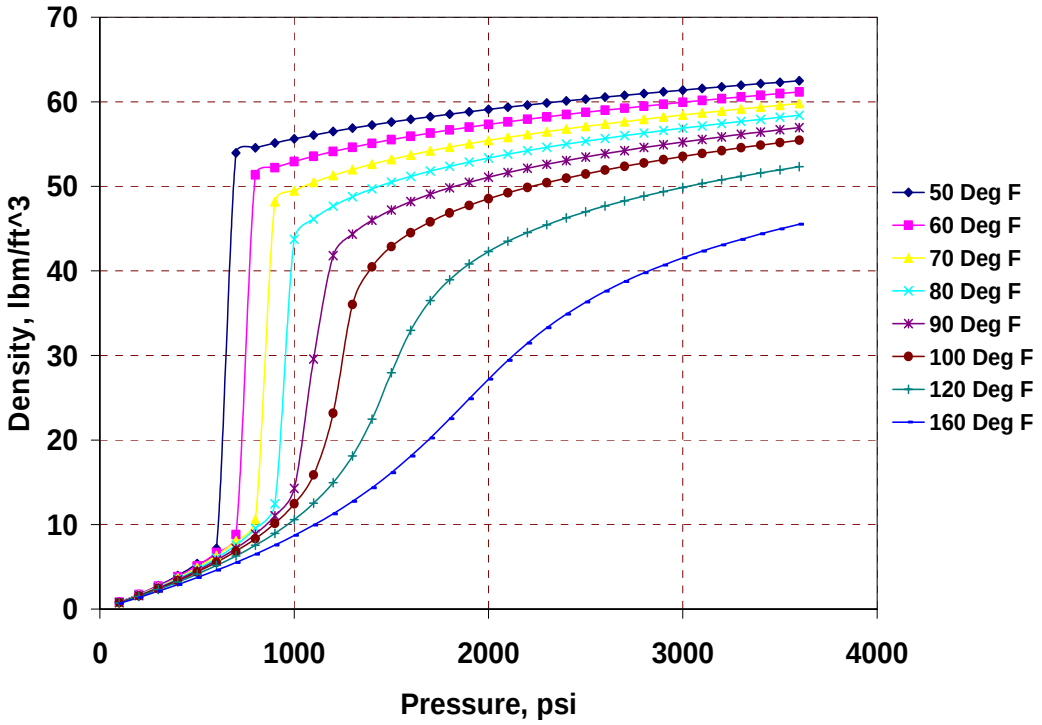

Fig. 4.2 - Density of CO_2 shows abrupt changes at pressures below critical temperature.

4.2 Experimental parameters

Berea core was used for all the experiments. The cores were cut from a single block of Berea sandstone and have similar properties and dimensions with slight variations. The porosity of the cores determined from CT measurements revealed that the porosity varied from 19 to 23%. The properties of the core used are given in Table 4.1. The oil used for the experiments is a mixture of Soltrol 130^{TM} and 1-iodohexadecane. 1-iodohexadecane was used as the doping phase. The purpose of using this fluid is to artificially increase the CT number of the refined oil so as to obtain a clear contrast between the different phases during the course of the experiment. 1-iodohexadecane was chosen for the purpose due to its similar structure to the refined oil used. Previous measurements have shown that the iodohexadecane serves only as the doping phase and does not alter the interfacial tension between the fluids. The only problem associated with this doping phase is that it is sensitive to light and the attenuation properties decrease with constant exposure to bright light. This problem can be eliminated by using bromodecane, although the attenuation

coefficient for bromodecane is not as high as iodohexadecane. As mentioned earlier, the pressure and temperature for the experiments were maintained at 800 psi and 25º C for all experiments. These parameters were important to ensure that the displacements were immiscible and also obtain a clear contrast between the fluids in the CT scans. A plot of density versus pressure at the experimental conditions is shown in Fig. 4.3.

Table 4.1 – Berea core properties.

Berea Core Properties	
Length	13 cm
Diameter	2.5146 cm
Area	4.963 cm^2
Porosity	19 - 23 %
Permeability	200 md

In the experiments, cores were fully saturated with oil and no connate water saturation was considered. The displacing phase was CO_2 and this was used as a secondary recovery agent. Fluids were injected into cores at constant rates or at rates that were varied to maintain constant pressure. Produced fluids were collected in graduated cylinders. The displacement processes were studied during the experiment where the injection rates, production volumes and pressure drops were measured. Fluid saturation distributions were also indirectly measured using X-Ray CT. The overall efficiency of the process was analyzed by combining the CT measurements and the external effluent volume measurements.

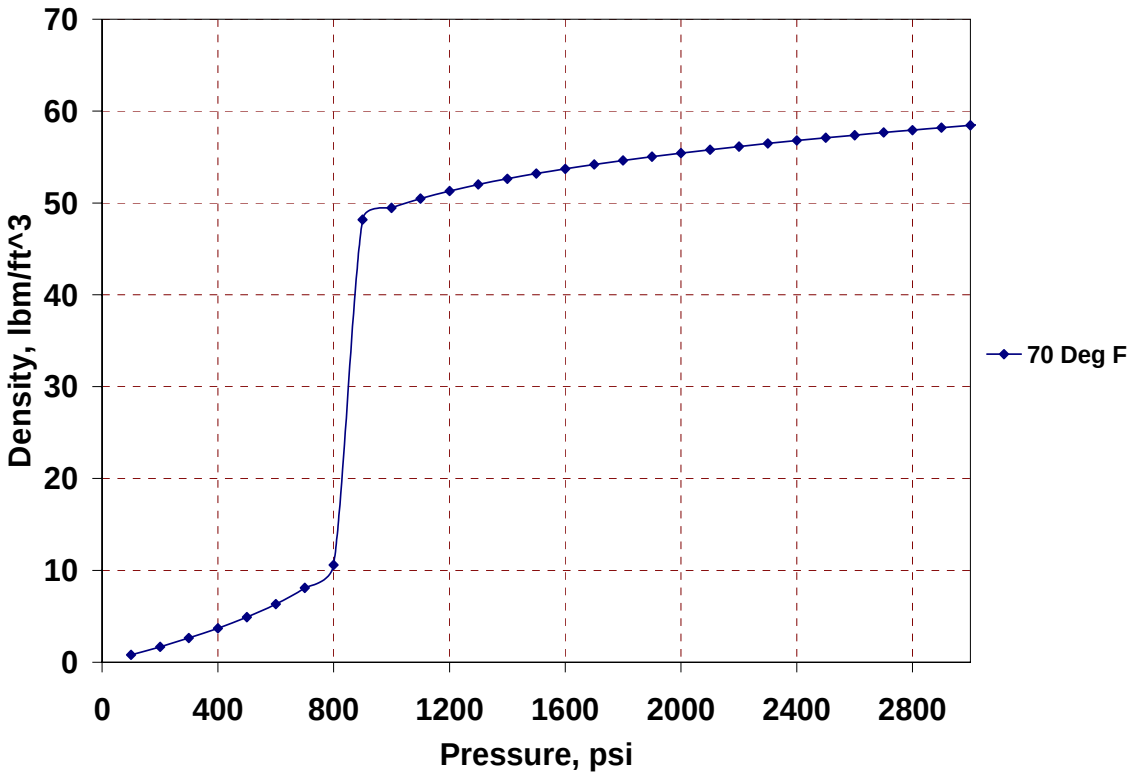

Fig. 4.3 – Density of CO_2 at experimental conditions.

4.3 Experimental procedure

A general outline of the experimental procedure is given below:

1. The core is first heated at about 150º F for a sufficient period of time to remove all residual water saturation.
2. The entire core is then evacuated using a vacuum pump
3. The evacuated dry core is scanned at a confining pressure of about 1000 psi.
4. For a fractured core experiment, the above steps are repeated after fracturing the core.
5. The core is flooded with CO_2 at the desired temperature and pressure to obtain the scans at 100% CO_2 saturation.
6. The core is then evacuated again in the vacuum chamber.
7. The evacuated core is saturated with doped oil in the vacuum chamber for a period of 48 hours.

8. The oil saturated core is transferred to the aluminum core holder and about 15 pore volumes of oil are injected to ensure complete saturation.
9. The backpressure regulator at the outlet is fully closed and the pressure in the core holder is allowed to build up. Care is taken that the overburden pressure is always at least 300 psi higher than the pressure inside the sleeve.
10. Once the desired pressure is reached, oil injection is stopped.
11. The oil saturated core is now scanned again.
12. The pressure in the CO_2 accumulator is increased to be about 50 psi higher than the pressure in the coreflood cell to prevent back flow of oil.
13. CO_2 is now allowed to enter the coreflood cell and any excess pressure above the desired pressure is released using a valve available for this purpose.
14. Injection is then started at the desired rate.
15. The core is scanned at various times to visualize fluid flow and determine saturations at various times.
16. For a WAG experiment, doped/viscosified water is injected when desired and the core is scanned during the injection process.
17. For the experiment with the cross-linker, the gel is injected into the fracture prior to CO_2 injection.

In general, CO_2 experiments make use of a gas chromatograph to analyze the produced CO_2 after breakthrough. This is because the CO_2 produced would carry trace amounts of light hydrocarbons, which is a sign of miscible displacement by a vaporizing drive. But since our experiments were of the immiscible type and the refined oil is made up of much fewer components compared to actual crude oil, a gas chromatograph was not used in the process.

4.4 Cross-sectional scans

During the scanning process, scans were taken at different locations along the length of the core. The scan spacing was usually 3mm, but for certain experiments where greater resolution was required, the scans were spaced at 1mm. For the fractured cores, the fracture was oriented vertically and scanned at different locations. Pressure was applied

radially along the length of the core, which corresponds to the overburden. A schematic of the cross-sectional scans is provided in Fig. 4.4.

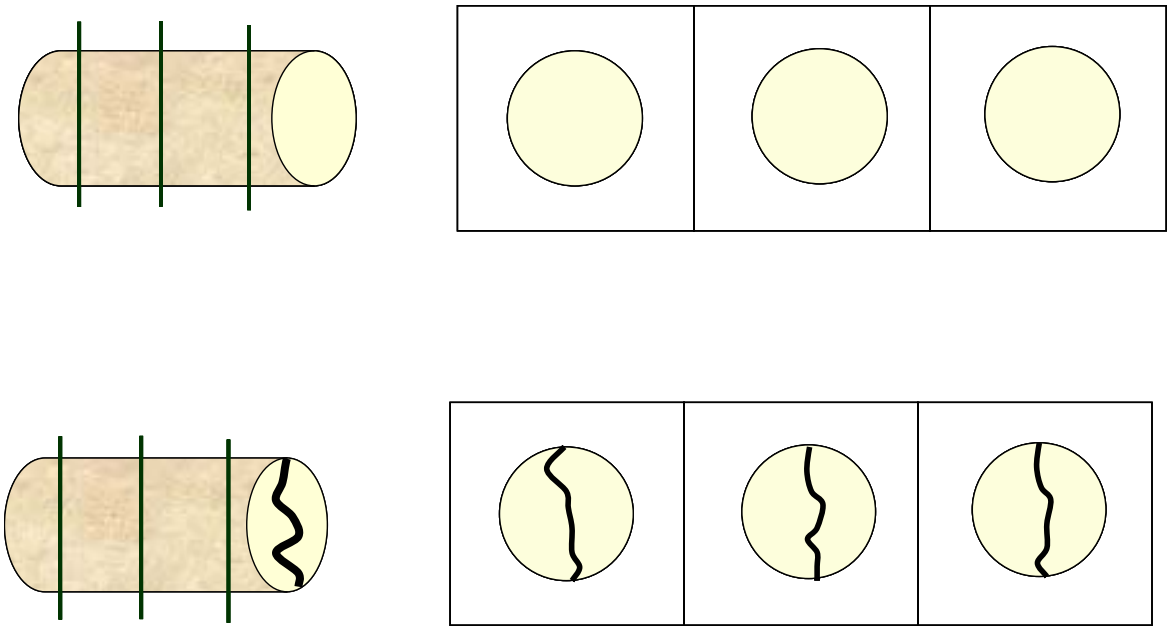

Fig. 4.4 – Schematic of cross-sectional scans.

CHAPTER V

EXPERIMENTAL RESULTS AND DISCUSSION

Several experiments were performed to analyze the displacement of oil by CO_2 in homogeneous (unfractured) and heterogeneous (fractured) media. These experiments can be classified into three major categories:

1. Continuous CO_2 injection in unfractured and fractured cores.
2. Analyzing WAG performance in a fractured system.
3. Use of polymer gel for conformance in a fractured system.

A detailed discussion of each of the above experiments is given below.

5.1 Experiments using unfractured cores

One of the important factors to consider when designing a CO_2 flood is the reservoir heterogeneity. In an unfractured reservoir, this heterogeneity may be in the form of differences in porosity and permeability in the reservoir. In the case of a carbonate reservoir, it is not very uncommon to encounter secondary porosity in the form of vugs. As with all flooding processes, highly variable permeability adversely affects the process. In the presence of high permeability streaks, CO_2 tends to flow through those zones and form a preferential path. As time progresses, the saturation of CO_2 increases in these preferential paths and flow tends to occur only through these paths and hence a considerable amount of oil is bypassed. These unfavorable mobility ratios thus often lead to viscous fingering. In general, it can be said that the CO_2 flooding process is most applicable to reservoirs with a low vertical permeability. CO_2 has low viscosity and high mobility and tends to form a gravity tongue at the top of the zone. Hence, thin permeable zones are considered the best for a good CO_2 flood. Another important factor when considering a CO_2 flood is the injection rate. The two objectives when performing a CO_2 flood are to increase the oil recovery by acting as a secondary or tertiary recovery agent and to maintain reservoir pressure. The second objective requires that a large amount of CO_2 be injected into the reservoir in a short time. But this might be detrimental for the economics of the project because the amount of CO_2 injected has a direct relation to the breakthrough time. The higher the amount of CO_2 injected, the faster is the breakthrough

of CO_2. But a low injection rate may not be favorable in terms of the time taken for oil recovery. The importance of these factors can be understood better from the results of the experiments.

Two experiments were performed using unfractured cores: a high injection rate case where CO_2 was injected at about 1 cc/min and a low injection rate case where CO_2 was injected at 0.03 cc/min. The goal of these two experiments was to investigate bypassing mechanisms at the two injection rates and also observe the difference in sweep in the two cases.

5.1.1 High injection rate

Fig. 5.1 represents the dry core scans with the first scan being the injector end and the last scan being the producer end. In these scans the bright blue color represents regions of high density whereas the dark blue represents regions of low density.

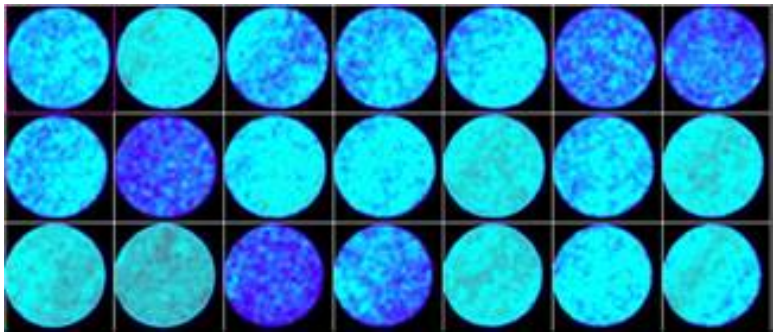

Fig. 5.1 - Dry core scans.

The differences in density contribute to the heterogeneity of the core. The differences in color are essentially due to the differences in CT number which is directly proportional to the density. When the core is saturated with oil, the void spaces in the core material are now replaced by the doped oil and hence the CT number of the oil saturated core is higher than the dry core. Fig. 5.2 represents the scans taken when the core is 100% oil saturated. Here, the red color represents regions of higher CT numbers and this increase is seen to be in agreement with the dry core scans with the dry core scans. Once CO_2 injection is started, invasion of CO_2 into the core can be identified by the blue spot that is seen at the center, as shown in Fig. 5.3. It can be observed that the CO_2 invasion decreases as we proceed from the injector towards the producer end of the core. It can also be seen that there is a small green smudge at the producer end of the core which indicates that CO_2 has already broken through. Subsequent images as shown in Fig. 5.4 to Fig. 5.7 show an increase in CO_2 saturation inside the core. The last set of scans as shown in Fig. 5.7 show a uniform blue color throughout the cross-section indicating that the core is now almost fully saturated with CO_2. At this point, the produced fluid was only CO_2 and about 95% of the oil had been recovered. However, more than 5 PV of CO_2 had to be injected to obtain this recovery. Almost complete saturation of CO_2 was also confirmed by comparing the CT numbers with a core that was previously fully saturated with CO_2 in the absence of any other fluid.

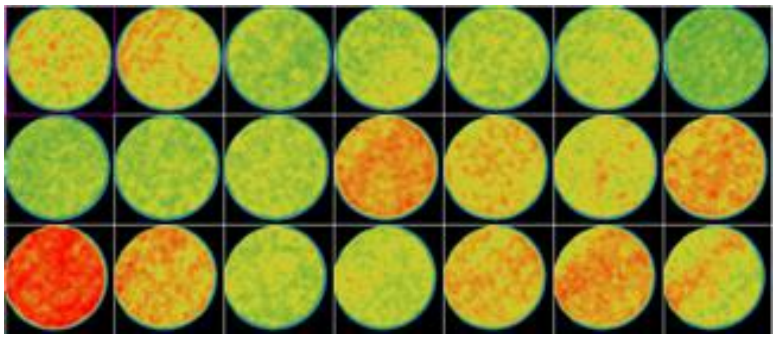

Fig. 5.2 – Oil saturated core scans.

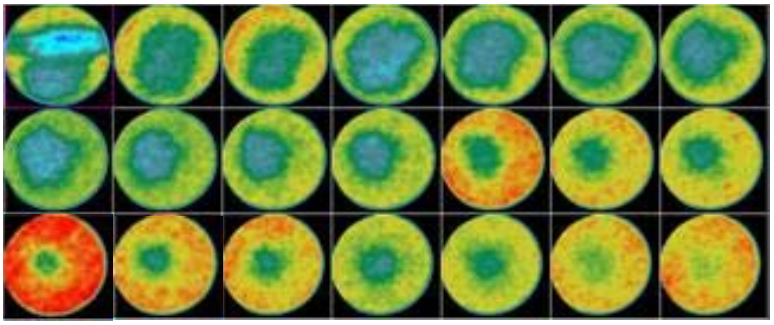

Fig. 5.3 – Scans taken at 0.3 PV of CO_2 injection.

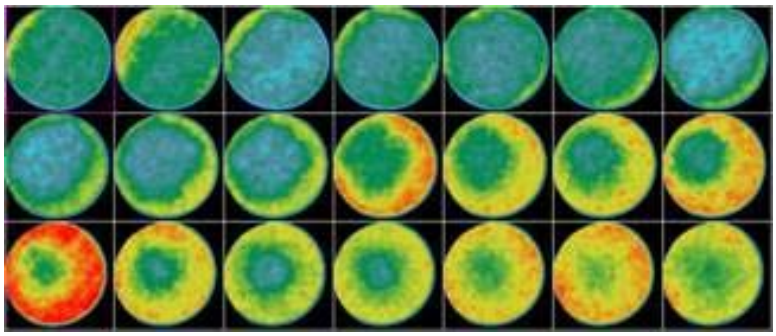

Fig. 5.4 – Scans taken at 0.5 PV of CO_2 injection.

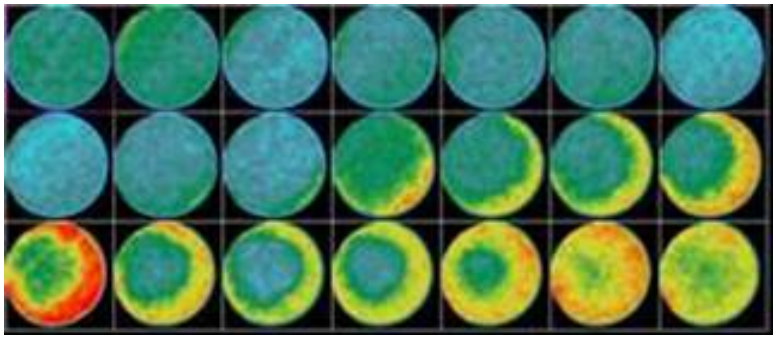

Fig. 5.5 – Scans taken at 1.5 PV of CO_2 injection.

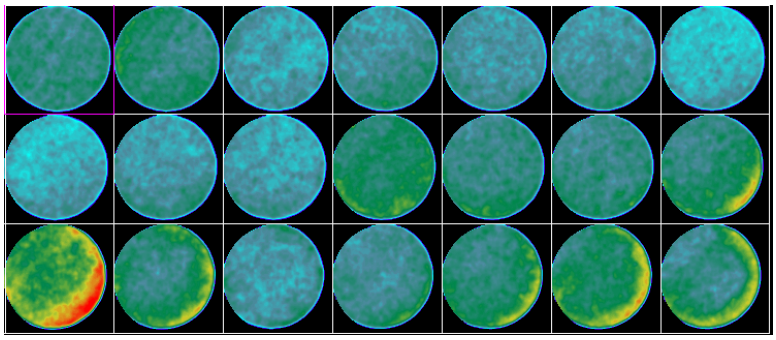

Fig. 5.6 – Scans taken at 3 PV of CO_2 injection.

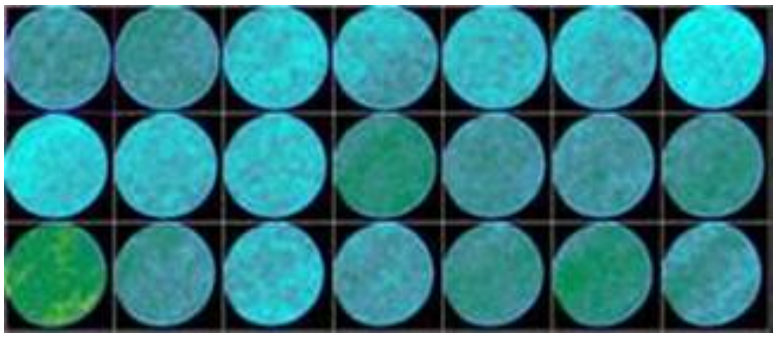

Fig. 5.7 – Scans taken at 5.4 PV of CO_2 injection.

Fig. 5.8 depicts the difference in the CT numbers between the dry core, oil saturated core and after CO_2 invades the core. It is seen that CO_2 can be identified by a decrease in the CT number in the invaded region. A better understanding of the fluid flow inside the core can be achieved by looking at the ortho-reconstructions of the cross-sectional images. Fig. 5.9 shows the reconstructions, where it can be seen that when the injection is first started, The injected CO_2 enters the core sweeping most of the oil near the injection port (left) but tends to flow through the center of the core near the producing port (right), hence bypassing a considerable amount of oil. Continuous injection of CO_2 for a sufficient amount of time allowed CO_2 to contact all regions of the core and squeezed the oil out of those regions. This type of flow commonly occurs in homogeneous cores.

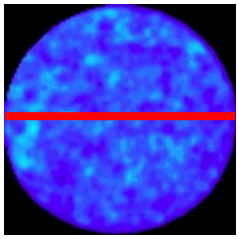

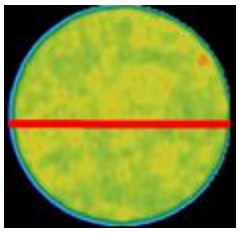

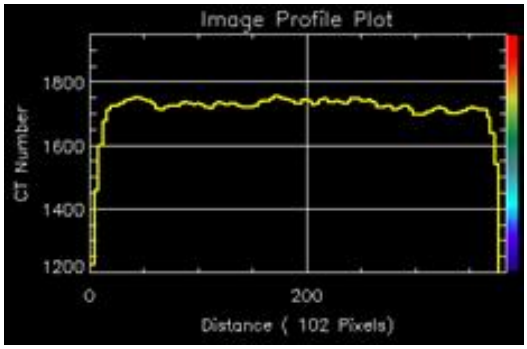

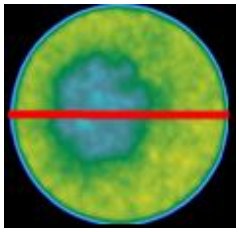

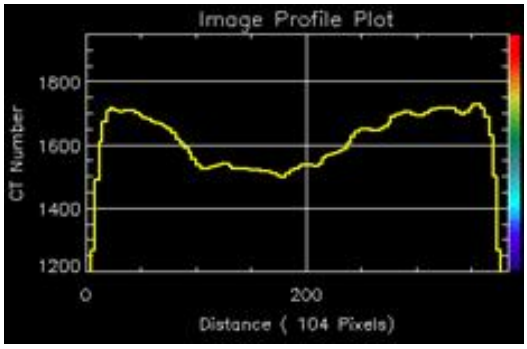

Fig. 5.8 – Comparison of CT number plot at different stages during the experiment.

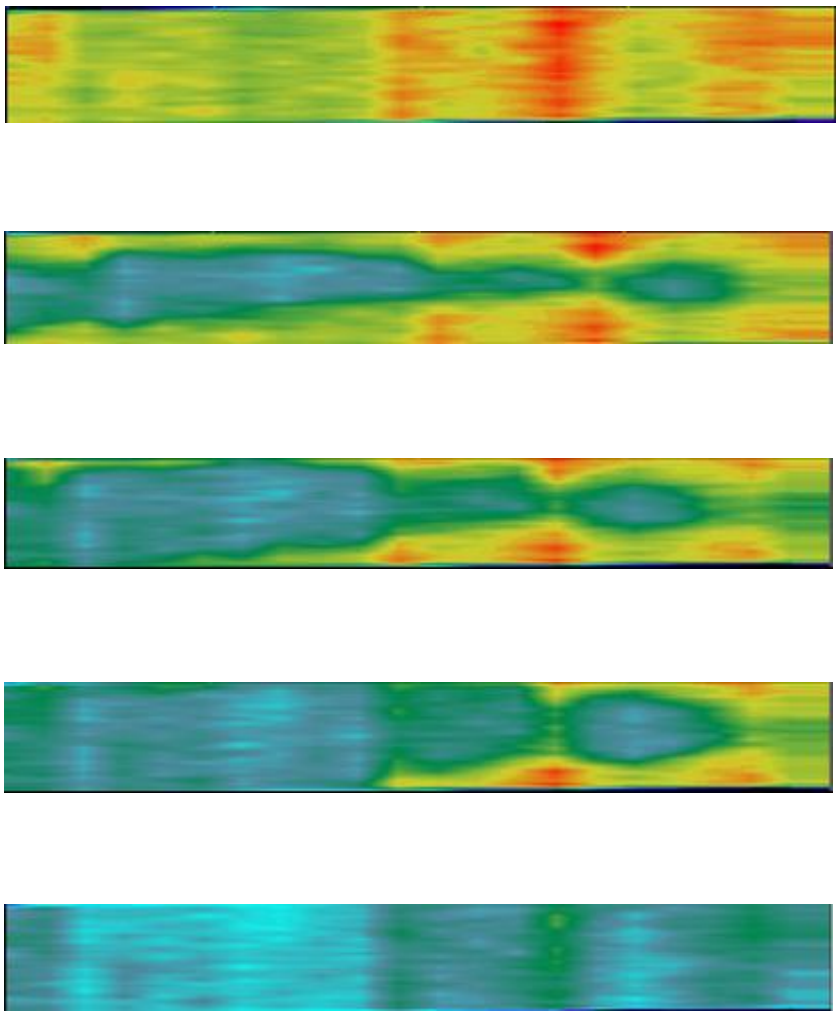

Fig. 5.9 – Ortho reconstructions at various stages showing heterogeneous regions.

However, Fig. 5.9 shows that even in a supposedly homogeneous core, some degree of heterogeneity is still present. The red colored spots on the side of the producing port (right) in Fig. 5.9 represents the heterogeneity in the core. It can be seen that the CO_2 flow line thins down at particular regions and remains that way for some time. This phenomenon is also observed in the cross-sectional images.

The cross-sectional images showed in the previous figures are CT number images and only provide a qualitative representation of the CO_2 saturation in the core. In order to obtain the actual values of saturations, these images need to be converted to a saturation

basis. This was done using the equations discussed previously. The saturation images at various times during the experiments are shown in Fig. 5.10 to Fig. 5.14. Here the color scale has been chosen such that the red color represents regions of higher saturation while the green and blue colors represent regions of lower saturations. A small amount of CO_2 at the producer end in the first stage of injection as shown in Fig. 5.9 confirms the CO_2 breakthrough as was observed earlier in the CT scan images.

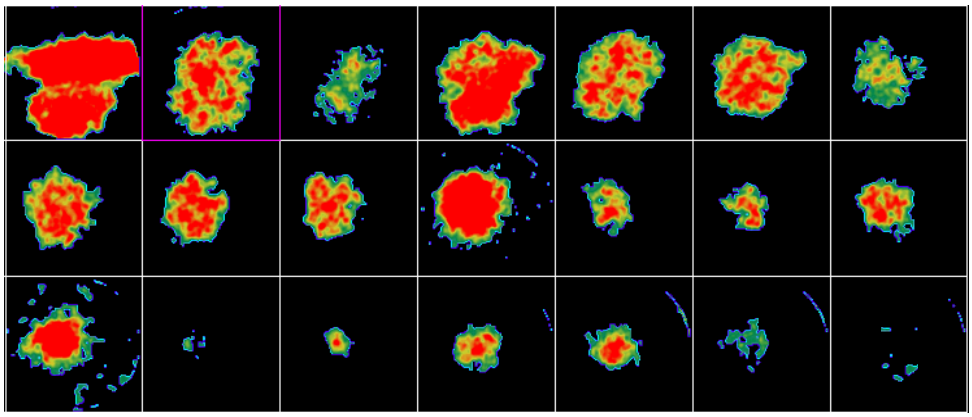

Fig. 5.10 – CO_2 saturations at 0.3 PV of injection.

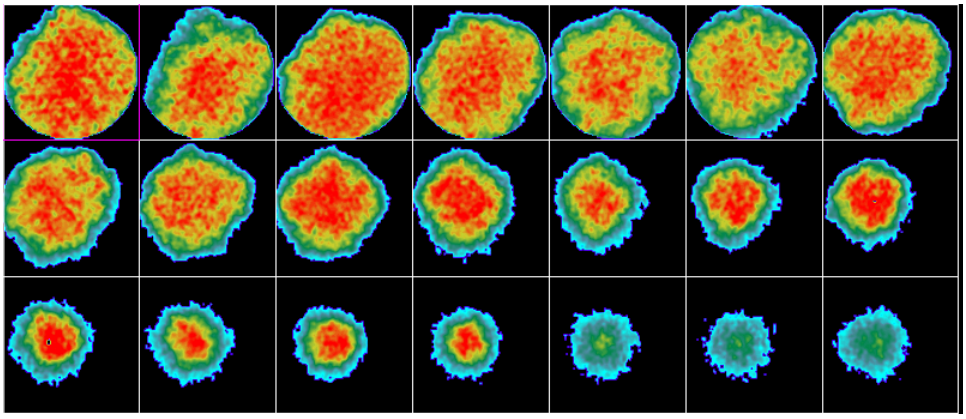

Fig. 5.11 – CO_2 saturations at 0.5 PV of injection.

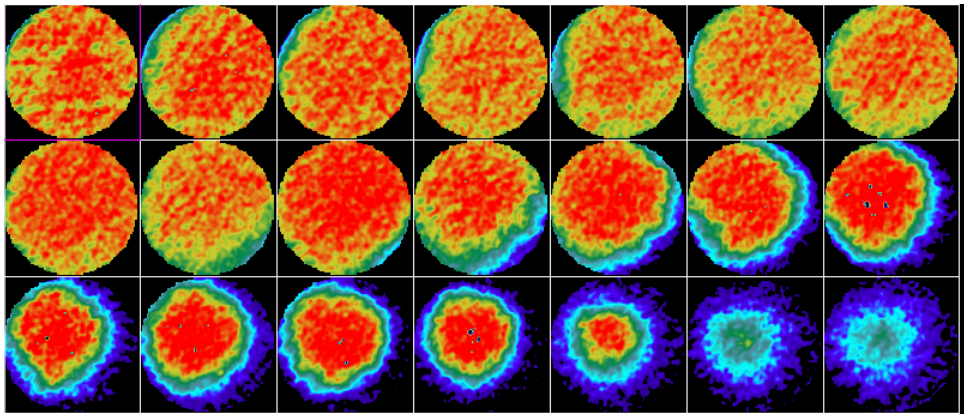

Fig. 5.12 – CO_2 saturations at 1.5 PV of injection.

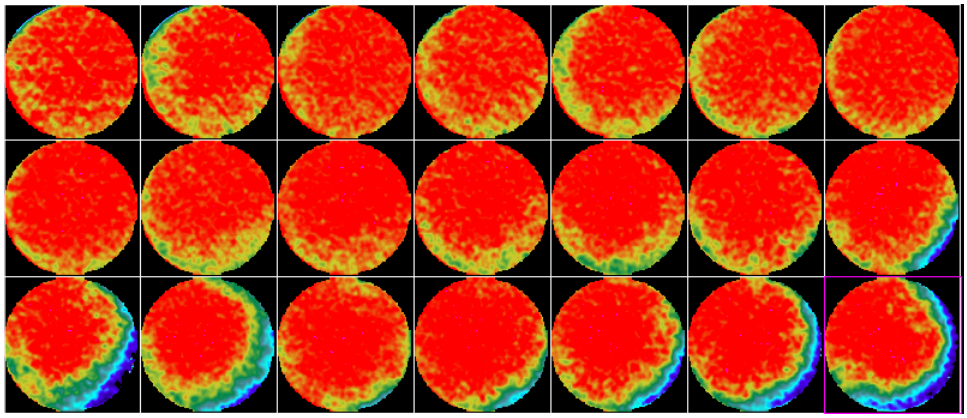

Fig. 5.13 – CO_2 saturations at 3 PV of injection.

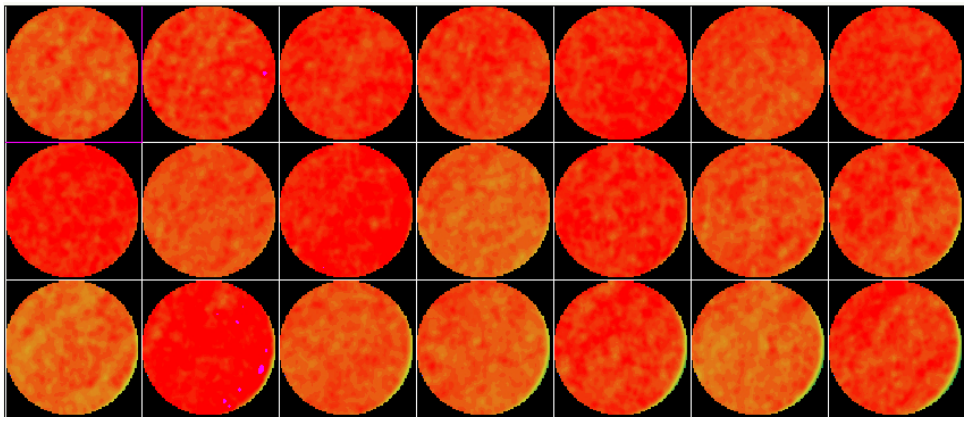

Fig. 5.14 – CO_2 saturations at 5.4 PV of injection.

The distribution of CO_2 saturations can be better understood when observed as a 3D image. *Petro3D*, a commercial image processing software, was used to convert the 2D saturation images to 3D distributions. Fig. 5.15 to Fig. 5.21 show the 3D saturation of CO_2 at different times. In Fig. 5.15, CO_2 is clearly observed to follow a cone like distribution with the tip of the cone towards the producer end. In these images, the white streaks represent the regions inside the core that possess at least a minimum value of saturation, as specified in the image. For example, in Fig. 5.15, pore spaces with a value of CO_2 saturation of at least 7% have been displayed. This was done to ensure that the producer end at which the breakthrough occurred, having regions with CO_2 saturations less than or equal to 7%, is displayed. Similarly, in Fig. 5.16, pore spaces containing at least 40% CO_2 saturation have been displayed. Subsequent 3D images show an increase in the CO_2 saturation with time, and in Fig. 5.21, it can be seen that in most of the regions, the CO_2 saturation is greater than 95%. It is to be noted that, in these images, the distance does not represent the actual length of the core. These numbers are assigned by the software based on the number of slices used for reconstruction of 3D images.

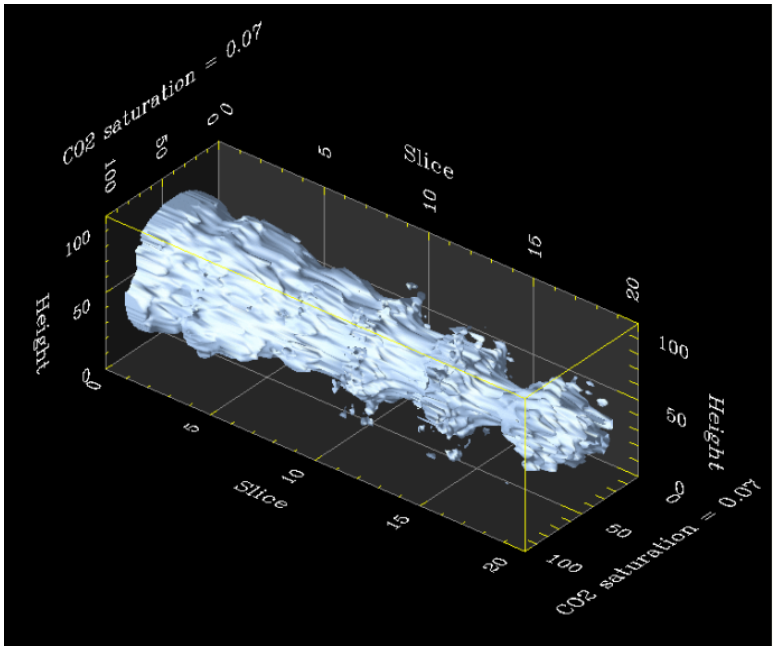

Fig. 5.15 – Regions with a minimum saturation of 7% at 0.3PV of injection.

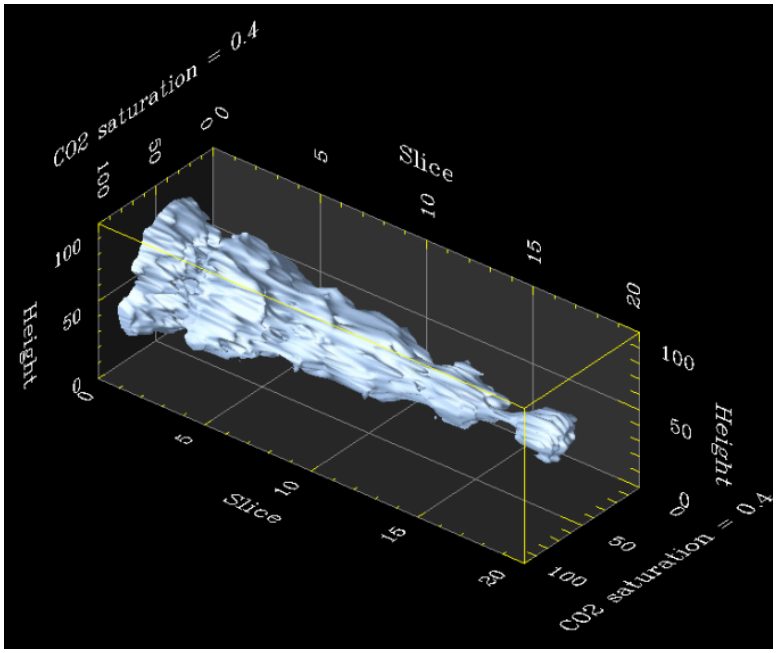

Fig. 5.16 – Regions with a minimum saturation of 40% at 0.3PV of injection.

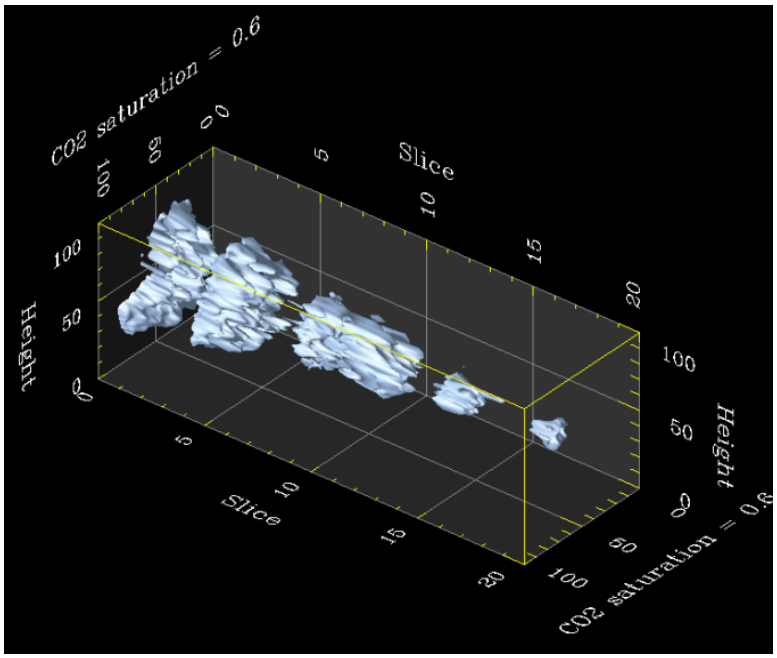

Fig. 5.17 – Regions with a minimum saturation of 60% at 0.3PV of injection.

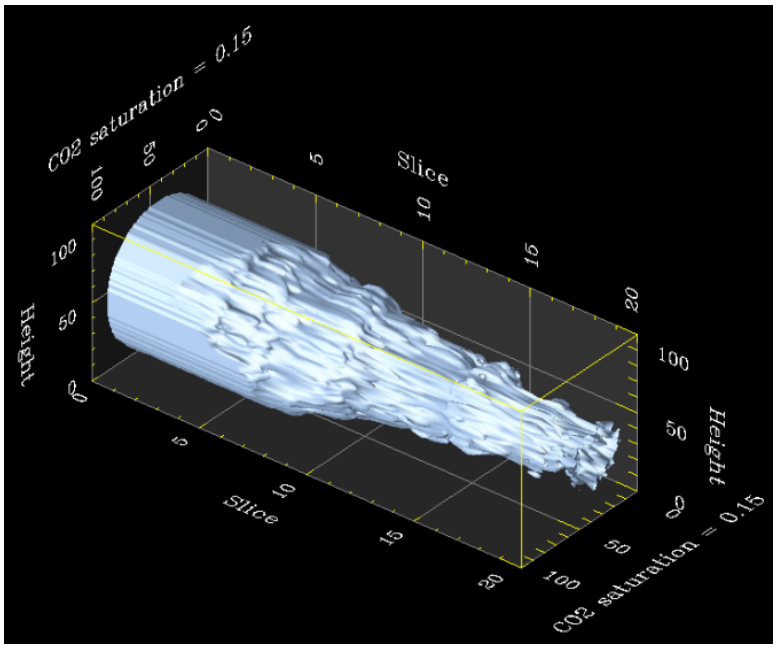

Fig. 5.18 – Regions with a minimum saturation of 15% at 0.5PV of injection.

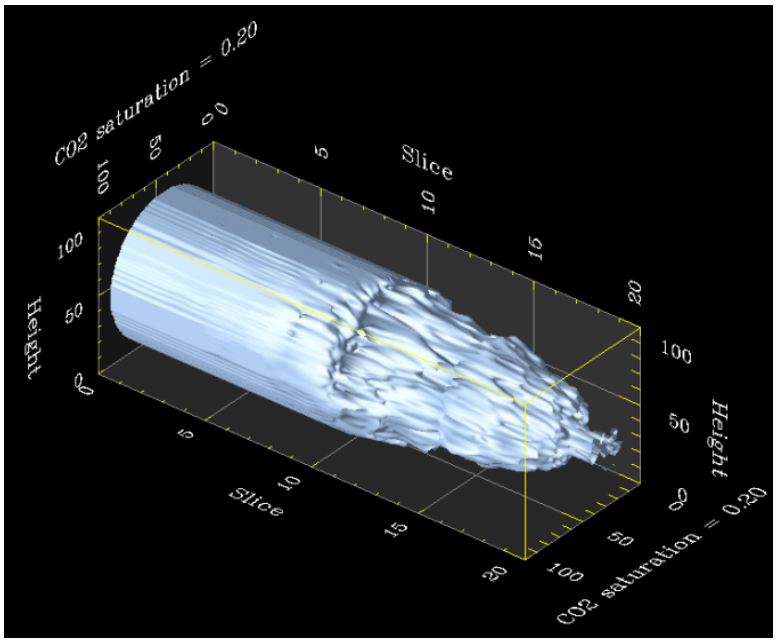

Fig. 5.19 – Regions with a minimum saturation of 20% at 1.5 PV of injection.

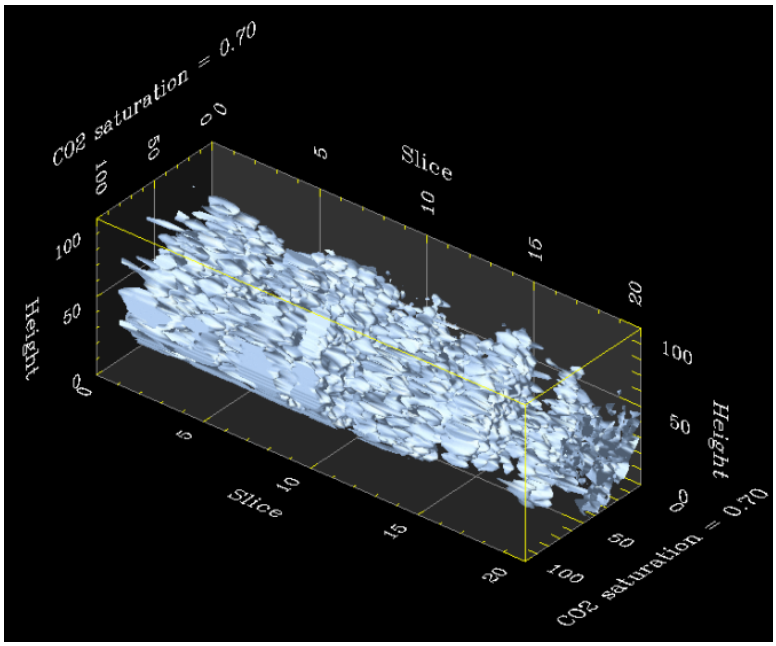

Fig. 5.20 – Regions with a minimum saturation of 70% at 3 PV of injection.

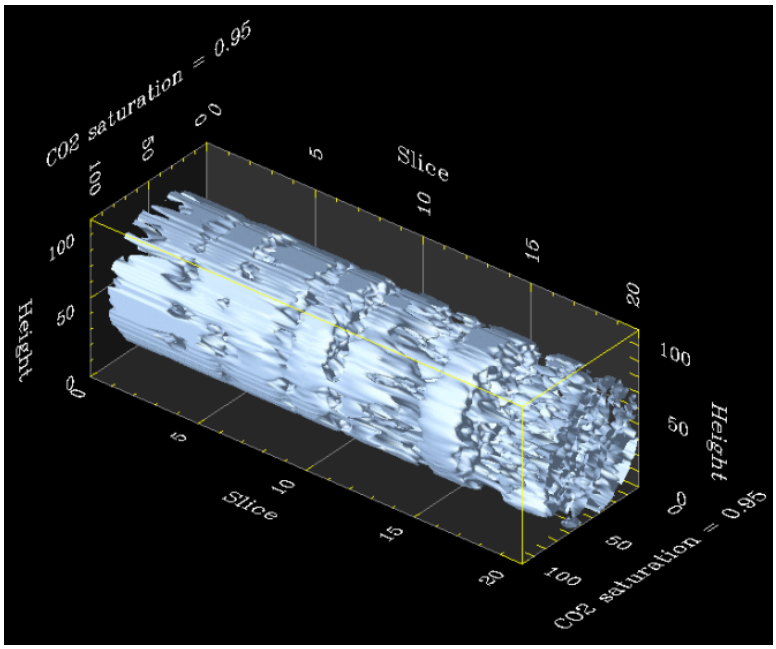

Fig. 5.21 – Regions with a minimum saturation of 95% at 5.4 PV of injection.

These saturation images can be used to obtain actual values of saturation. A commercial software, VOXELCALC^{TM}, is available for this purpose. The output from this software is in the form of spreadsheets containing the saturation data for each pixel in a particular image. A Visual Basic program was developed to accept input from this software, determine average values of saturation for each stage and output the saturations in the form of Excel plots. The plot of saturations obtained at different times is shown in Fig. 5.22.

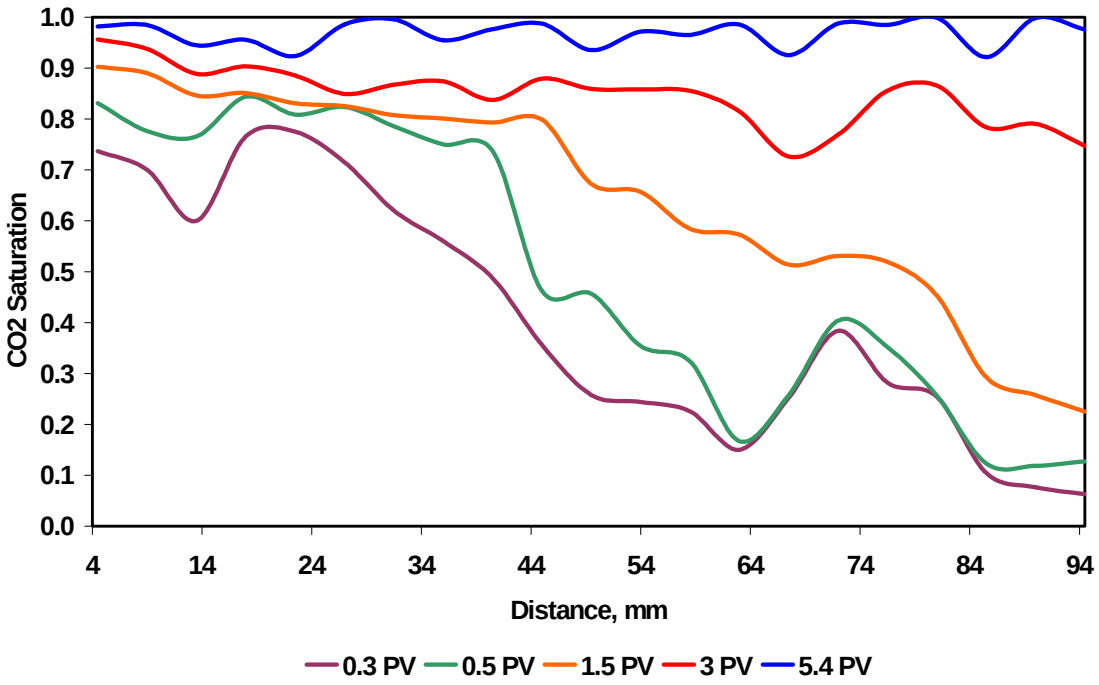

Fig. 5.22 – Spatial variation of saturation at high injection rates.

In the above plot, the left side of the plot corresponds to the injector end of the core while the right side corresponds to the producer end. CO_2 breakthrough can clearly be observed at the producer end in the curve corresponding to 0.3 PV of injection where the value of CO_2 saturation is slightly above zero. An analysis of this plot indicates that the regions where there is some amount of heterogeneity present, the saturation of CO_2 decreases. More amount of CO_2 is required to completely saturate these regions. The effect of heterogeneity is also observed in the low injection rate case discussed in the following section.

5.1.2 Low injection rate

A similar procedure was followed for this experiment. Fig. 5.23 to Fig. 5.27 show the cross-sectional scans obtained at different times during the experiment. These images clearly depict the effect of injection rate on sweep and utilization of CO_2.

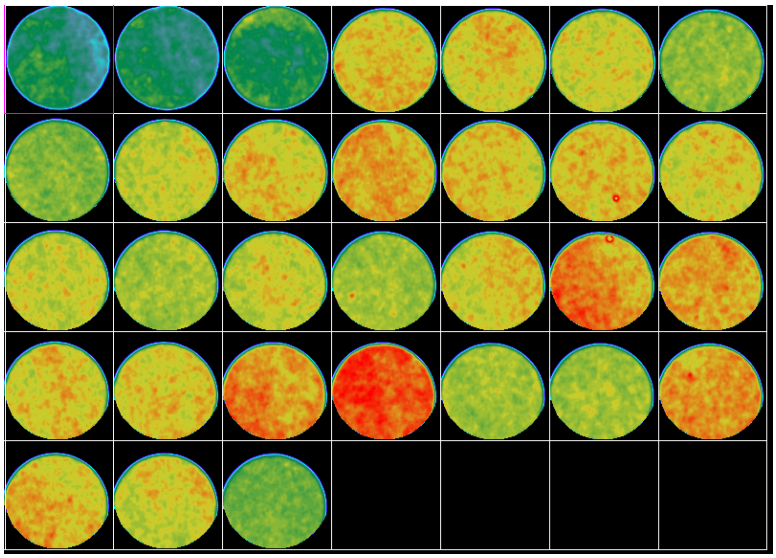

Fig. 5.23 – Scans taken at 0.11 PV of CO_2 injection.

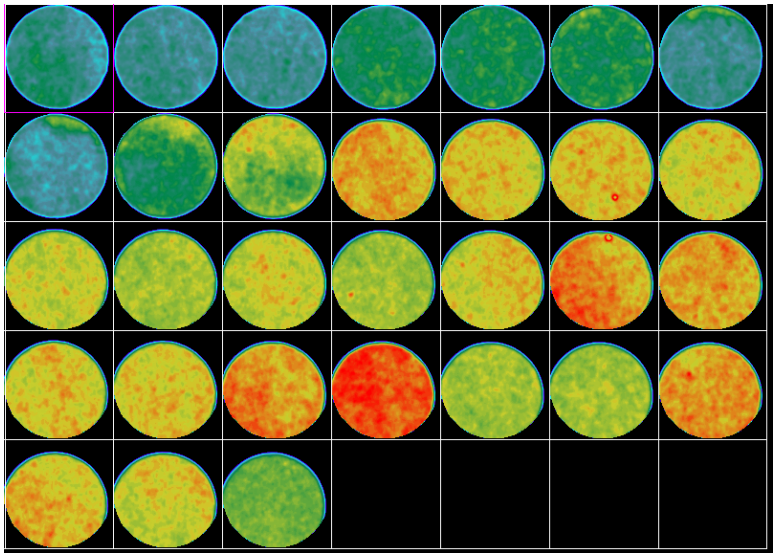

Fig. 5.24 – Scans taken at 0.22 PV of CO_2 injection.

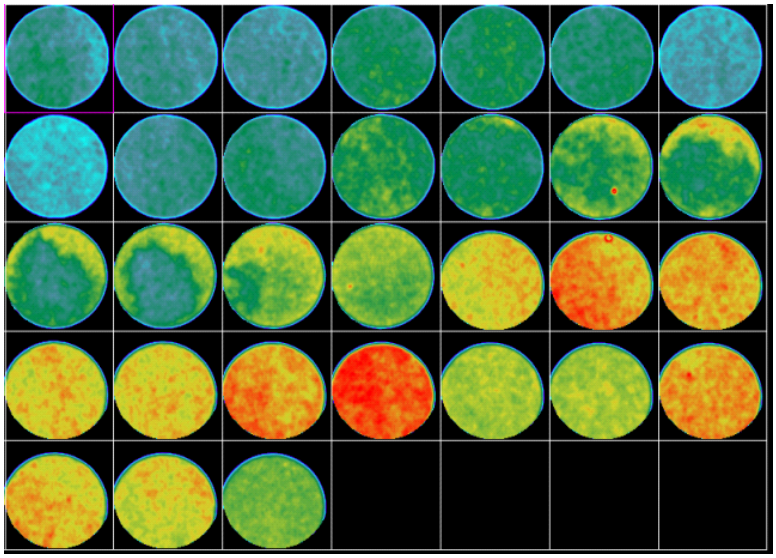

Fig. 5.25 – Scans taken at 0.45 PV of CO_2 injection.

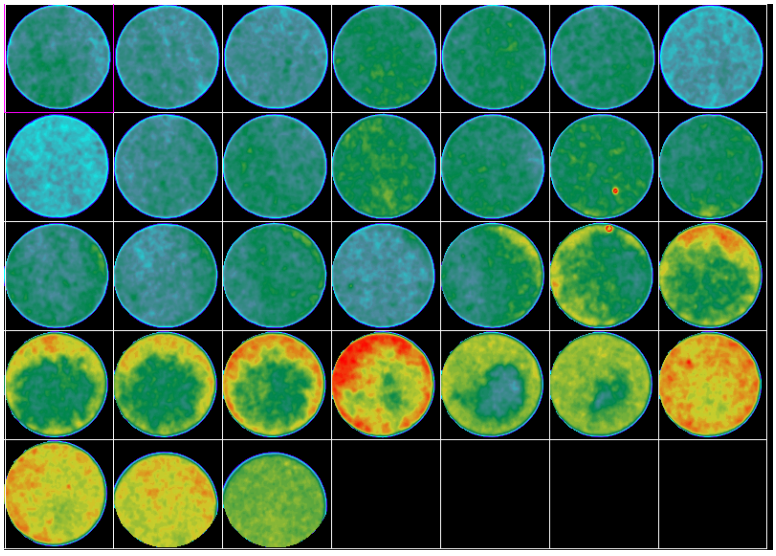

Fig. 5.26 – Scans taken at 0.57 PV of CO_2 injection.

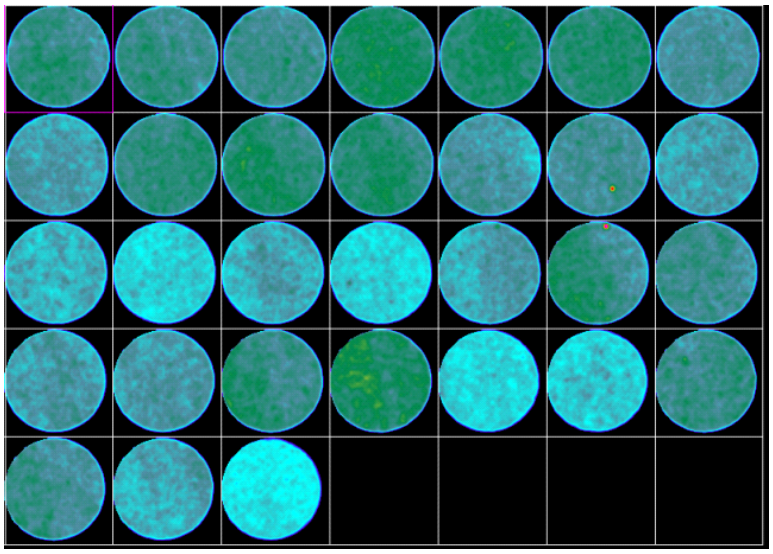

Fig. 5.27 – Scans taken at 1.1 PV of CO_2 injection.

It can clearly be observed that at this injection rate, CO_2 does not bypass oil and a very good sweep is obtained. In this case CO_2 does not flow through the centre of the core and a uniform distribution of CO_2 is obtained. This is because of the fact that there is enough time for CO_2 to diffuse uniformly into all parts of the core. Also, the breakthrough time of CO_2 increased considerably compared to the previous case. The effect of heterogeneity observed in this case is similar to the previous case as shown in Fig. 5.28. Saturation distributions were obtained in this case using the cross-sectional scans. The number of pore volumes of CO_2 injected corresponding to each reconstruction can be seen in Fig 5.29, which shows the plot of CO_2 saturation versus distance for low injection rate case. It can be seen that breakthrough occurs after about 0.57 PV of CO_2 injection for the low injection rate whereas in the high injection rate case breakthrough occurred at only about 0.3 PV of injection. The figure also shows that the final recovery obtained in this case is consistently above the 90% range, with an average final recovery of 96%. Fig. 30 shows 3D saturations obtained using *Petro3D* shows at the end of the experiment.

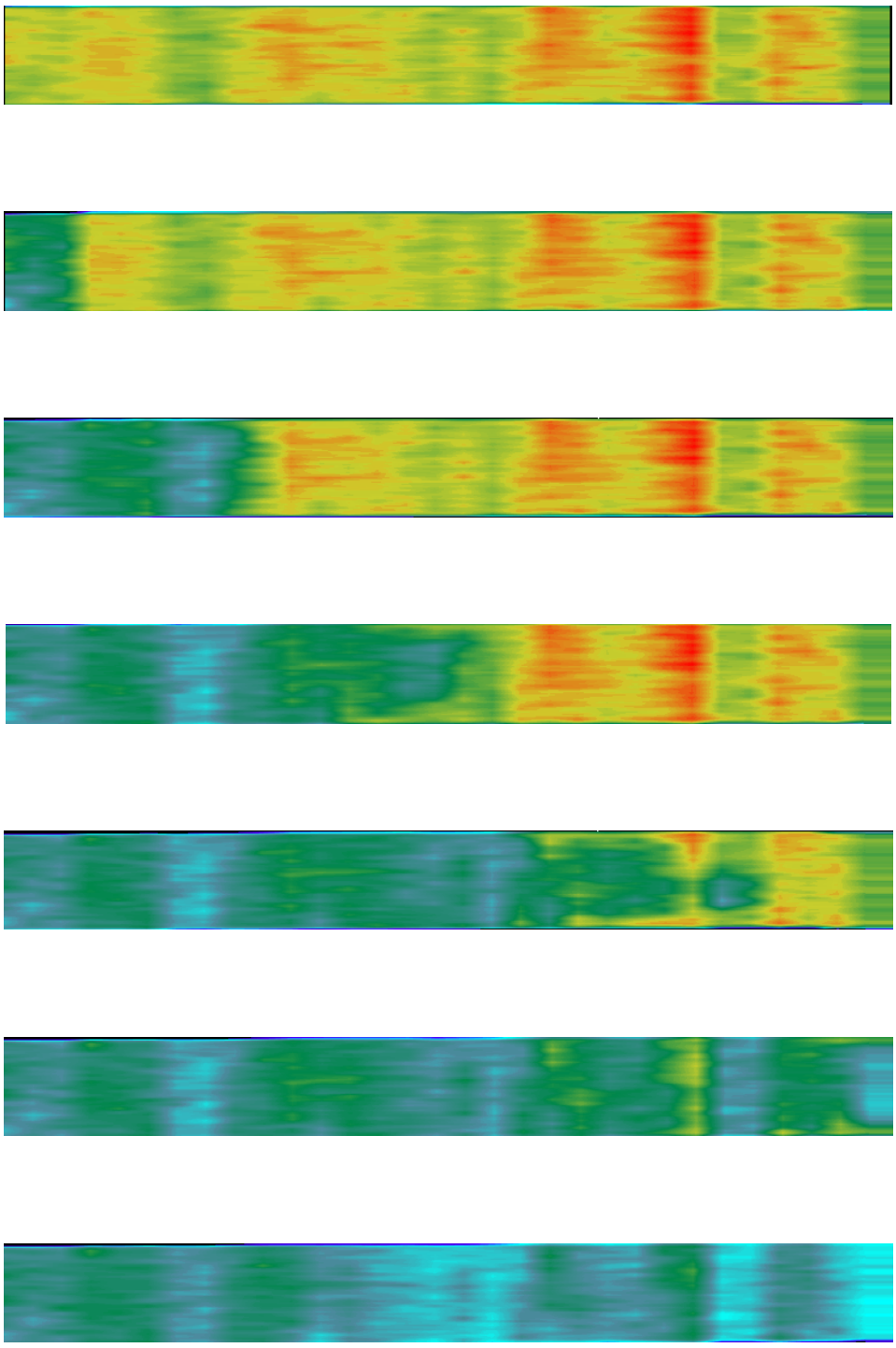

Fig. 5.28 - Reconstructions of cross-sectional scans for low injection rate case shows good sweep.

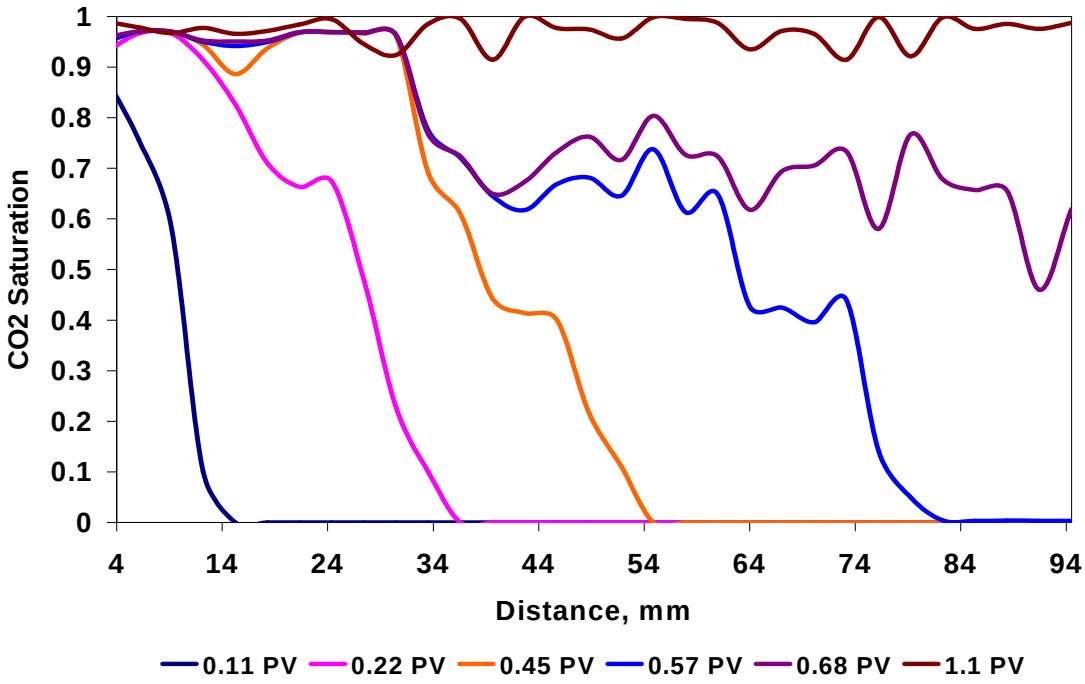

Fig. 5.29 - CO_2 saturations along the length of the core at different stages of injection.

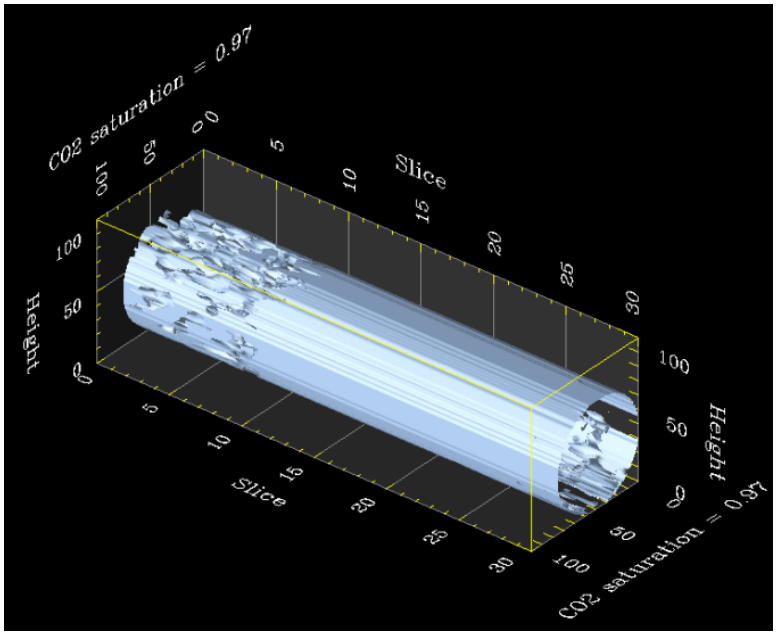

Fig. 5.30 – Regions with minimum saturation of 97% at the end of the experiment.

The important point to be noted here is that although the final recovery obtained in both the cases is almost the same, there is a huge difference in the amount of CO_2 used to obtain such a high recovery. Such a high value of oil recovery obtained even when the displacement is immiscible can be attributed to the light, low viscosity oil used in the experiments. Figure 5.31 shows the oil recovery obtained using CT saturations for the two cases. This plot, showing the oil recovery versus the pore volumes of CO_2 injected, is a more familiar plot and indicates the efficiency of a secondary or tertiary recovery process. The resolution of the plot is not very high due to the fact that scans taken were intermittent and were limited by the capacity of the scanner. From the plot, it is clearly seen that the low injection rate case is much more efficient compared to the high injection rate case with respect to the utilization of CO_2. This is because, for almost the same amount of oil recovered, the high rate case uses almost 5.4 PV of CO_2 whereas the low injection rate case uses only about 1.2 PV. But it should also be noted that although the sweep is very good in the low rate case, the time taken to obtain such a recovery is much higher (about 300 minutes) compared to the high injection rate case, which took only about 60 minutes. This time taken would be magnified many times in an actual field application and this would prove detrimental to the economics of the project. Also, at a very low rate, the viscous forces are extremely low and a possibility of the gas forming a gravity tongue always exists. Also, the pressure of the reservoir should not be allowed to drop too much. Hence it is important that the injection rates be optimized before the start of injection and a balance be obtained between achieving the highest possible recovery and obtaining such a recovery in the lowest possible time.

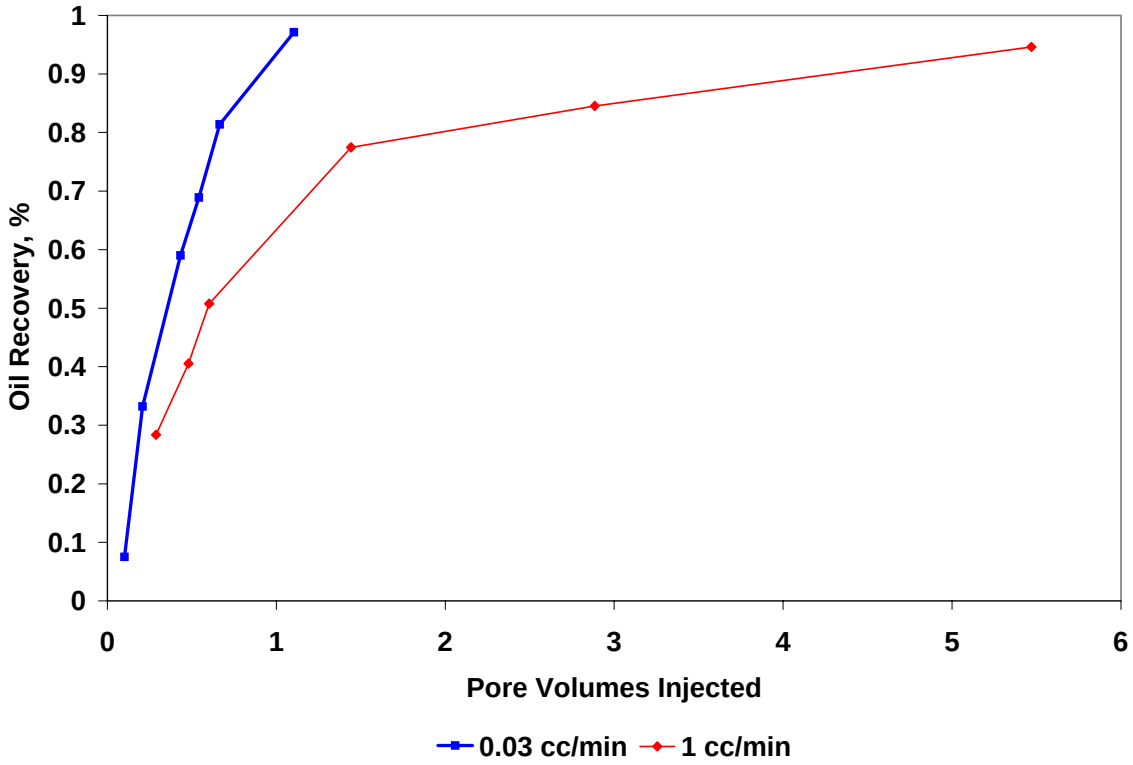

Fig. 5.31 - Higher oil recovery is obtained for lesser pore volumes injected in the low injection rate case.

5.2 Experiments using fractured cores

For these experiments, the cores were artificially fractured in the laboratory. The major difference that is to be observed between a naturally and an artificially fractured core is the presence of mineralization in the former. But obtaining a naturally fractured core is difficult in the first place. Also, with our current experimental setup, the maximum size of core that can be used is limited to a diameter of 1 inch. At this size, it is almost impossible to obtain a naturally fracture core. But an artificially fracture core should still serve the purpose considering the fact that the distribution of apertures in both the cores is the same[25].

Experiments were performed in the fractured cores with the objective of analyzing breakthrough mechanisms and the effectiveness of various methods that are currently being used for mobility and conformance control.

5.2.1 Continuous CO_2 injection

The permeability of a fracture is typically about 10^3 to 10^6 times greater than the permeability of the porous rock. In a fractured system, the tendency of the fluid would be to flow through the high permeability fracture which leads to early breakthroughs. In the case of gas injection, the injection rate plays an important role. In the case of waterflooding, a low injection rate facilitates dynamic imbibition of the wetting phase into the matrix, when gravity effects are neglected. Babadagli[26] found that, for water wet cores very low injection rates helped in obtaining a better oil recovery due to imbibition. But when the injection rate exceeded a particular value, no oil was produced, no matter how much water was injected. In this case, viscous forces played a minor role while capillary forces played an important role in recovery. But in the case of gas injection, the process is one of drainage and gas is the non-wetting phase. Here, the drainage mechanism could be either one of counter or co-current drainage. In counter current drainage, diffusion of gas into the matrix causes an equivalent amount of oil to flow into the matrix. In the case of co-current drainage, the gas causes viscous displacement of oil in the direction of flow. A schematic of the drainage process is provided in Fig. 5.32. In gas injection, the gravity and capillary forces play an important role in the recovery process. During the injection process, the viscous forces are high at the injector end and reduce as we proceed towards the producer end. Hence, the recovery of oil at the injector end is higher due to the diffusion of gas into the matrix and the recovery from the producer end is lower and the time taken for complete recovery is very high. Continuous CO_2 injection was started at a very low rate of approximately 0.03 cc/min in a fractured core with a vertical fracture. Only a very small amount of oil was recovered after about 1.5 PV of injection, most of which was from the fracture. In this case, the breakthrough from the fracture was almost instantaneous. Scans were taken at different time during the experiments. The flow of CO_2 through the fracture was identified by the decrease in the CT number in the fracture and the change in color in the cross-sectional scans in the fracture. Fig. 5.33 and Fig. 5.34 show the oil saturated core scans and the scans after CO_2 injection was started respectively.

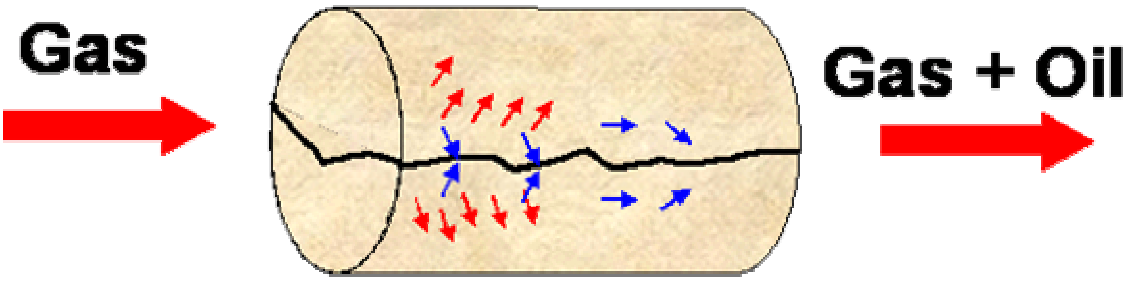

Fig. 5.32 – Schematic of drainage process.

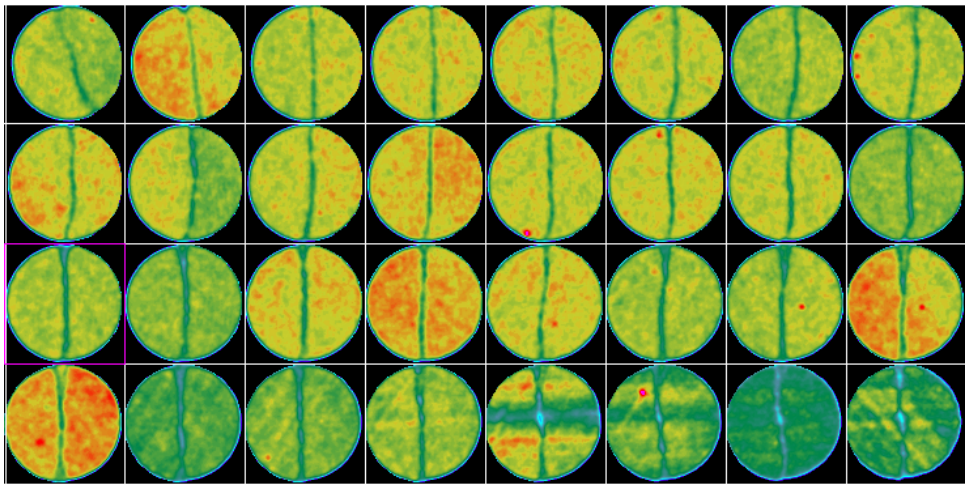

Fig. 5.33 – Oil saturated core scans with the fracture seen at the center.

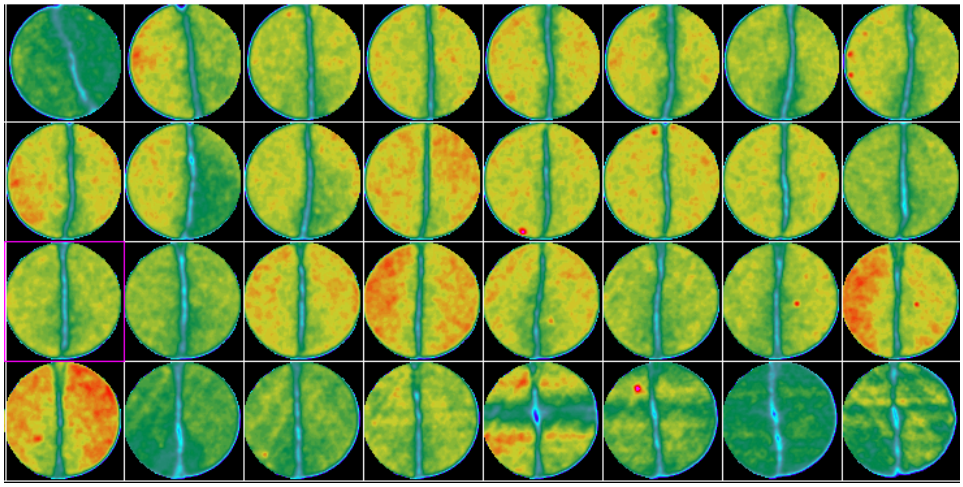

Fig. 5.34 – CO_2 flow can be identified by a change in color at the fracture.

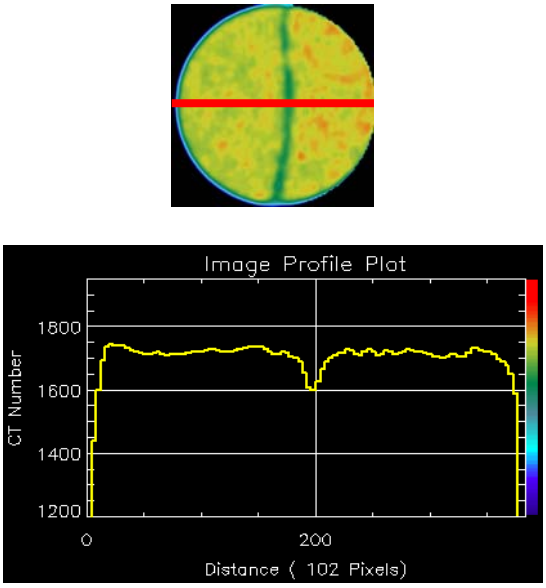

Fig. 5.35 – CT number of oil saturated core.

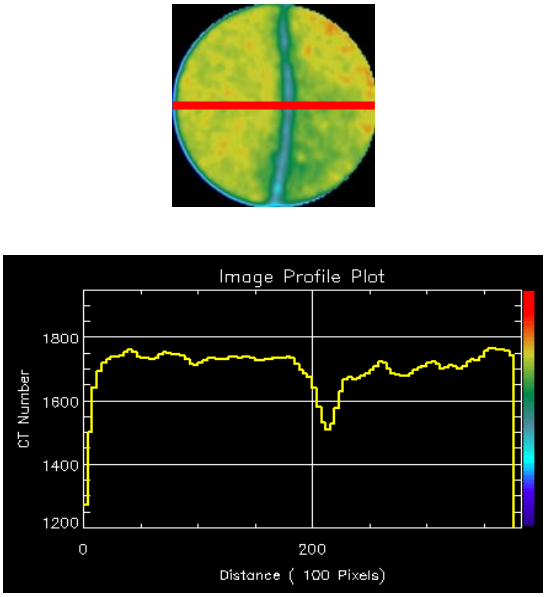

Fig. 5.36 – CT number after CO_2 injection was started.

The flow of CO_2 through the fracture was also identified by the reduction in the CT number at the fracture after injection was started as shown in Fig 5.35 and Fig. 5.36. Reconstructions of the horizontal scans also indicate the CO_2 flowing over the fracture surface. This can be seen in Fig. 5.37. In this reconstruction, the bottom reconstruction represents a cross-section parallel to the fracture surface (along the fracture) while the top reconstruction represents section perpendicular to the fracture surface (which shows the fracture as a blue streak at the center).

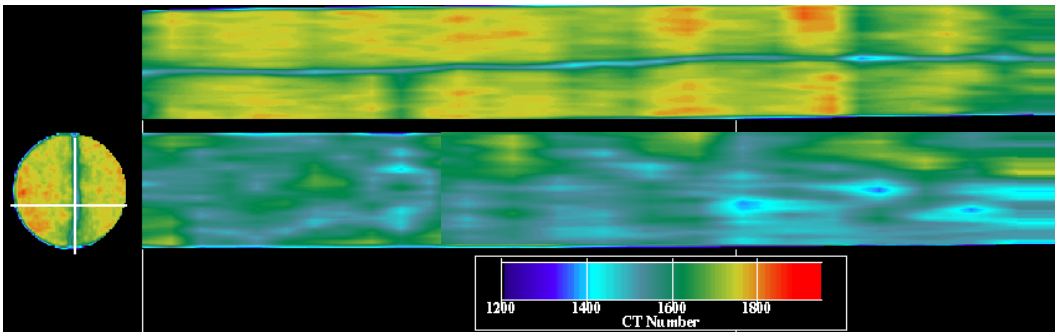

Fig. 5.37 – Reconstructions parallel and perpendicular to the fracture surface.

Following this, another experiment was performed with a higher injection rate of 0.1 cc/min. The fracture configuration used in this case was similar to the previous case. The breakthrough of CO_2 occurred after about 10 minutes corresponding to about 0.09 PV of injection. Although this was not as early as the previous case, this can still be considered very early for economic operation. Fig. 5.38 to Fig. 5.41 show the various scans taken during the course of the experiment.

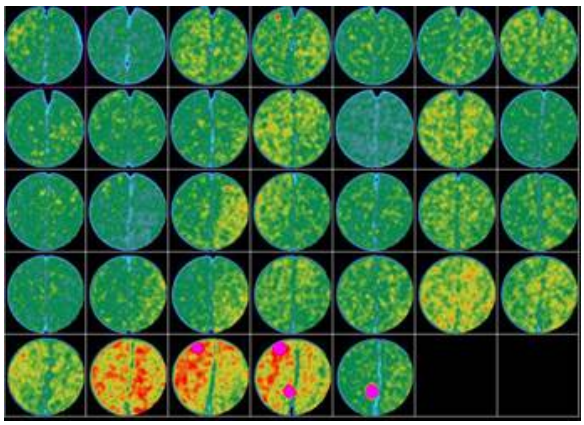

Fig. 5.38 – Oil saturated core scans during continuous CO_2 injection.

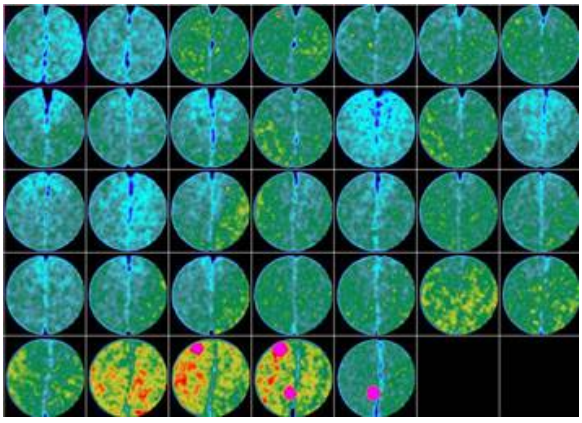

Fig. 5.39 – Scans taken at about 0.7 PV of injection indicate irregular saturation of CO_2 and breakthrough from fracture.

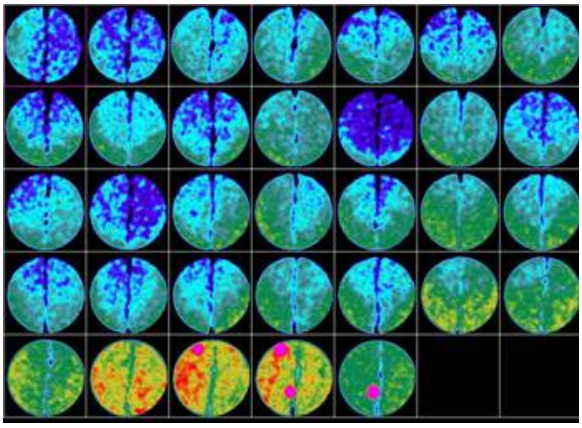

Fig. 5.40 – Scans taken at about 1.3 PV of injection.

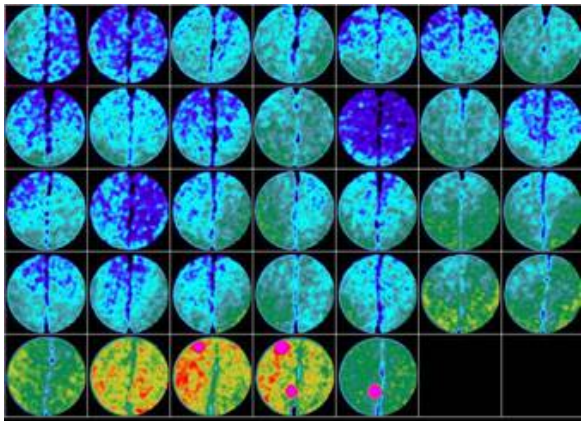

Fig. 5.41 – Scans taken at the end of the experiment.

In these scans the color scale has been chosen such that the blues indicate the lowest CT numbers while red and pink indicate the highest CT numbers with green and yellow being the intermediates. Thus, with an increase in CO_2 saturation, the CT number decreases and hence the color changes to a dark shade of blue. The color scale for these CT numbers is shown in Fig. 5.42.

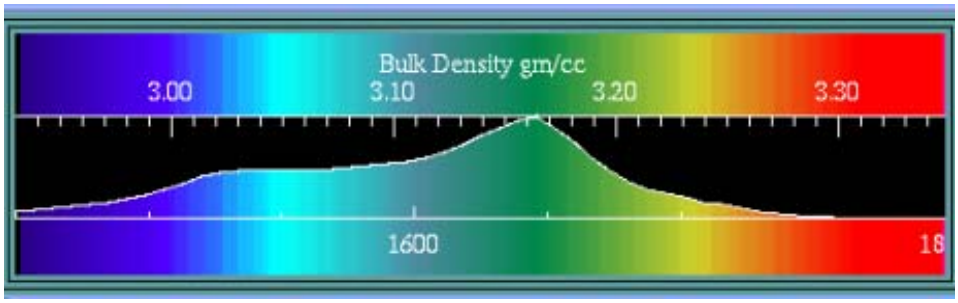

Fig. 5.42 – Scale showing colors and their corresponding CT numbers.

In order to better understand the displacement process and to calculate the saturations, the CT number images were converted to saturations and 3D images were also obtained using these saturations. The CO_2 saturations from the continuous CO_2 injection process are shown in Fig. 5.43 to Fig. 5.45.

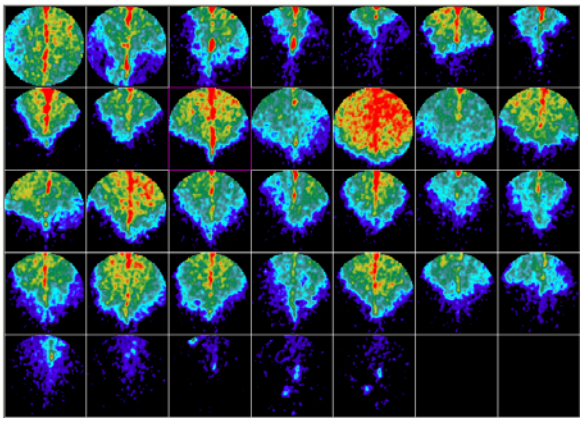

Fig. 5.43 – CO_2 saturations at 0.7 PV of injection.

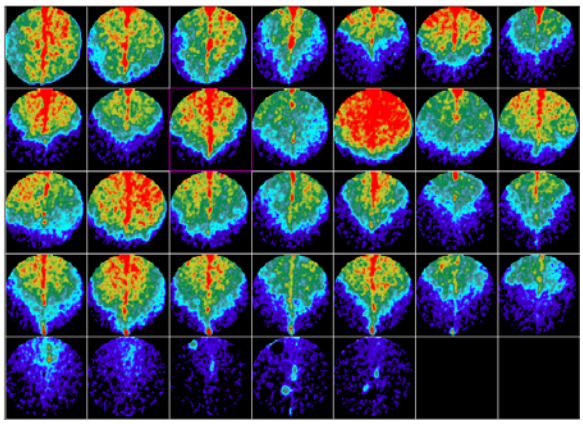

Fig. 5.44 – CO_2 saturations at 1.3 PV of injection.

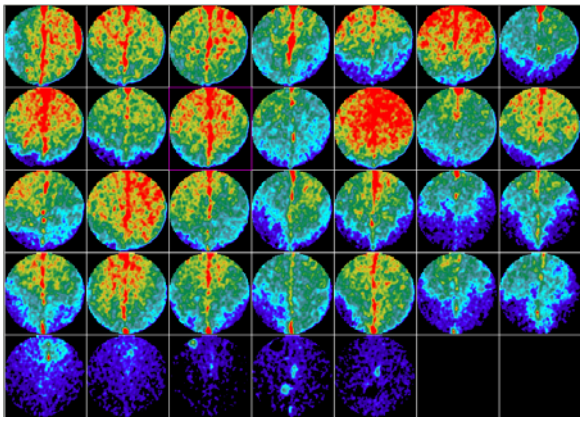

Fig. 5.45 – CO_2 saturations at the end of the experiment.

The CO_2 saturation images give a clear insight into the displacement mechanism acting in the flooding process. It is well known that gravity drainage is an important oil recovery mechanism in naturally fractured reservoirs. In some cases it is the only mechanism that allows oil recovery and production of oil from the matrix blocks. Oil recovery by gravity drainage strongly depends on the height of the capillary continuity. Hence gravity drainage has always been associated with tall matrix blocks. But these saturation images obtained, clearly show the influence of gravity segregation in the displacement process. The fact that the oil recovery takes place mainly from the top part

of the core and some amount of oil is recovered towards the bottom as time progresses, indicates that gravity segregation is possible in a 1 inch core. The force required for CO_2 to flow sideways into the matrix is provided by the viscous drive mechanism. Thus the displacement is seen to be a combination of gravity and viscous forces. It can be seen that although CO_2 has invaded a large portion of the core, the recovery of oil from these regions is not complete. This can be explained by observing the color scale for the saturation images, shown in Fig. 5.46.

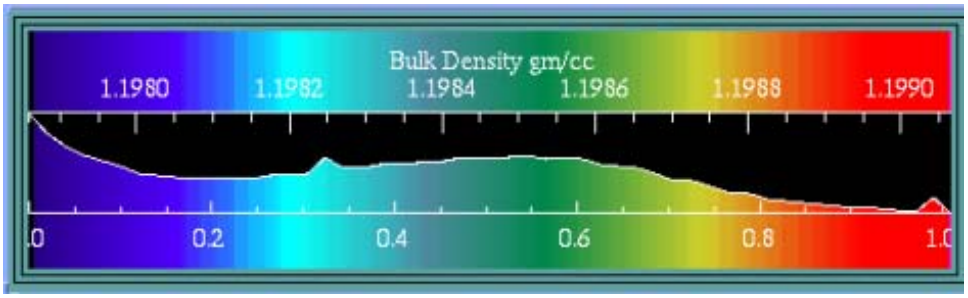

Fig. 5.46 – Color scale indicating red color with high values of saturation.

Looking at the color scale and comparing it with the saturation images, it is observed that the maximum saturation of CO_2 occurs at the fracture, indicating that CO_2 is following the path of least resistance. The oil recovery curve from the displacement process is shown in Fig. 5.47. This curve shows that the initial recovery is high and this reduces as time progresses. Towards the end of the experiment, the recovery obtained is seen to be a constant low value. In this kind of displacement, there is always some amount of CO_2 that breaks through without contacting any oil, thus greatly reducing the sweep efficiency. The diffusion process is extremely slow, and given enough time and CO_2, a good recovery may be obtained. The final recovery obtained in this experiment after about 2.2 PV of injection is about 58%.

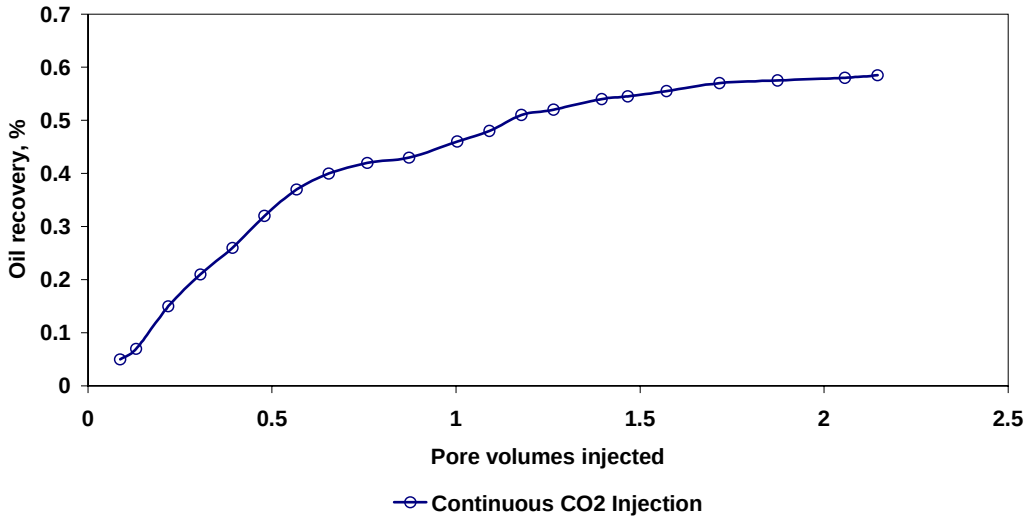

Fig. 5.47 – Oil recovery vs. pore volumes injected for continuous CO_2 injection.

5.2.2 Water Alternating Gas (WAG)

In the recent years, there has been an increasing interest in the WAG process, both miscible and immiscible. The continuous CO_2 injection process is an important process to identify displacement mechanisms but is not likely to be economic in practice unless significant recycling of gas is employed[27]. Inherent in all gas injection processes is the lack of mobility and gravity control (areal and vertical sweep) necessary to sweep significant portions of the reservoir. Therefore, the replacement of high cost CO_2 by a cheaper chase fluid such as water for horizontal displacements appears economically attractive.

The WAG process involves alternate injections of small pore volumes (5% or less) of CO_2 and water until the desired volume of CO_2 has been injected. The oil recovery by WAG has been attributed to the contact of unswept zones, especially the recovery of attic or cellar oil by exploiting the segregation of gas to the top or accumulating water towards the bottom[28]. Since the microscopic displacement oil by gas normally is better than by water, the WAG injection combines the improved displacement efficiency of gas flooding with an improved macroscopic sweep by the injection of water. This has resulted in an improved recovery (compared to pure water injection) for most field cases.

WAG has been applied with success in most field trials. Very few field trials have been reported as unsuccessful though operational problems have been reported.

The WAG process can be grouped in many ways. The most common is to distinguish between the miscible and the immiscible WAG process. In the miscible WAG process, a multi-contact gas-oil miscibility is obtained, although a lot of uncertainty exists about the actual displacement process. For the miscible process to be observed, the pressure of the reservoir must be above the minimum miscibility pressure (MMP) of the oil. The reservoir is often repressurized to this pressure before the initiation of the WAG process. In many cases, it is not possible to maintain the reservoir pressure above the MMP, especially in gas injection and hence the process oscillates between miscible and immiscible. The immiscible WAG process has usually been applied with the aim of improving frontal stability or contacting unswept zones. The application has mainly been in reservoirs where gravity stable gas injection has been difficult because of limited gas availability or unfavorable reservoir properties like low dip or strong heterogeneities. There are other WAG process like the hybrid WAG where a large slug of gas is followed by small slugs of alternate water and gas, and the simultaneous WAG or SWAG where water and gas are injected simultaneously.

WAG has been used for mobility control in a wide variety of rock types like low permeability chalk[29], high permeability sand stone[30]and other lithologies. Several field cases[31,32,33,34] and laboratory experiments[35,36] indicate that the WAG process has been an effective mobility control method in most cases. In a fairly homogeneous system, water invades the zones previously invaded by the gas, subsequently diverting the gas into other zones[37]. But a completely different situation prevails in the presence of extreme heterogeneities like fractures. In such a case, the conformance control agent must be able to effectively divert the fluid into the matrix, thereby delaying breakthrough and reducing oil bypass. But the performance of WAG in terms of mobility control in fractures has not been adequately studied.

Experiments were performed to test the performance of WAG in the presence of extreme heterogeneities like fractures. The first task was to test the mobility of water in the core. Brine was prepared and tagged with both sodium iodide and potassium iodide to artificially its CT number. The properties of brine are provided in Table 5.1. This tagged

brine was injected into an oil saturated core at a rate of about 0.1 cc/min. During the experiment, it was observed that the water mobility in the core was very high, Berea being a core with very high permeability. The presence of a fracture in the core increased the mobility even more and a very early breakthrough was observed, at about 0.12 PV of injection.

Table 5.1 – Synthetic Brine Composition

Brine Properties	
Composition	**Concentration**
Nacl	122699 mg/L
$Cacl_2.2H_2O$	7497 mg/L
NaI	500 ppm
KI	500 ppm

This early breakthrough of brine indicated that pure brine by itself will not be able to delay the breakthrough of CO_2 from the fracture. The mobility of water in the fracture had to be reduced and this requires that its viscosity be increased. A conventional WAG process involves alternate injection of specific pore volumes of gas and water to reduce the relative permeability of the gas and hence its mobility. But here, our aim is to delay CO_2 breakthrough and hence we decided to inject the viscosified water into the fracture to "heal" it to some extent so as to the reduce CO_2 mobility in fracture. Xanthan was chosen to increase the viscosity of water due to its good injectivity and relative insensitivity of its viscosity to salinity[38]. Sufficient amount of Xanthan was added to the iodated brine to increase the viscosity to about 20 cp. This was then injected into the core with the injection port aligned with the fracture. Although no problems were encountered with the injectivity of the liquid, it was observed that there was a large amount of liquid "leakoff" into the matrix. Liquid "leakoff" is a term used to describe the loss of water into the matrix, from the viscosified mixture in the fracture. This causes the fracture to be left open for CO_2 flow. By the time the liquid filled the entire fracture and breakthrough occurred, a considerable quantity had leaked off into the rock and more than 65% of the

oil had already been recovered. Fig. 5.48 to Fig. 5.51 show the scans obtained at various times during the experiment.

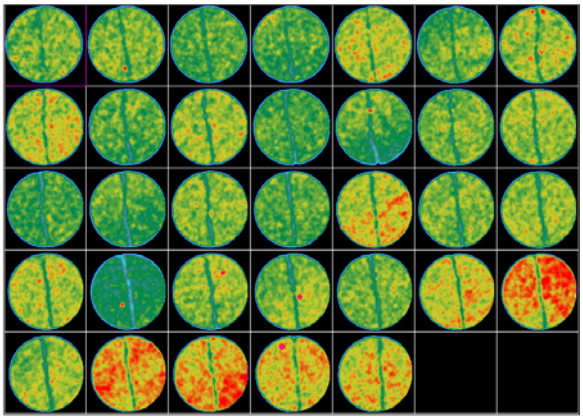

Fig. 5.48 – Oil saturated core scans during WAG injection.

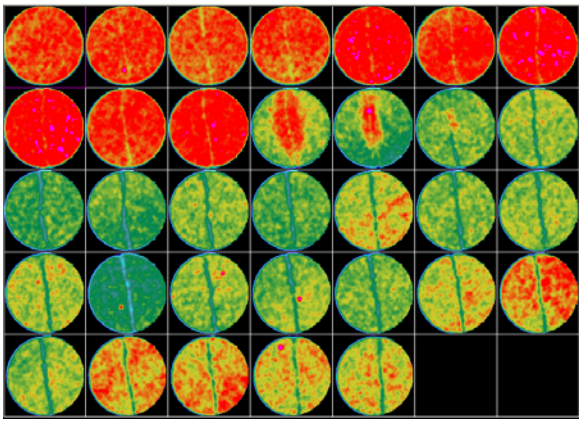

Fig. 5.49 – Scans taken at about 0.08 PV of injection where red color indicates higher CT numbers due to doped brine.

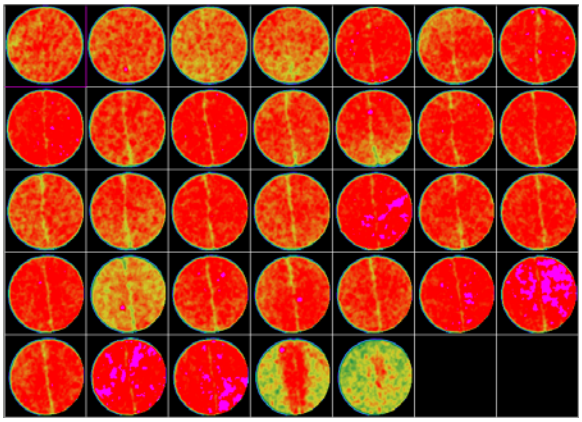

Fig. 5.50 – Scans taken at viscosified water breakthrough (0.25 PV).

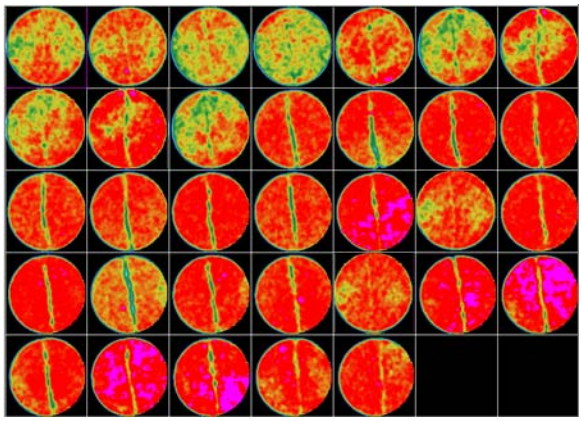

Fig. 5.51 – Scans taken at CO_2 breakthrough indicating CO_2 diverted into many regions inside the matrix.

In these scans the red color represents the higher CT numbers where the viscous brine has invaded the pore spaces. Once breakthrough of brine was observed, injection of brine was stopped and CO_2 injection started. By the time CO_2 displaced the remaining brine in the tubing and reached the core, about 80% of the oil had been recovered. This was considered to be the residual oil saturation for the core to water. CO_2 injection resulted in an incremental recovery of only about 4.5% during which time, viscosified brine was also observed at the outlet. Although, the incremental recovery obtained in this case was low,

the important result obtained is that the breakthrough of CO_2 was delayed considerably compared to the continuous CO_2 injection case. Here, the breakthrough of CO_2 occurred after 0.44 PV of injection. Although the overall recovery obtained was higher than that obtained by continuous CO_2 injection, most of the recovery was due to the viscous water and very little due to CO_2. This again might be due to the strong water-wet nature of the cores and the very low viscosity of the oil used. Using brine of higher viscosity (about 30 cp) also gave us similar results. The success of this process depends on preventing liquid leakoff into the matrix, because in actual conditions, the reservoir is likely to be at residual oil conditions and any entry of water into the matrix will not help in recovering more oil and only result in leaving the fracture open for CO_2 flow. Liquid leakoff into the porous rock can be minimized by using suspended particulate matter[39]. Also, in an oil-wet core, the amount of water imbibing into the porous rock would obviously be lesser and hence the viscous liquid can remain in the fracture, healing it to some extent. But this liquid can still flow and would be produced when CO_2 flows through the fracture. So CO_2 and liquid have to be injected alternately similar to the WAG process. Another method suggested in the literature to minimize leakoff is the addition of a cross-linker to form a gel, when its propagation becomes extremely slow or negligible[40]. Fig. 5.52 represents the oil recovery curve for this experiment. Here the red curve represents the oil recovery due to viscosified water and the green curve represents the incremental oil recovery. It can be seen that the green curve is flat for most part. This is because most of the fluid recovered was brine and very little oil was recovered.

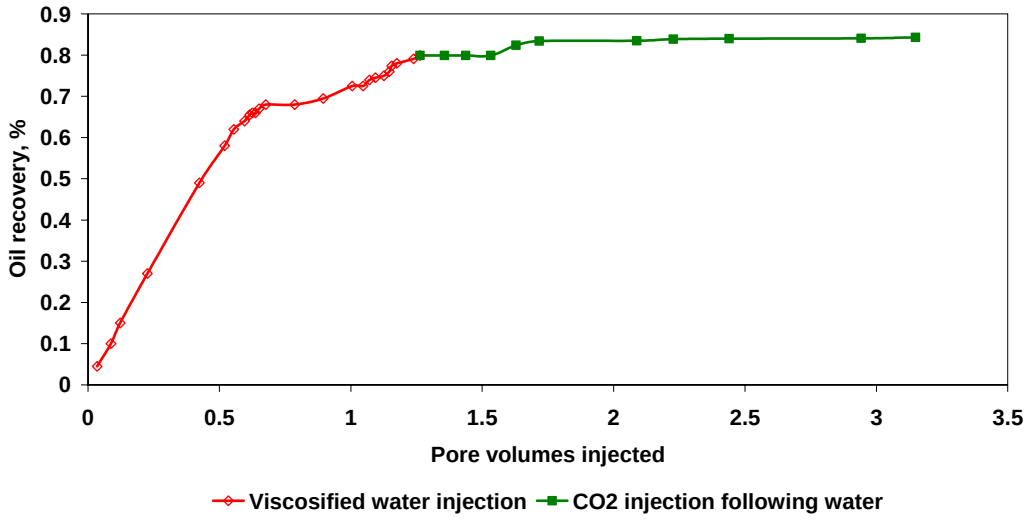

Fig. 5.52 – Oil recovery vs. pore volumes injected for WAG injection.

5.2.3 Experiment using cross-linked gel

It was seen in the previous experiments using a polymer without cross-linker that there was excessive leakoff of the viscous fluid into the matrix. Also, alternate injection of brine and CO_2 was required to prevent CO_2 breakthrough from fracture. These two problems can effectively be eliminated by injecting a pre-formed or a delayed cross-link gel into the fracture.

5.2.3.1 Introduction

In oil recovery operations, several different types of processes have been proposed to reduce channeling of fluids through fractures and streaks of very high permeability. These include several processes like gels, particulates, precipitates, microorganisms, foams and emulsions. Of these, processes that use cross-linked polymers or other types of gels have been the most common[41]. The goal of gel treatment to date has been fairly simple – to improve the macroscopic sweep efficiency by providing a fairly uniform sweep across the entire reservoir. This is true when water is the displacing fluid. Several other EOR processes are also used to improve the microscopic sweep efficiency by

recovering the hydrocarbon that is stuck to the reservoir rock. The performance of several kinds of gels have been have been tested on a lab scale. Cr(III)/acetate/HPAM, Cr(III)/Xanthan, Xanthan solution with cross-linker and resorcinol/formaldehyde are some of the commonly used ones[41]. Typically, a gel is composed of a gelant (which is usually a polymer in an aqueous solution) mixed with a small quantity of cross-linker which causes gelling. The type of gel to be used is decided based on the resistance factors that develop during the injection of the gelant into the fracture. Apart from the type of gel to be used, there are several factors that affect the success of a gel treatment process. These include gel placement, gelant leakoff into the matrix, effect of gravity on gel placement, permeability reduction properties of the gels and the stability of the gel system. Each of these factors needs to be considered before the treatment process is started. A brief description of each of the determining factors is provided in the following sections.

5.2.3.2 Gel placement

Gel placement in a fractured system has been an important topic of research. In a fractured system, with either a hydraulic or a natural fracture, the fracture may extend part of or all the way between the injector well and the producer well. Because of its orientation and conductivity, this fracture may significantly reduce the sweep efficiency. In order to improve the sweep efficiency of the process, the most ideal condition would be that the gel completely fills the fracture and completely negate its existence[42]. This case would increase the sweep efficiency greatly. But problems occur when the matrix permeability becomes extremely low. In such a case, the injectivity is greatly reduced and this injectivity loss associated with the healing of the fracture may not be acceptable in most cases.

In order to maintain a high injectivity and also obtain a good sweep, the gel has to be places at proper locations in the fracture. For fractured injection wells, the best locations would be far from the wellbore rather than near the wellbore[42]. This is because, the part of the fracture far from the wellbore is most likely to allow the injected fluid to bypass the oil due to a variety of reasons like low viscous forces, gravity effects etc. Thus, plugging this part is most likely to improve the sweep efficiency. Also, if the near wellbore part is open to fluid flow, then injectivity problems are drastically reduced.

In the case of stratified reservoirs where the fracture cuts multiple strata, it might be important to plug those zones that are more likely to be saturated with water than those that are oil saturated. However, for injection wells, reducing the conductivity of the fracture is more important than selectively plugging the matrix of different strata[42].

5.2.3.3 Gelant leakoff into the matrix

As discussed earlier, the fracture typically has a much higher permeability compared to the matrix. Hence, the gelant when injected into the fracture can travel to a much longer distance along the fracture than it does into the adjacent matrix. But there is always some amount of gelant that enters the matrix and this plays an important role in determining how effectively the gel treatment can reduce channeling. If the gelant leakoff into the matrix is too high, then both productivity and oil-recovery efficiency become very less[42]. For an effective gel treatment, the fracture must be healed to an extent such that there is still a viable flow path between the injection and the production well. In general, the amount of leakoff that occurs into the matrix is more for a high viscosity gelant than for a low viscosity gelant. Several methods have been suggested to minimize the leakoff of the gelant into the fracture. The use of suspended particulate matter is one of the most common and effective methods to reduce leakoff during gel treatments. Cross-linking the gel is another solution, but in this case injectivity might be affected. Early in the gelation process, the gelants can penetrate a significant distance, but once the gel is formed, gel propagation becomes extremely slow and negligible. This is because of the increase in the resistance factors. This resistance factor increases with the increase in viscosity. Seright[42],(1995) performed several experiments using different types of gelants to confirm these concepts. He found that before the gel aggregates become larger than the size of pore throats, gelants penetrated readily into the pore spaces, but after gelation occurred, the propagation became negligible. Thus, two methods can be adopted to minimize gelant leakoff in fractured systems. The first method would be to allow sufficient gelation to occur before the gelant leaves the wellbore so that the gelant will not penetrate into the rock. For this method to be possible, the gel must be pumpable for some period of time without excessive increase in pressure. The second and more commonly used method is to add particulate matter to the gelant. Both these methods are still under consideration and require further research.

5.2.3.4 Effect of gravity on placement

The process of gel placement in a fractured system is usually divided into two stages for most commercial treatments. First, the gelant is injected in a fluid form. Second, the well is shut in to allow gelation to take place[42]. During the first stage, when the gelant is being injected at a high rate, the viscous forces virtually dominate over the gravity forces. In such a case, the gravity number is very low, much less than one. The dimensionless gravity number, G, provides a way to compare the importance of gravity forces relative to the viscous forces during a displacement process. For gel treatments in fractured production wells, the gel treatment rates are typically high – in the range of 50 to 500 bbl-d/ft of pay[42]. For these rates, the gravity number becomes very low. Hence, during the injection process, the position of the gelant or the gel front will not be affected significantly by gravity during injection. However, after the injection is stopped, gravity plays an important role and the dense gel starts to move downwards. Using gravity to clear a portion of the fracture to form a conduit for oil to flow to the production wells could be advantageous in most cases. Sometimes, gels can help curbing the problem of excess water production, if the source is an underlying aquifer.

5.2.3.5 Gel stability

The stability of the gel used is another important aspect to consider in a gel treatment. Several important factors such as the setting time of the gels, time for which the gel remains without breaking up, effect of shear on the gel and the stability of the gel at elevated temperatures are to be taken into account. About 50% of the oil that can be recovered by chemical flooding exist in reservoirs that have temperatures over 140 F. In such cases it is important to examine the performance of the gel at these elevated temperatures. Several experiments have been performed on gel systems where water is the displacing fluid. But when the displacing phase is a reactive substance like CO_2, care should be taken to confirm that the gel system remains stable. Laboratory experiments need to be performed to investigate the stability of gel systems in the presence of CO_2.

5.2.3.6 Field cases

Several successful field cases have been reported where gelled polymer has been successful in reducing channeling problems and improving conformance[43,44]. Sydansk[45], (1988) reported 29 successful Cr(III)-carboxylate/acrylamide-polymer (CC/AP) gel

treatments in the naturally fractured Big Horn Basin of Wyoming between 1985-1988. Of these 29 treatments, 17 were applied to injection wells as sweep improvement treatments and 12 were applied to production wells as water-shutoff treatments. The sweep improvement treatments recovered 3,650,000 bbls of incremental oil recovery. Borling[46], (1991) reported using this gel at the Wertz field CO_2 project in the Wind River Basin of Wyoming. The ten injection-well gel treatment resulted in an incremental oil recovery of up to 140,000 bbls per pattern. Hild and Wackowski[47], (1998) reported the application of CC/AP gel treatment on 44 injection wells using large volumes (10,000 bbls) of polymer gel at the CO_2 flooding project of the Rangely Weber Sand Unit of Colorado from 1994-1997. They concluded that the gel treatment program shows conformance improvement success rate of 80%. Average incremental oil was increased by 21 bbls and average incremental water was reduced by 98 bbls. Although there have been many successful field applications, all these treatments have been used for conformance control during waterflood operations. There have not been any field cases or lab experiments to investigate conformance control during CO_2 flooding.

5.2.3.7 Experimental procedure

In this experiment, the main objective was to investigate the performance of CO_2 in the presence of gel for conformance control. Here, a delayed cross-link gel was used to delay breakthrough and improve recovery. For this purpose, Guar gum was used with a borate cross-linker. Our aim here is not to investigate the use of different types of gels and any gel that can heal the fracture effectively would serve the purpose. Guar and borate cross-linker were chosen because of their easy availability and the gel was formed using this combination. One of the important considerations in using a gel for conformance is the injection pressure. As discussed earlier, once the gel is formed by the cross-link process, there is a huge increase in the resistance to flow. But gels with low resistance factors can be injected into the fracture without experiencing “screen out”. In this case, the partially formed gel with the borate cross-linker was injected directly into the fracture and allowed to set for a period of 16 hours. Fig. 5.53 to Fig. 5.55 depict the scans taken at different times after CO_2 injection was started.

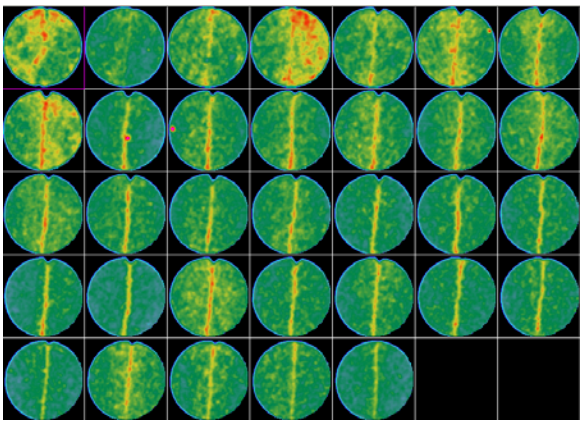

Fig. 5.53 – Oil saturated core scans with the gel seen as a yellow streak in the fracture.

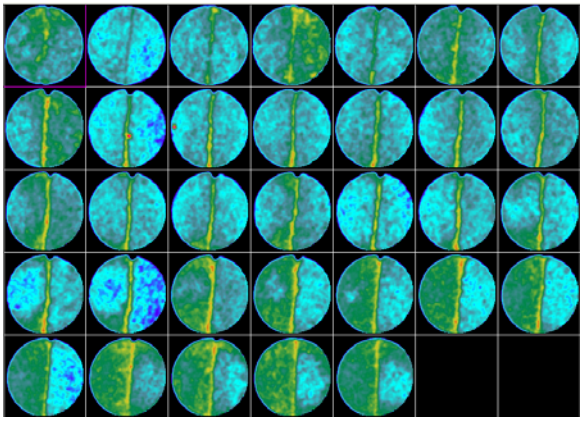

Fig. 5.54 – Scans at CO_2 breakthrough.

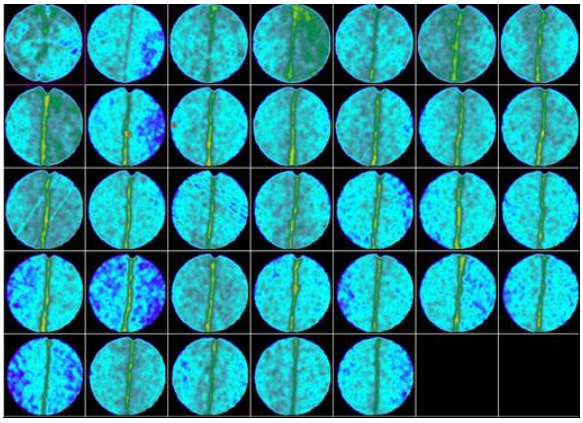

Fig. 5.55 – Scans obtained at the end of injection.

In this experiment, the brine used for forming the gel was doped with sodium iodide and potassium iodide. This was to ensure that the gel was clearly visible once injected into the fracture. It was also important to note the amount of leak off that occurred into the matrix. As can be seen from the figures, the leak off in this case is not very high. This might be due to the fact that the gel was partially formed before being injected into the fracture. Thus the gel is seen as a bright yellow streak at the centre throughout the fracture. The injection of the gel was carried out slowly by scanning different portions of the core and ensuring that the fracture was completely filled with the gel. Once CO_2 injection is started, CO_2 invasion in the core is identified by the change in color to a shade of blue. But the important thing to be noted is that the gel which is seen to be yellow at the beginning of the experiment is still seen to be intact at the end of the experiment. During the experiment, CO_2 is seen to preferentially move into one half of the core compared to the other. Investigation after the experiment showed that two of the grooves on the injection face were blocked by the gel, on one side. This caused most of the injected CO_2 to flow to the other half of the injection face (open grooves). This also led to a much earlier breakthrough than one would have expected. But it can clearly be observed from the cross-sections and the reconstructions that a good sweep has been obtained on both halves of the core. The final recovery in this case was about 95% after approximately 2.5 PV of injection. The movement of CO_2 inside the core can be better understood by looking at the ortho reconstructions shown in Fig. 5.56 to Fig. 5.58.

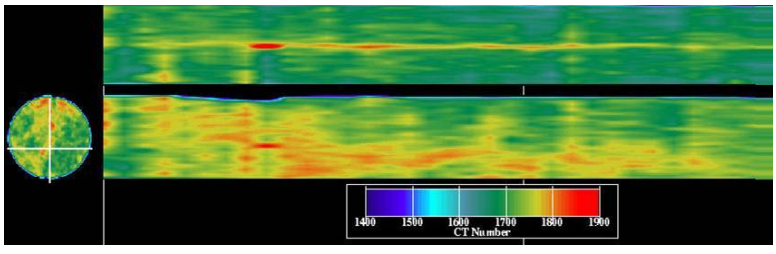

Fig. 5.56 - Ortho reconstruction showing gel in the fracture (top) and on the fracture surface (bottom).

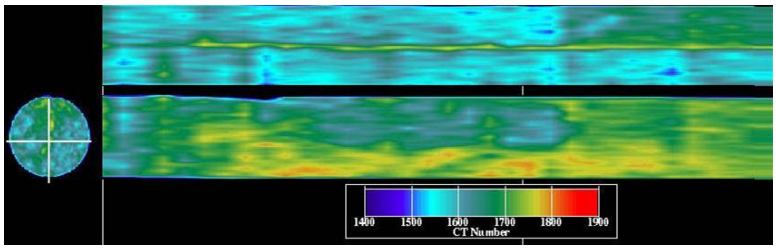

Fig. 5.57 - Reconstructions of cross-sectional scans showing preferential movement of CO_2 on one half of the core.

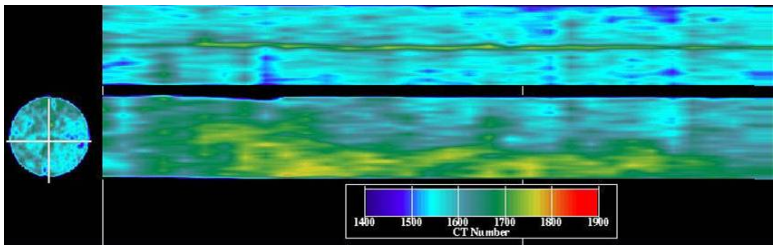

Fig. 5.58 - Ortho reconstructions showing gel intact at the end of the experiment.

In the above reconstructions, the top reconstruction was made using sections perpendicular to the fracture, while the bottom reconstructions were made using sections along the fracture surface. Fig. 5.59 shows the saturation of CO_2 inside the core at the end of CO_2 injection. Also shown in Fig. 5.60 is the color scale indicating the values of CO_2 saturation. It can be seen that most of the core is almost fully saturated with CO_2. The centre of the image where the gel was previously present shows a CO_2 saturation value of zero, confirming that no CO_2 is flowing through the fracture and the gel is still intact at the end of he experiment.

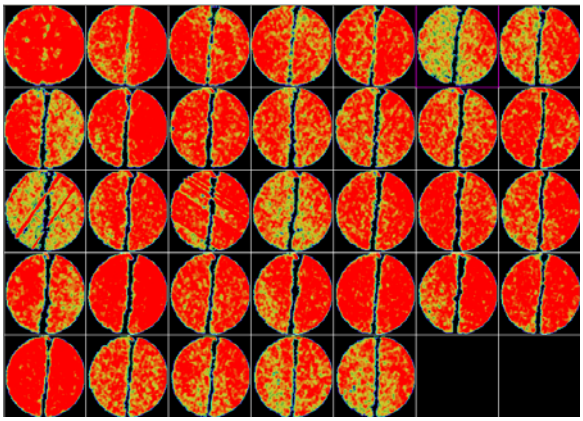

Fig. 5.59 – CO_2 saturations at the end of the experiment.

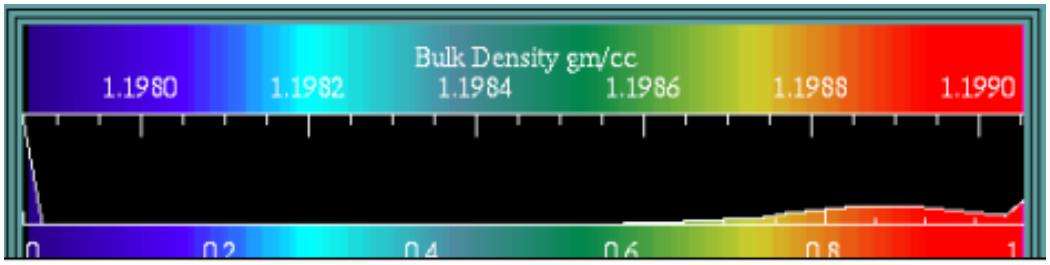

Fig. 5.60 – Color scale where red indicates high values of saturation.

.

Fig. 5.61 shows the plot of oil recovery obtained versus the number of pore volumes of CO_2 injected. Also shown in Fig. 5.62 is a comparison of the oil recovery obtained from the three different experiments. It can be seen that the process with the cross-linked gel indicates the highest efficiency.

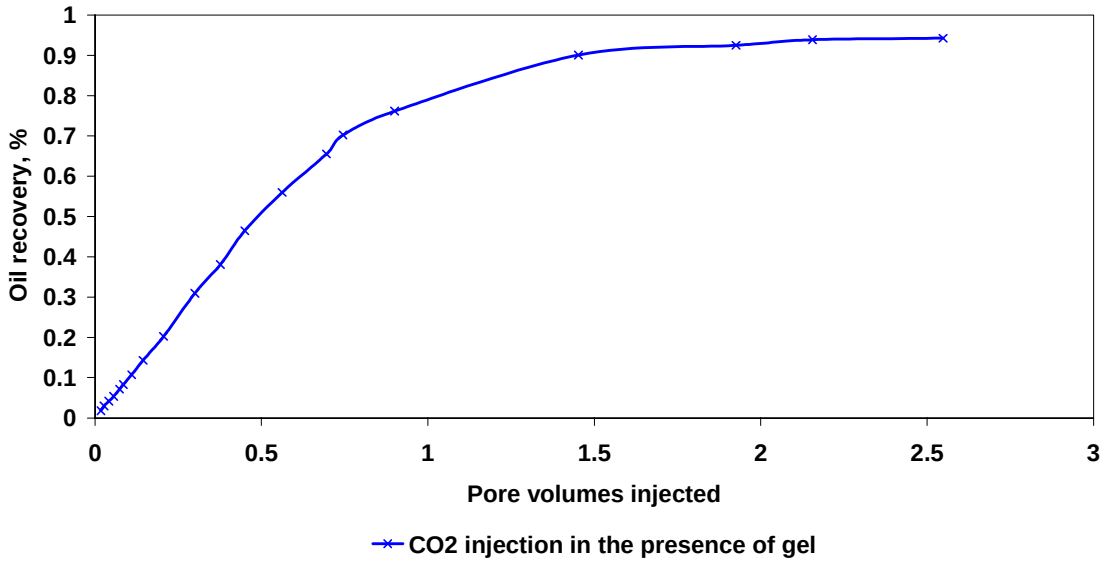

Fig. 5.61 – Oil recovery vs. pore volumes injected for CO_2 injection in the presence of cross-linked gel.

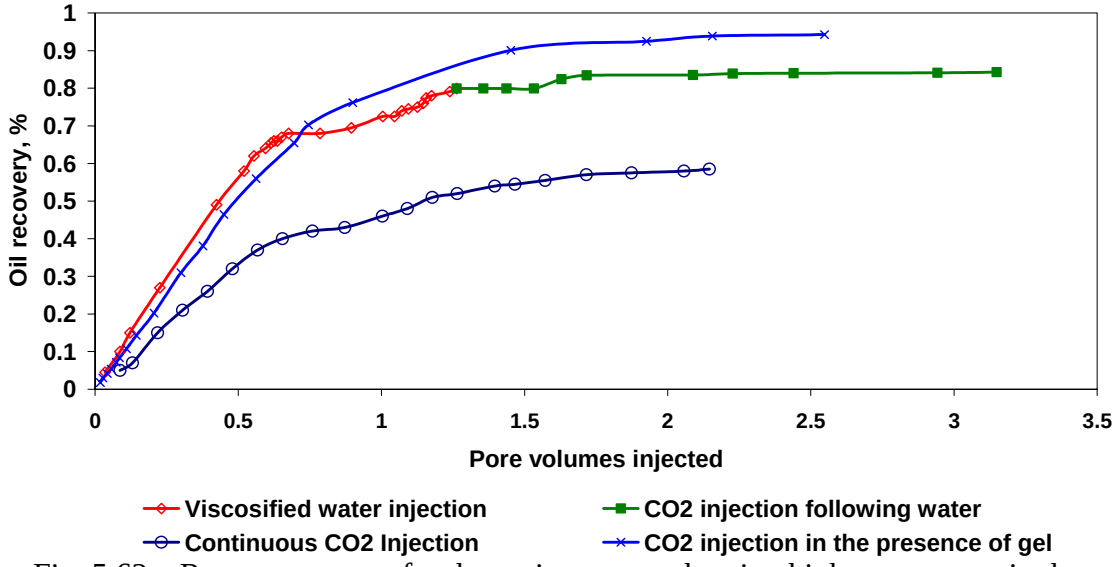

Fig. 5.62 – Recovery curves for the various cases showing highest recovery in the presence of gel.

CHAPTER VI

CONCLUSIONS AND RECOMMENDATIONS

6.1 Conclusions

The following conclusions can be derived from the coreflooding experiments performed in the laboratory:

1. Injection rates and heterogeneity play an important role in determining oil recovery and breakthrough. Although quantification of the effect of heterogeneity is very difficult, it can be said that heterogeneities always lead to a poor sweep during a flooding process.
2. Early breakthrough and irregular sweep are observed at high injection rates. The utilization of CO_2 at high injection rates would be much higher if CO_2 forms preferential paths in the regions of higher gas saturation. The amount of oil bypassed is seen to be very high during high injection rates.
3. Low injection rates give better sweep and lesser utilization of CO_2. Since viscous forces are low, gravity would play an important role at low injection rates.
4. Neither very high nor very low injection rates are good for the economic success of a project. Injection rates need to be optimized before the start of injection and a balance should be achieved between obtaining the highest possible recovery in the lowest possible time.
5. In a fractured system, the high permeability fracture serves as the preferred path for the injected fluid. This leads to early breakthrough and higher oil bypass.
6. In the presence of fractures, the recovery of oil from the matrix is a very slow process. Considerable amount of time and CO_2 are required to obtain a good recovery.
7. The coreflood experiments in the presence of fractures indicate that gravity drainage can be an important recovery mechanism even in very short matrix blocks.
8. Coreflood experiments using water viscosified with a polymer suggest that this technique can delay CO_2 breakthrough, provided the liquid “leak off” into the

matrix is not very high. Leak off into the matrix might be low in oil wet rocks, but more work is needed to establish this.

9. Using a cross-linked gel for conformance control reduces the liquid leak off to a great extent. Certain partially formed gels can be injected into the fracture without facing “screen out” problems.
10. Cross-linked gels are effective in improving the sweep efficiency and oil recovery during CO_2 flooding. The type and composition of gel to be used in the presence of CO_2 needs more investigation.

6.2 Recommendations

1. The coreflood experiments carried out were of the immiscible type and can be justified since the oil used is very light. Miscible CO_2 flood experiments are needed when experiments are performed with actual crude oil.
2. In order to better observe gravity effects, larger cores are recommended. With larger cores, connate water saturation can also be considered and CO_2 can be used as a tertiary recovery agent.
3. Investigation of the type and composition of gel that can be used without stability problems in the presence of CO_2 is recommended.

REFERENCES

1. Martin, D.F. and Taber, J.J.: "Carbon Dioxide Flooding," *JPT* (April 1992) 394-400.
2. Roebuck, I.F.: "Gas-Injection Pressure Maintenance in Oil Reservoirs," in *Petroleum Engineering Handbook,* B.H. Bradley (ed.), SPE, Richardson, Texas, (1992) Chap. 43, 1-17.
3. Uleberg, K. and Hoier, L.: "Miscible Gas Injection in Fractured Reservoirs," paper SPE 75136 presented at the 2002 SPE/DOE 10^{th} Symposium on Improved Oil Recovery, Tulsa, Oklahoma, 13-17 April.
4. Holm, L.W. and O'Brien, L.J.: "Factors to Consider When Deciding a CO_2 Flood," paper SPE 14105 presented at the 1986 International Meeting on Petroleum Engineering, Beijing, China, 17-20 March.
5. Mungan, N.: "An Evaluation of CO_2 Flooding," paper SPE 21672 presented at the 1991 SPE Western Regional Meeting, Long Beach, California, 20-22 March.
6. Bergosh, J. L., Marks, T. R. and Mitkus, A. F.: "New Core Analysis Techniques for Naturally Fractured Reservoirs," paper SPE 13653 presented at the 1985 Annual Regional Meeting, Bakersfield, California, 27-29 March.
7. Honarpour, M. M., Cromwell, V., Hatton, D. and Satchwell, R.: "Reservoir Rock Descriptions Using Computed Tomography (CT)," paper SPE 14272 presented at the 1986 Annual Technical Conference and Exhibition, Las Vegas, 22-25 September.
8. Honarpour, M. M., McGee, K. R., Crocker, M. E., Maerefat, N. L. and Sharma, B.: "Detailed Core Description of a Dolomite Sample from the Upper Madison Limestone Group," paper SPE 15174 presented at the 1986 Rocky Mountain Regional Meeting, Billings, Montana, 19-21 May.
9. Narayanan, K. and Deans, H. A.: "A Flow Model Based on the Structure of Heterogeneous Porous Media," paper SPE 18328 presented at the 1988 Annual Technical Conference and Exhibition, Houston, Texas, 2-5 October.
10. Jasti, J., Jesion, G. and Feldkamp, L.: "Microscopic Imaging of Porous Media Using X-Ray Computer Tomography," paper SPE 20495 presented at the 1990 Annual Technical Conference and Exhibition, New Orleans, 23-26 September.

11. Hidajat, I., Mohanty, K.K., Flaum, M. and Hirasaki, G.: “Study of Vuggy Carbonates Using X-Ray CT Scanner and NMR,” paper SPE 77396 presented at the 2002 SPE Annual Technical Conference and Exhibition, San Antonio, Texas, 29 September - 2 October.
12. MacAllister, D. J., Miller, K. C., Graham, S. K. and Yang, C.T.: “Application of X-Ray CT Scanning to the Determination of Gas-Water Relative Permeabilities,” paper SPE 20494 presented at the 1990 Annual Technical Conference and Exhibition, New Orleans, 23-26 September.
13. Withjack, E. M.: “Computed Tomography for Rock-Property Determination and Fluid-Flow Visualization,” paper SPE 16951 presented at the 1987 SPE Annual Technical Conference and Exhibition, Dallas, Texas, 27-30 September.
14. Wellington, S. L and Vinegar, H. J: “X-Ray Computerized Tomography,” paper SPE 16983, *JPT* (August 1987) 885-898..
15. Hicks Jr., P.J. and Narayanan, R. K.: “An Experimental Study of Miscible Displacements in Heterogeneous Carbonate Cores Using X-Ray CT,” paper SPE 20492, *SPE Formation Evaluation* (March 1994) 55-60.
16. Wellington, S. L. and Vinegar, H. J.: “CT Studies of Surfactant- Induced CO_2 Mobility Control,” paper SPE 14393 presented at the 1985 SPE Annual Technical Conference and Exhibition, Las Vegas, 22-25 September.
17. Yamamoto, J., Satoh, T., Ishii, H. and Okatsu, K.: “An Analysis of CO_2 WAG Coreflood by Use of X-Ray CT,” paper SPE 38068 presented at the 1997 SPE Asia Pacific Oil and Gas Conference, Kuala Lumpur, Malaysia, 14-16 April.
18. Oshita, T., Okabe, H. and Namba, T.: “Early Water Breakthrough – X-Ray CT Visualizes How It Happens in Oil-Wet Cores,” paper SPE 59246 presented at the 2000 SPE Asia Pacific Conference on Integrated Modeling for Asset Management, Yokohama, Japan, 25-26 April.
19. Alajmi, A.F. and Grader, A.S.: “Analysis of Fracture-Matrix Fluid Flow Interactions Using X-Ray CT,” paper SPE 65628 presented at the 2000 Eastern Regional Meeting, Morgantown, West Virginia, 17-19 October.
20. ECL Technology Ltd.: “Gas Injection Studies,” www.ecltechnology.com/subsur/ior/gasinj.htm, April 1999.

21. Holm, W.: “Evolution of the Carbon Dioxide Flooding Process,” *JPT* (November 1987) 1337-1342.
22. Qadeer, S., Dehghani, K., Ogbe, D.O., and Ostermann, R.H.: “Correcting Oil/Water Relative Permeability Data for Capillary End Effect in Displacement Experiments,” paper SPE 17423 presented at the 1988 SPE California Regional Meeting, Long Beach, California, 23-25 March.
23. Holm L.W. and Josendal, V.A.: “Mechanisms of Oil Displacement by Carbon Dioxide,” paper SPE 4736, *JPT* (December 1974) 1427 – 1438.
24. Holm, L. W.: “Evolution of the Carbon Dioxide Flooding Process,” *JPT* (November 1987) 1337-1342.
25. Alfred, D.: “Modeling Fluid Flow Through a Single Fracture Using Experimental, Stochastic and Simulation Approaches,” Master’s thesis, Texas A&M University, College Station, 2003.
26. Babadagli, T.: “Injection Rate Controlled Capillary Imbibition Transfer in Fractures Systems,” paper SPE 28664 presented at the 1994 Annual Technical Conference and Exhibition, New Orleans, 25-28 September.
27. Christensen, J. R., Stenby, E.H. and Skauge, A.: “Review of WAG Field Experience,” paper SPE 39883 presented at the 1998 SPE International Petroleum Conference and Exhibition, Villahermose, Mexico, 3-5 March.
28. Rogers, J. D., and Grigg, B. R.: “A Literature Analysis of the WAG Injectivity Abnormalities in the CO_2 Process,” *SPE Reservoir Evaluation and Engineering* (October 2001), 375-386.
29. Baojun, F. and Xingjia, D.: “Pilot Test of Water Alternating Gas Injection in Heterogeneous Thick Reservoir of Positive Rhytm Sedimentation of Daqing Oil Field,” paper SPE 30482, *SPE Advanced Technology Series* (October 1995) 33-39.
30. Grigg, R.B., and Schechter, D. S. : “State of the Industry in CO_2 Floods,” paper SPE 38849 presented at the presented at the 1997 Annual Technical Conference and Exhibition, San Antonio, Texas, 5-8 October.
31. Hsie, J.C. and Moore, J.S.: “The Quarantine Bay 4RC CO_2-WAG Pilot Project: A Post Flood Evaluation,” paper SPE 15498 presented at the 1986 SPE Annual Technical Conference and Exhibition, New Orleans, 5-8 October.

32. Holm, L.W. and O'Brien, L.J.: "Carbon-Dioxide Test at the Mead-Strawn Field," paper SPE 3103, *JPT* (April 1971) 431-432.
33. Kane, A.V.: "Performance Review of a Large-Scale CO_2-WAG Enhanced Recovery Project - SACROC Unit- KELLY SNYDER," *JPT* (February 1979) 217.
34. Aarra, M.G, Skauge, A. and Martinsen, H.A.: "FAWAG: A Breakthrough for EOR in the North Sea," paper SPE 77695 presented at the 2002 SPE Annual Technical Conference and Exhibition, San Antonio, Texas, September 29 – October 2.
35. Prieditis, J., Wolle, C.R. and Notz, P.K.: "A Laboratory and Field Injectivity Study: CO_2 WAG in the San Andres Formation of the West Texas," paper SPE 22653 presented at the 66th Annual Technical Conference and Exhibition, Dallas, Texas, October 6-9.
36. Akervoll, I., Talukdar, M.S., Midtlyng, S.H. and Torsaeter, O.: "WAG Injection Experiments with In-Situ Saturation Measurements at Reservoir Conditions and Simulations," paper SPE 59323 presented at the 2000 SPE/DOE Improved Oil Recovery symposium, Tulsa, Oklahoma, April 3-5.
37. Holm, L.W.: "CO_2 FLOODING: Its Time Has Come," paper SPE 11592, *JPT* (December 1982) 2739-2745.
38. Cannella, W.J., Huh, C. and Seright, R.S.: "Prediction of Xanthan Rheology in Porous Media," paper SPE 18089 presented at the 63rd Annual Technical Conference and Exhibition, Houston, October 2-5.
39. Seright, R.S. and Lee, R: "Gel Treatments for Reducing Channelling in Naturally Fractured Reservoirs," paper SPE 39802 presented at the 1998 SPE Permian Basin Oil and Gas Recovery Conference, Midland, Texas, 25-27 March.
40. Seright, R.S.: "Use of Preformed Gels for Conformance Control in Fractured Systems," *SPE Production & Facilities Journal* (February 1997), 59-65.
41. Seright, R.S. and Liang, J.: "A Comparison of Different Types of Blocking Agents," paper SPE 30120 presented at the 1995 European Formation Damage Conference, The Hague, Netherlands, May 15-16.
42. Seright, R.S.: "Gel Placement in Fractured Systems," paper SPE 27740, *SPE Production & Facilities Journal* (November1995), 241-248.
43. Martin, F.D. and Kovarik, F.S.: "Gels for CO_2 Profile Modification," paper SPE/DOE

17330 presented at the 1988 Improved Oil Recovery Symposium, Tulsa, Oklahoma, 17-20 April.

44. Sydansk, R.D.: “A New Conformance-Improvement-Treatment Chromium(III) Gel Technology,” paper SPE/DOE 17329 presented at the 1988 Improved Oil Recovery Symposium, Tulsa, Oklahoma, 17-20 April.
45. Sydansk, R.D. and Southwell, G.P.: “More than 12 Years’ Experience with a Successful Conformance-Control Polymer-Gel Technology,” *SPEPF* (Nov. 2000) 270-278.
46. Borling, D.C.: “Injection Conformance Control Case Histories Using Gels at the Wertz Field CO_2 Tertiary Flood in Wyoming,” paper SPE/DOE 27825 presented at the 1994 Symposium on Improved Oil Recovery, Tulsa, Oklahoma, 17-20 April.
47. Hild, G.P. and Wackowski, R.K.: “Results of the Injection Well Polymer Gel Treatment Program at the Rangely Weber Sand Unit, Rangely, Colorado,” paper SPE/DOE 39612 presented at the 1998 Symposium on Improved Oil Recovery, Tulsa, Oklahoma, 19-22 April.

APPENDIX A

CALCULATION OF POROSITY

Porosity was calculated before the start of the experiment. Two methods were employed to calculate the porosity. First, a core from the set of cores was used to calculate the porosity by material balance method. This resulted in a porosity of about 19%. The CT scanner was then used to calculate the porosity based on the CT scans of the dry core and the fluid saturated core. The procedure is as follows:

1. The core is heated at about 200° C for a period of about two days to ensure that the core is completely free of water.
2. The dry core is then transferred to the core holder and scans are obtained at different locations along the length of the core.
3. The starting and the ending positions of the scans are marked and noted down.
4. The oil in which the core is to be saturated is then prepared by mixing it with the doping phase.
5. A beaker of oil is then scanned to obtain its CT number.
6. The core is saturated in the oil in a vacuum chamber for a period of about 48 hours.
7. It is then rapidly transferred to the coreflood cell and oil saturated core scans are obtained at the same locations as the dry core scans.

   The CT number of the oil when scanned in the beaker was about 800. Using the formula described earlier, the porosity obtained was in the range of 0.16 to 0.22 with an average porosity of about 0.18. The porosity images are shown in Fig. A.1. It can be seen that the porosity varies to some extent along the length of the core. The color scale showing the values of porosity is shown in Fig. A.2. 3-D images showing the porosity profile are also shown in Fig. A.3 and Fig. A.4. Fig. A.4 shows that almost all regions in the core have a porosity value of around 18%.

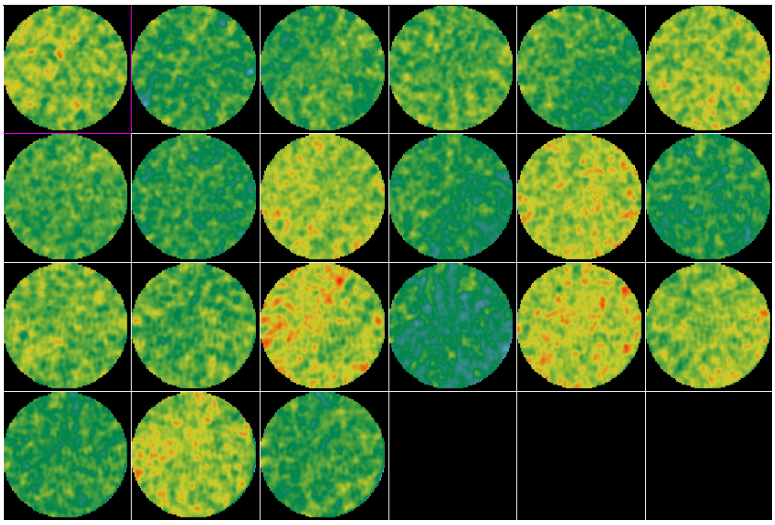

Fig. A.1 – Porosity variations along the length of the core.

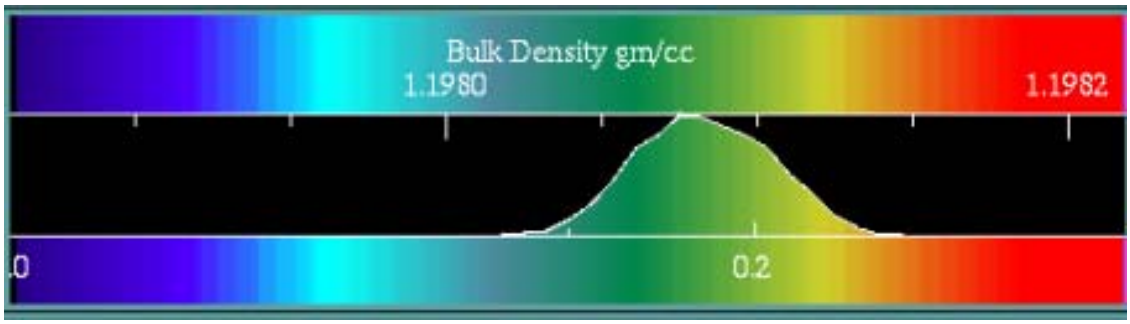

Fig. A.2 – Color scale showing average porosity value to be around 18%.

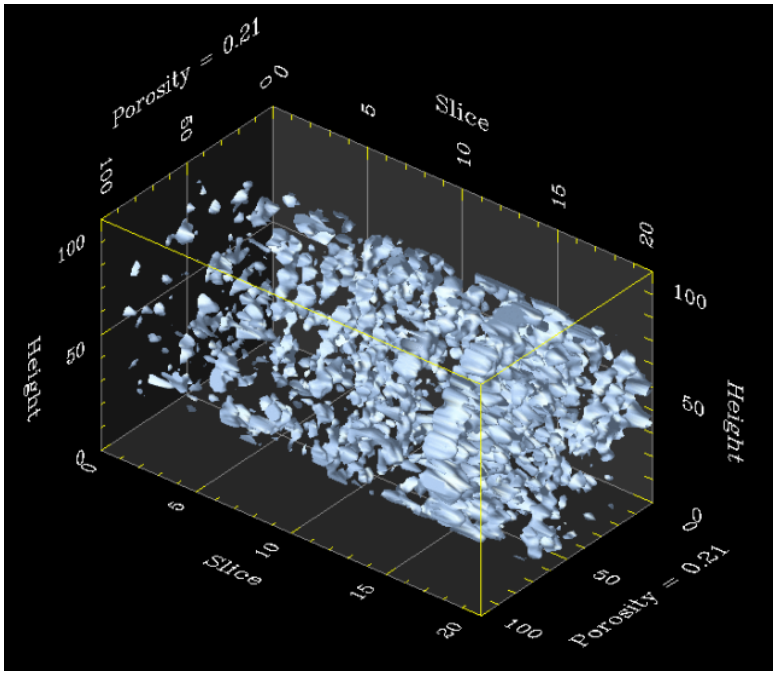

Fig. A.3 – Regions with porosity value in the range of 21%.

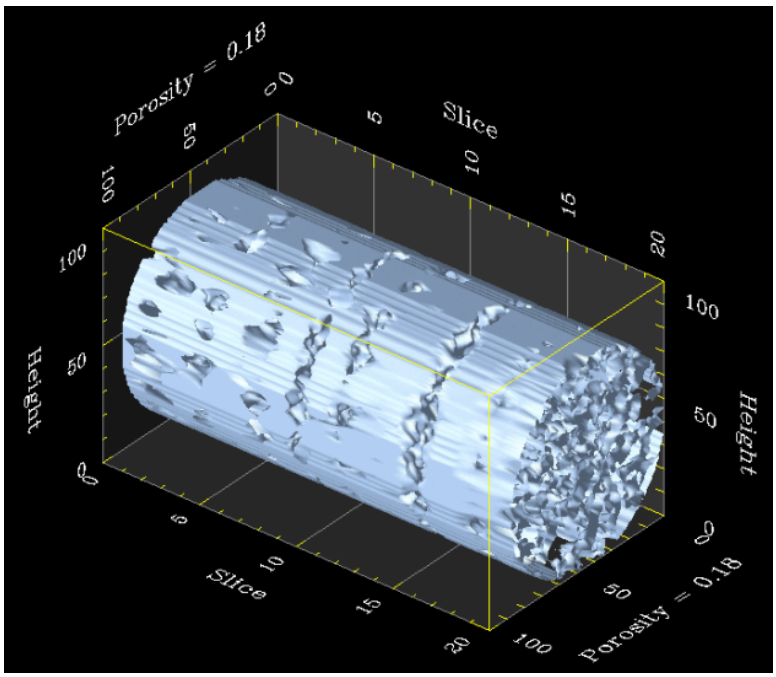

Fig. A.4 – Regions with a porosity value of at least 18%.

APPENDIX B

COMPUTER PROGRAMS

The Visual Basic programs used to calculate the saturations are listed in this appendix.

Program	Function
1. DH.vbp	Main program containing different modules.
2. modPublic.bas	Public declaratin module.
3. modFileFormat.bas	Format RAW files to compute saturations.
4. modFileops.bas	Perform file operations from interface.
5. modUtils.bas	Modify file content.
6. modCalc.bas	Calculate saturations.

DH.vbp

modPublic.bas

```
'modFileops Variables
Public strfilename As String 'Variable for file name
Public strNewName As String  'Variable for file name
Public strCheckName As String
Public strSaveName As String 'Final save file name
Public strExt As String      'To store file extension
Public strTrunc As String
Public boolSave As Boolean   'Save check
Public boolOpen As Boolean   'Open check
Public boolComp As Boolean   'File compatibility check
Public boolOnce As Boolean
Public intLen As Integer     'Store length of file name
Public intYNCan As Integer   'Variables for yes or no
Public intYNOp As Integer    'questions
Public intYNEx As Integer    'Last two or three letters
Public intYNCl As Integer    'denote subroutine
Public intYNDel As Integer
Public intYNSave As Integer

'modUtils Variables
Public intCTR As Integer     'General Counter variable
Public intRCNT As Integer    'Increment rows
```

```
'modFileFormat Variables
Public intRow As Integer     'Vary rows
Public intCol As Integer     'Vary Columns
Public intCount As Integer   'Counter
Public intRange As Integer
Public intYNchange As Integer
Public intYNsplit As Integer
Public intR1 As Integer      'These are to fix range
Public intR2 As Integer
Public intC1 As Integer
Public intC2 As Integer
Public rngPivot As Range     'Pivot used in splitting
Public rngCut As Range
Public lngCum As Long
Public lngEnd As Long        'Row for a particular image
Public boolDelimit As Boolean
Public boolInterChange As Boolean
Public boolSplit As Boolean

'frmAnalyze variables
Public objExcelApp As New Excel.Application 'Open a new
excel application object

Public ExcWB As Excel.Workbook     'Excel workbook object
Public ExcWS As Excel.Worksheet    'Excel Worksheet object

'modCalc variables
Public NOS As Integer              'Number of sheets in a
file
```

modFileFormat.bas

```
Public Sub Delimit()
    On Error GoTo Error_Delimit

    If boolOpen = False Then
        MsgBox "Please open file before editing",
vbExclamation, "Delimit Error"
        Exit Sub
    End If

    With ExcWB.Worksheets(1)

         Columns("A:A").Select
```

```
        Selection.TextToColumns Destination:=Range("A1"),
_
        DataType:=xlDelimited, _
        TextQualifier:=xlDoubleQuote, _
        ConsecutiveDelimiter:=True, _
        Tab:=True, _
        Semicolon:=False, _
        Comma:=False, _
        Space:=True, _
        Other:=False, _
        FieldInfo:=Array(Array(1, 1), Array(2, 1),
Array(3, 1), Array(4, 1), Array(5, 1)), _
        TrailingMinusNumbers:=True

        Selection.Delete Shift:=xlToLeft
        MsgBox "Delimit Complete", vbInformation,
"Delimit"
        boolDelimit = True
    End With

Error_Delimit:
    Select Case Err.Number
        Case 0:
        Case 424:
            MsgBox "Program Bug. Object has not been
properly referenced", _
                   vbCritical + vbOKOnly, "Delimit Error"
        Case Else
            MsgBox "Error No.: " & Err.Number & vbCrLf &
"Error: " & Err.Description, _
                   vbCritical, "Delimit Error"
    End Select

End Sub

Public Sub Interchange()
    On Error GoTo Error_Change

    If boolOpen = False Then
        MsgBox "Please open file before editing",
vbExclamation, "Interchange Error"
        Exit Sub
    End If

    If boolDelimit = False Then
        intYNchange = MsgBox("Click Ok if the File has been
Delimited. Else Press" & _
```

```
 "Cancel and Delimit Before Proceeding.", _
  vbExclamation + vbOKCancel, "Warning")
    End If

    Select Case intYNchange
        Case vbOK
        Case vbCancel
            If boolDelimit = False Then Exit Sub
    End Select

    With ExcWB.Worksheets(1)

        Columns("A:D").Select

        Selection.Sort Key1:=Range("C1"), _
        Order1:=xlAscending, _
        Header:=xlGuess, _
        OrderCustom:=1, _
        MatchCase:=False, _
        Orientation:=xlTopToBottom, _
        DataOption1:=xlSortNormal

        Columns("C:C").Select
        Selection.Cut
        Columns("A:A").Select
        Selection.Insert Shift:=xlToRight

        MsgBox "Interchange Complete", vbInformation,
"Interchange"
        boolInterChange = True
    End With
    Call modUtils.Change_Sheet_Name(1, "Main")

Error_Change:
    Select Case Err.Number
        Case 0:
        Case 424:
            MsgBox "Program Bug. Object has not been
properly referenced", _
                   vbCritical + vbOKOnly, "Interchange
Error"
        Case Else
            MsgBox "Error No.: " & Err.Number & vbCrLf &
"Error: " & Err.Description, _
                   vbCritical, "Interchange Error"
    End Select
End Sub
```

```
Public Sub SplitData()

    Dim lngLast_Row As Long
    Dim LR_With_Value As Long
    Dim intImageNumber As Integer

    ExcWB.Worksheets.Add           'New worksheet to store
split data
    intRange = 1
    Call Change_Sheet_Name(1, "Split")
    lngLast_Row = LastRowInColumn(intRange)
    lngEnd = lngLast_Row
    intImageNumber = 0
    intC1 = 1
    intC2 = 4
    ExcWB.Worksheets("Main").Activate
        Set rngPivot = Range("A1").Cells(1, 1)
        Do
            Do While rngPivot.Value = intImageNumber
                intCount = intCount + 1
                Set rngPivot = Cells(intCount + 1, intC1)
            Loop
            lngCum = lngCum + intCount
            If lngCum = lngLast_Row Then Exit Sub
            intImageNumber = intImageNumber + 1
            Set rngCut = Range(Cells(intCount + 1, intC1),
Cells(lngEnd, intC2))
            intC1 = intC1 + 5
            intC2 = intC2 + 5
            rngCut.Select
            Selection.Cut
            Cells(1, intC1).Select
            ActiveSheet.Paste
            lngEnd = lngEnd - intCount
            intCount = 0
        Loop
    MsgBox "Complete"
End Sub

Sub Split_Data()

    If boolInterChange = False Then
        intYNsplit = MsgBox("Click Ok if Interchange has
been Performed. Else Press" & _
                            " Cancel and Interchange Before
Proceeding.", _
```

```
                                vbExclamation + vbOKCancel,
"Warning")
    End If

    Select Case intYNsplit
        Case vbOK
        Case vbCancel
            If boolInterChange = False Then Exit Sub
    End Select

    Dim wsIn As Worksheet: Set wsIn =
ExcWB.Worksheets("Main")
    Dim rngSourceRange As Range: Set rngSourceRange =
wsIn.Range("A1").CurrentRegion
    Dim rngListRange As Range
    Dim rngTargetRange As Range
    Dim ws As Worksheet
    Dim rngC As Range
    Dim lngRStart As Long, lngREnd As Long

    Application.ScreenUpdating = False
    wsIn.Range("A1:E1").EntireColumn.Insert    'Takes all
data and puts it in column F

    Set rngListRange = wsIn.Range("A1")

    rngSourceRange.Columns(1).AdvancedFilter
Action:=xlFilterCopy, _
    CopyToRange:=rngListRange, Unique:=True    'Copies
0,1,2,3,4,5,6,7 into column 1
    Set rngListRange = wsIn.Range("a1").CurrentRegion

    rngListRange.Offset(0, 1).FormulaR1C1 = "=MATCH(RC[-
1]," & _
    rngSourceRange.Resize(rngSourceRange.Rows.Count, 1). _
                        Address(True, True, xlR1C1) & ")"
    lngRStart = 0

    For Each rngC In rngListRange.Offset(1, 0). _
                      Resize(rngListRange.Rows.Count - 1,
1).Cells
        Set ws = Worksheets.Add
        ws.Name = CStr(rngC.Value)
        lngREnd = rngC.Offset(0, 1).Value
        Set rngTargetRange = ws.Range("A1",
ws.Cells(lngREnd - lngRStart, 4))
```

```
        rngTargetRange.Value =
Range(rngSourceRange.Cells(lngRStart + 1, 1), _

rngSourceRange.Cells(lngREnd, 4)).Value
        lngRStart = lngREnd
    Next rngC

    wsIn.Columns("A:E").Delete
    Application.ScreenUpdating = True
    MsgBox "Split Complete!", vbInformation, "Split"

Error_Split:
    Select Case Err.Number
        Case 0:
        Case Else:
            MsgBox "Error No.: " & Err.Number & vbCrLf &
"Error: " & Err.Description, _
                    vbCritical, "Interchange Error"
    End Select


End Sub

Option Explicit
Option Base 1
```

modFileops.bas

```
Sub File_Open()
    On Error GoTo Error_Open
    If boolOpen = True Then
        If boolSave = False Then
            intYNOp = MsgBox("File " & strfilename & " has
not been saved. " & _
                             "proceed ?", vbExclamation +
vbYesNo, "Close")
        Else
            Call Close_File
        End If
    boolOnce = True
    GoTo 10
    End If
    Select Case intYNOp
        Case vbYes
            Call Close_File
        Case vbNo
```

```
            Exit Sub
    End Select
10  If frmAnalyze.txtName(0).Text = "" Then
        MsgBox "Please select file to be opened",
vbExclamation, "Error"
        Exit Sub
    Else
        strfilename = frmAnalyze.txtName(0).Text
    End If
    Call Check_Comp(strfilename, 0)
    If boolComp = False Then Exit Sub
    If boolOnce = False Then Set objExcelApp =
CreateObject("Excel.Application")
    Set ExcWB = objExcelApp.Workbooks. _
                            Open(frmAnalyze.filFile(0).Path
& "\" & strfilename)
    boolOpen = True
    MsgBox "File open for computation", vbInformation,
"Ready"

Error_Open:
    Select Case Err.Number
        Case 0:
        Case 1004:
            MsgBox Err.Description, vbCritical, "Error
Opening File"
        Case Else
            MsgBox "Error No.: " & Err.Number & vbCrLf &
"Error: " & Err.Description, _
                    vbCritical, "Interchange Error"
    End Select
End Sub

Sub File_Save()
    On Error GoTo Error_Save
    If boolOpen = False Then
        MsgBox "Please open file before attempting save!",
vbExclamation, "Save"
        Exit Sub
    End If

    If frmAnalyze.txtName(1).Text = "" Then
        MsgBox "Please enter valid file name",
vbExclamation, "Save Error"
        Exit Sub
    End If
```

```
    strNewName = frmAnalyze.txtName(1).Text
    Call Save_File(strNewName, 1)
    Exit Sub

Error_Save:
    Select Case Err.Number
        Case 0:
        Case 1004:
            MsgBox "Cannot complete save. Please check if
the file is: " & vbCrLf & _
                   "> Read Only, or" & vbCrLf & "> In use
by another program", _
                   vbCritical, "Save Error"
        Case Else:
            MsgBox "Error No.: " & Err.Number & vbCrLf &
"Error: " & Err.Description, _
                    vbCritical, "Interchange Error"
    End Select
End Sub

Sub Program_Exit()
    If boolOpen = True And boolSave = False Then
        intYNEx = MsgBox("File has not been saved. Do you
still want to exit ?", _
                    vbExclamation + vbYesNo, "Save File")
    Else
        intYNEx = MsgBox("Are you sure you want to quit ?",
_
                    vbQuestion + vbYesNo, "Exit")

        Select Case intYNEx
        Case vbYes
            If boolOpen = True Then
                Call modUtils.Close_File
            End If
            Call Exit_Prg
        Case vbNo
            Exit Sub
        End Select
    End If
    Select Case intYNEx
        Case vbYes
            If boolOpen = True Then
                Call Close_File
            End If
            Call Exit_Prg
        Case vbNo
```

```
            Exit Sub
    End Select
End Sub

Sub File_Delete()
    On Error GoTo Error_Delete
        If frmAnalyze.txtName(1).Text = "" Then
            MsgBox "Please specify File", vbExclamation,
"Error"
        Else
            intYNDel = MsgBox("File will be permanently
deleted. Are you sure?", _
                                vbYesNo + vbExclamation,
"Confirm File Delete")
        End If
    Select Case intYNDel
        Case vbYes
            Kill (frmAnalyze.filFile(1).Path & "\" &
frmAnalyze.txtName(1).Text)
            frmAnalyze.filFile(1).Refresh
            frmAnalyze.txtName(1).Text = ""
        Case vbNo
            Exit Sub
    End Select
Error_Delete:
    Select Case Err.Number
        Case 0:
        Case 75:
            MsgBox "Delete failed. Check if -" & vbCrLf & _
                   "> The file is read-only, or" & vbCrLf &
_
                   "> The file is being used by another
program", vbCritical, _
                   "File Delete Error"
        Case Else:
        MsgBox "Error No.: " & Err.Number & vbCrLf &
"Error: " & Err.Description, _
                vbCritical, "Interchange Error"
    End Select
End Sub

Sub File_Cancel(Index As Integer)
    If boolOpen = True Then
        intYNCan = MsgBox("This will close the currently
open file. Proceed ?", _
                          vbExclamation + vbYesNo,
"Cancel")
```

```
    Else
        frmAnalyze.txtName(Index).Text = ""
    End If

    Select Case intYNCan
        Case vbYes
            Call Close_File
            frmAnalyze.txtName(Index).Text = ""
            strfilename = ""
        Case vbNo
            Exit Sub
    End Select

End Sub
```

modUtils.bas

```
Sub Find_Add_Ext(ByRef strCheckName As String, ByVal Index
As Integer)
    intLen = Len(strCheckName)
    Select Case intLen
        Case Is < 5
            If frmAnalyze.filFile(Index).Pattern = "*.*"
Then
                strExt = ".xls"
                MsgBox "File will be saved with the
extension .xls", vbInformation, _
                       "Save"
                strCheckName = strCheckName & strExt
                Exit Sub
            End If
            strCheckName = strCheckName &
Mid(frmAnalyze.filFile(Index).Pattern, 2, 4)
            intLen = Len(strCheckName)
            strExt = Mid(strCheckName, intLen - 3, 4)
        Case Is > 5
            strTrunc = Mid(strCheckName, intLen - 3, 1)
            If strTrunc <> "." Then
                strCheckName = strCheckName &
Mid(frmAnalyze.filFile(Index).Pattern, 2, 4)
                intLen = Len(strCheckName)
                strExt = Mid(strCheckName, intLen - 3, 4)
            Else
                If Index = 1 Then
                    strCheckName = Mid(strCheckName, 1,
intLen - 4)
```

```
                    strExt =
Mid(frmAnalyze.filFile(Index).Pattern, 2, 4)
                    stecheckname = strCheckName & strExt
                Else
                    strExt =
Mid(frmAnalyze.filFile(Index).Pattern, 2, 4)
                End If
            End If
    End Select
End Sub

Sub Check_Comp(ByVal strCheckName As String, Index As
Integer)
    Call Find_Add_Ext(strCheckName, Index)
    If strExt = ".raw" Or strExt = ".xls" Then
        boolComp = True         'Compatibility set to true
    Else
        MsgBox "Incompatible file type. Please choose
files" & vbCrLf _
             & "of type .xls or .raw", vbCritical, "File
Access Error"
        frmAnalyze.txtName(Index).Text = ""
        boolComp = False        'Compatibility set to false
    End If
End Sub

Sub Save_File(ByVal strSaveName As String, Index As
Integer)
    Call Find_Add_Ext(strSaveName, Index)
    If strExt = ".raw" Then
        ExcWB.SaveAs (frmAnalyze.filFile(Index).Path & "\"
& strSaveName)
    Else
        ExcWB.SaveAs (frmAnalyze.filFile(Index).Path & "\"
& strSaveName), _
                                FileFormat:=xlNormal
    End If

    ExcWB.Saved = True
    boolSave = True
    MsgBox "File save successful", vbInformation, "Save"
End Sub

Sub Change_Sheet_Name(ByVal SheetNo As Byte, strSheetName
As String)
    ExcWB.Worksheets(SheetNo).Name = strSheetName
End Sub
```

```
Sub Close_File()
    If boolOpen = True Then
        ExcWB.Saved = True
        ExcWB.Close
        Set ExcWB = Nothing
        boolOpen = False
    End If
End Sub
Sub Exit_Prg()
    Unload frmAnalyze
    End
End Sub

Sub Decide_Range()
    modFileFormat.intRow = 1
    modFileFormat.intCol = 1
End Sub

Function LastRowInColumn(intCol As Integer) As Long

    Dim xlWs As Excel.Worksheet
    Dim LastRow As Long

    On Error GoTo Error_LastRow
    Set xlWs = ExcWB.Worksheets("Main")
    LastRow = xlWs.UsedRange.Rows.Count +
xlWs.UsedRange.Row

    While
Application.WorksheetFunction.CountA(xlWs.Rows(LastRow)) =
0
        LastRow = LastRow - 1
    Wend

    LastRowInColumn = LastRow

Error_LastRow:
    Select Case Err.Number
        Case 0:
        Case Else:
            MsgBox "Error Number = " & Err.Number & "   " &
Err.Description
    End Select
End Function
```

modCalc.bas

```
Option Explicit
Option Base 1

Public Sub Calc_Sat()
    Dim i As Integer
    Dim j As Integer
    Dim dummy As Double
    ExcWB.Worksheets("Main").Activate
    Cells.Select
    Selection.ClearContents
    Cells(1, 1) = "Image"
    Selection.Font.Bold = True
    Cells(1, 2) = "Saturations"
    Selection.Font.Bold = True
    Columns("B:B").EntireColumn.AutoFit
    Columns("A:B").Select
    With Selection
        .HorizontalAlignment = xlCenter
        .VerticalAlignment = xlBottom
        .WrapText = False
        .Orientation = 0
        .AddIndent = False
        .IndentLevel = 0
        .ShrinkToFit = False
        .ReadingOrder = xlContext
        .MergeCells = False
    End With

    With ExcWB.Worksheets(1)
        NOS = .Cells(1, 1)
    End With
    NOS = NOS + 1
    j = NOS
    For i = 1 To NOS
         ExcWB.Worksheets(i).Activate
         Range("E1").Select
         ActiveCell.FormulaR1C1 = "=AVERAGE(C[-1])"
         dummy = ActiveCell.Value
         ExcWB.Worksheets("Main").Activate
         Cells(j + 1, 1) = j - 1
         Cells(j + 1, 2) = dummy
         j = j - 1
    Next
    MsgBox "Finished Computation!", vbInformation,
"Saturation"
```

```
End Sub

Public Sub Calc_Area()

End Sub
```

VITA

Deepak Chakravarthy holds a B.E degree in mechanical engineering from PSG Institute of Technology, India. He is currently involved with the U.S Department of Energy sponsored pilot project “Investigation of Efficiency Improvements during CO_2 Injection in Hydraulically and Naturally Fractured Reservoirs”. His research areas include experimental and simulation analysis of water and gas flooding in fractured systems and multiphase pumping.

His address: 2600 Lazy Hollow Dr.

Apt # 1406

Houston, TX 77063

USA